BULLETIN OF RUSSIAN STATE MEDICAL UNIVERSITY

BIOMEDICAL JOURNAL OF PIROGOV RUSSIAN NATIONAL RESEARCH MEDICAL UNIVERSITY

EDITOR-IN-CHIEF Denis Rebrikov, DSc, professor

DEPUTY EDITOR-IN-CHIEF Alexander Oettinger, DSc, professor

EDITORS Valentina Geidebrekht, PhD; Nadezda Tikhomirova

TECHNICAL EDITOR Evgeny Lukyanov

TRANSLATORS Nadezda Tikhomirova, Vyacheslav Vityuk

DESIGN AND LAYOUT Marina Doronina

SUBMISSION

EDITORIAL BOARD

Averin VI, DSc, professor (Minsk, Belarus)
Azizoglu M, MD PhD (Istanbul, Turkey)
Alipov NN, DSc, professor (Moscow, Russia)
Belousov VV, DSc, professor (Moscow, Russia)
Bozhenko VK, DSc, CSc, professor (Moscow, Russia)
Bylova NA, CSc, docent (Moscow, Russia)
Gainetdinov RR, CSc (Saint-Petersburg, Russia)
Gendlin GYe, DSc, professor (Moscow, Russia)
Ginter EK, member of RAS, DSc (Moscow, Russia)
Gorbacheva LR, DSc, professor (Moscow, Russia)
Gordeev IG, DSc, professor (Moscow, Russia)
Gudkov AV, PhD, DSc (Buffalo, USA)
Gulyaeva NV, DSc, professor (Moscow, Russia)
Gusev EI, member of RAS, DSc, professor (Moscow, Russia)
Danilenko VN, DSc, professor (Moscow, Russia)
Zarubina TV, DSc, professor (Moscow, Russia)
Zatevakhin II, member of RAS, DSc, professor (Moscow, Russia)
Kagan VE, professor (Pittsburgh, USA)
Kzyshkowska YuG, DSc, professor (Heidelberg, Germany)
Kobrinskii BA, DSc, professor (Moscow, Russia)
Kozlov AV, MD PhD, (Vienna, Austria)
Kotelevtsev YuV, CSc (Moscow, Russia)
Lebedev MA, PhD (Darem, USA)
Manturova NE, DSc (Moscow, Russia)
Milushkina OYu, DSc, professor (Moscow, Russia)
Mitupov ZB, DSc, professor (Moscow, Russia)
Moshkovskii SA, DSc, professor (Moscow, Russia)
Munblit DB, MSc, PhD (London, Great Britain)
Negrebetsky VV, DSc, professor (Moscow, Russia)
Novikov AA, DSc (Moscow, Russia)
Polunina NV, corr. member of RAS, DSc, professor (Moscow, Russia)
Poryadin GV, corr. member of RAS, DSc, professor (Moscow, Russia)
Razumovskii AYu, corr. member of RAS, DSc, professor (Moscow, Russia)
Rebrova OYu, DSc (Moscow, Russia)
Rudoy AS, DSc, professor (Minsk, Belarus)
Rylova AK, DSc, professor (Moscow, Russia)
Semiglazov VF, corr. member of RAS, DSc, professor (Saint-Petersburg, Russia)
Skoblina NA, DSc, professor (Moscow, Russia)
Smirnov VM, DSc, professor (Moscow, Russia)
Spallone A, DSc, professor (Rome, Italy)
Starodubov VI, member of RAS, DSc, professor (Moscow, Russia)
Stepanov VA, corr. member of RAS, DSc, professor (Tomsk, Russia)
Suchkov SV, DSc, professor (Moscow, Russia)
Takhchidi KhP, member of RAS, DSc, professor (Moscow, Russia)
Trufanov GE, DSc, professor (Saint-Petersburg, Russia)
Tumanova UN, MD (Moscow, Russia)
Favorova OO, DSc, professor (Moscow, Russia)
Filipenko ML, CSc, leading researcher (Novosibirsk, Russia)
Khazipov RN, DSc (Marsel, France)
Chundukova MA, DSc, professor (Moscow, Russia)
Schegolev AI, MD, professor (Moscow, Russia)
Shimanovskii NL, corr. member of RAS, Dsc, professor (Moscow, Russia)
Shishkina LN, DSc, senior researcher (Novosibirsk, Russia)
Yakubovskaya RI, DSc, professor (Moscow, Russia)

SUBMISSION http://vestnik.rsmu.press/login?lang=en
CORRESPONDENCE editor@rsmu.press
COLLABORATION manager@rsmu.press
ADDRESS ul. Ostrovityanova, d. 1, Moscow, Russia, 117997

Indexed in Scopus. CiteScore 2024: 0.7

Indexed in WoS. JIF 2024: 0.4

Five-year h-index is 11

SCImago Journal & Country Rank 2024: 0.166

Indexed in DOAJ

Open access to archive

Issue DOI: 10.24075/brsmu.2026-01
Mass media registration certificate No. 012769, issued on July 29, 1994.
ISSN (Print): 2500-1094, ISSN (Online): 2542-1204.
Founder and publisher: Pirogov Russian National Research Medical University (Moscow, Russia).
The journal is indexed in the following scientific databases: Scopus, Web of Science, Google Scholar, SJR, DOAJ, Scilit, CyberLeninka, Embase, EZB, Lens.org, MIT Libraries, OpenAlex, Research4Life, Scholia, Wikidata, and ZDB.

The journal is distributed under the terms of the Creative Commons Attribution 4.0 International License (www.creativecommons.org).

Approved for print 28.02.2026
Circulation: 100 copies. Printed by Print.Formula
www.print-formula.ru

ВЕСТНИК РОССИЙСКОГО ГОСУДАРСТВЕННОГО МЕДИЦИНСКОГО УНИВЕРСИТЕТА

НАУЧНЫЙ МЕДИЦИНСКИЙ ЖУРНАЛ РНИМУ ИМ. Н. И. ПИРОГОВА

ГЛАВНЫЙ РЕДАКТОР Денис Ребриков, д. б. н., профессор

ЗАМЕСТИТЕЛЬ ГЛАВНОГО РЕДАКТОРА Александр Эттингер, д. м. н., профессор

РЕДАКТОРЫ Валентина Гейдебрехт, к. б. н.; Надежда Тихомирова

ТЕХНИЧЕСКИЙ РЕДАКТОР Евгений Лукьянов

ПЕРЕВОДЧИКИ Надежда Тихомирова, Вячеслав Витюк

ДИЗАЙН И ВЕРСТКА Марины Дорониной

ПОДАЧА РУКОПИСЕЙ

РЕДАКЦИОННАЯ КОЛЛЕГИЯ

В. И. Аверин, д. м. н., профессор (Минск, Белоруссия)
М. Азизоглу, MD PhD (Стамбул, Турция)
Н. Н. Алипов, д. м. н., профессор (Москва, Россия)
В. В. Белоусов, д. б. н., профессор (Москва, Россия)
В. К. Боженко, д. м. н., к. б. н., профессор (Москва, Россия)
Н. А. Былова, к. м. н., доцент (Москва, Россия)
Р. Р. Гайнетдинов, к. м. н. (Санкт-Петербург, Россия)
Г. Е. Гендлин, д. м. н., профессор (Москва, Россия)
Е. К. Гинтер, академик РАН, д. б. н. (Москва, Россия)
Л. Р. Горбачева, д. б. н., профессор (Москва, Россия)
И. Г. Гордеев, д. м. н., профессор (Москва, Россия)
А. В. Гудков, PhD, DSc (Буффало, США)
Н. В. Гуляева, д. б. н., профессор (Москва, Россия)
Е. И. Гусев, академик РАН, д. м. н., профессор (Москва, Россия)
В. Н. Даниленко, д. б. н., профессор (Москва, Россия)
Т. В. Зарубина, д. м. н., профессор (Москва, Россия)
И. И. Затевахин, академик РАН, д. м. н., профессор (Москва, Россия)
В. Е. Каган, профессор (Питтсбург, США)
Ю. Г. Кжышковска, д. б. н., профессор (Гейдельберг, Германия)
Б. А. Кобринский, д. м. н., профессор (Москва, Россия)
А. В. Козлов, MD PhD (Вена, Австрия)
Ю. В. Котелевцев, к. х. н. (Москва, Россия)
М. А. Лебедев, PhD (Дарем, США)
Н. Е. Мантурова, д. м. н. (Москва, Россия)
О. Ю. Милушкина, д. м. н., доцент (Москва, Россия)
З. Б. Митупов, д. м. н., профессор (Москва, Россия)
С. А. Мошковский, д. б. н., профессор (Москва, Россия)
Д. Б. Мунблит, MSc, PhD (Лондон, Великобритания)
В. В. Негребецкий, д. х. н., профессор (Москва, Россия)
А. А. Новиков, д. б. н. (Москва, Россия)
Н. В. Полунина, член-корр. РАН, д. м. н., профессор (Москва, Россия)
Г. В. Порядин, член-корр. РАН, д. м. н., профессор (Москва, Россия)
А. Ю. Разумовский, член-корр. РАН, д. м. н., профессор (Москва, Россия)
О. Ю. Реброва, д. м. н. (Москва, Россия)
А. С. Рудой, д. м. н., профессор (Минск, Белоруссия)
А. К. Рылова, д. м. н., профессор (Москва, Россия)
В. Ф. Семиглазов, член-корр. РАН, д. м. н., профессор (Санкт-Петербург, Россия)
Н. А. Скоблина, д. м. н., профессор (Москва, Россия)
В. М. Смирнов, д. б. н., профессор (Москва, Россия)
А. Спаллоне, д. м. н., профессор (Рим, Италия)
В. И. Стародубов, академик РАН, д. м. н., профессор (Москва, Россия)
В. А. Степанов, член-корр. РАН, д. б. н., профессор (Томск, Россия)
С. В. Сучков, д. м. н., профессор (Москва, Россия)
Х. П. Тахчиди, академик РАН, д. м. н., профессор (Москва, Россия)
Г. Е. Труфанов, д. м. н., профессор (Санкт-Петербург, Россия)
У. Н. Туманова, д. м. н. (Москва, Россия)
О. О. Фаворова, д. б. н., профессор (Москва, Россия)
М. Л. Филипенко, к. б. н. (Новосибирск, Россия)
Р. Н. Хазипов, д. м. н. (Марсель, Франция)
М. А. Чундокова, д. м. н., профессор (Москва, Россия)
Н. Л. Шимановский, член-корр. РАН, д. м. н., профессор (Москва, Россия)
Л. Н. Шишкина, д. б. н. (Новосибирск, Россия)
А. И. Щеголев, д. м. н., профессор (Москва, Россия)
Р. И. Якубовская, д. б. н., профессор (Москва, Россия)

ПОДАЧА РУКОПИСЕЙ https://vestnik.rsmu.press/login?lang=ru
ПЕРЕПИСКА С РЕДАКЦИЕЙ editor@rsmu.press
СОТРУДНИЧЕСТВО manager@rsmu.press
АДРЕС РЕДАКЦИИ ул. Островитянова, д. 1, г. Москва, 117997

Журнал включен в Scopus. CiteScore 2024: 0,7 — Журнал включен в WoS. JIF 2024: 0,4 — Индекс Хирша (h⁵) журнала по оценке Google Scholar: 11

SJR SCImago Journal & Country Rank 2024: 0,166 — Журнал включен в DOAJ — Здесь находится открытый архив журнала

DOI выпуска: 10.24075/vrgmu.2026-01
Свидетельство о регистрации средства массовой информации № 012769 от 29 июля 1994 г.
ISSN (Print): 2500-1094, ISSN (Online): 2542-1204.
Учредитель и издатель — Российский национальный исследовательский медицинский университет имени Н. И. Пирогова (Москва, Россия).
Журнал индексируется в научных базах Scopus, Web of Science, Google Scholar, SJR, DOAJ, Scilit, CyberLeninka, Embase, EZB, Lens.org, MITLibaries, OpenAlex, Research4Life, Scholia, Wikidata, ZDB.

Журнал распространяется по лицензии Creative Commons Attribution 4.0 International (www.creativecommons.org).

Подписано в печать 28.02.2026
Тираж 100 экз. Отпечатано в типографии Print.Formula
www.print-formula.ru

BULLETIN OF RSMU **1, 2026**
ВЕСТНИК РГМУ

Contents
Содержание

COMPARATIVE PROTEOMIC AND GENETIC TESTING METHODS IN MISCARRIAGE

Klimenko PA[1]✉, Lisitsa AV[2], Petushkova NA[2], Beiko NN[3], Kostyuk SV[3], Ershova ES[3], Klimenko MP[1], Gerasimova AA[4], Yusef OV[1], Vaschenko SI[1], Kurtser MA[1]

[1] Pirogov Russian National Research Medical University, Moscow, Russia
[2] Institute of Biomedical Chemistry, Moscow, Russia
[3] Institute of Biology of Aging and Healthy Longevity Medicine with a Clinic of Preventive Medicine, Petrovsky National Research Centre of Surgery, Moscow, Russia
[4] Peoples' Friendship University of Russia, Moscow, Russia

Biopsy is used for the diagnosis when treating miscarriage. However, it does not guarantee that a healthy oocyte will be acquired. The study aimed to identify proteins that are specific for pregnancy development and determine rDNA in the maternal and fetal genomes during embryogenesis. A total of 45 patients took part in the continuous prospective survey. Non-viable pregnancy was terminated in 25 patients. Another five underwent abortion due to teratogenic effects. Artificial abortion was performed in 15 cases (controls). To quantify proteins, tissues of the chorion and/or embryo and the decidua were collected from all the assessed individuals during surgery, along with blood from the cubital vein. DNA was isolated from all samples by the extraction method involving the use of organic solvents. The rDNA copy number in the DNA was determined by non-radioactive quantitative hybridization (NQH), and the chorion proteins were determined by panoramic mass spectrometry. In individuals with frozen pregnancy, decreased levels of some proteins specific for pregnancy, beta-1-glycoproteins (PSG), were revealed. The rDNA content was the same in blood cells and decidual cells of the same woman. Frozen pregnancy is associated with severe imbalance of the rDNA content in the embryonic and maternal genomes. In most cases, there are significantly less rDNA copies in the embryonic genome, than in the maternal genome and genomes of other embryos, the development of which has not been spontaneously interrupted. Thus, determination of specific proteins in chorionic villi and the rDNA copy number in the potential parents' genomes with subsequent rDNA copy number modeling in the embryo can help determine possible causes of infertility in married couples and improve the prenatal diagnosis quality.

Keywords: anembryony, decidua, frozen pregnancy, rDNA, teratogenic effect, IVF, embryo, mass spectrometry

Funding: the study was conducted as part of the Program for Basic Research in the Russian Federation for the Long Term (2021–2030) (No. 122030100170-5).

Acknowledgements: mass spectrometry measurements were conducted using the equipment of the Human Proteome SRF of the Institute of Biomedical Chemistry (Russia).

Author contribution: equally.

Compliance with ethical standards: the study was approved by the Ethics Committee of the Pirogov Russian National Research Medical University (protocol No. 228 dated 17 April 2023). All the surveyed individuals submitted the informed consent to take part in the study.

✉ **Correspondence should be addressed:** Pyotr A. Klimenko
Novatorov, 3, Moscow Москва, 119421, Russia; klimenko_pa@rsmu.ru

Received: 08.12.2025 **Accepted:** 19.01.2026 **Published online:** 28.01.2026

DOI: 10.24075/brsmu.2026.002

Copyright: © 2026 by the authors. **Licensee:** Pirogov University. This article is an open access article distributed under the terms and conditions of the Creative Commons Attribution (CC BY) license (https://creativecommons.org/licenses/by/4.0/).

СРАВНИТЕЛЬНЫЕ ПРОТЕОМНЫЕ И ГЕНЕТИЧЕСКИЕ МЕТОДЫ АНАЛИЗА ПРИ НЕВЫНАШИВАНИИ БЕРЕМЕННОСТИ

П. А. Клименко[1]✉, А. В. Лисица[2], Н. А. Петушкова[2], Н. Н. Вейко[3], С. В. Костюк[3], Е. С. Ершова[3], М. П. Клименко[1], А. А. Герасимова[4], О. В. Юсеф[1], С. И. Ващенко[1], М. А. Курцер[1]

[1] Российский национальный исследовательский медицинский университет имени Н. И. Пирогова, Москва, Россия
[2] Научно-исследовательский институт биомедицинской химии имени В. Н. Ореховича, Москва, Россия
[3] Институт биологии старения и медицины здорового долголетия с клиникой превентивной медицины ГНЦРФ РНЦХ имени Б. В. Петровского, Москва, Россия
[4] Российский университет дружбы народов имени Патриса Лумумбы, Москва, Россия

В прегравидарный период для оценки репродуктивного здоровья пациенток используют комплекс мероприятий (биопсию эндометрия, ультразвуковое определение ооцитов, желтого тела, гормонального баланса). Однако они не дают гарантии получения здоровой яйцеклетки. Целью исследования было идентифицировать специфичные для развития беременности белки и определить рДНК в геноме матери и плода в процессе эмбриогенеза. В сплошном проспективном обследовании участвовало 45 пациенток. У 25 пациенток выполнено удаление неразвивающейся беременности. Еще у пяти проведено прерывание беременности из-за тератогенных эффектов. В 15 случаях (контроль) проведен артифициальный аборт. Для определения количества белков у всех обследуемых в процессе операции отбирали ткани хориона и/или эмбриона и децидуальной оболочки, а также кровь из кубитальной вены. Из всех образцов выделяли ДНК методом экстракции органическими растворителями. Число копий рДНК в ДНК определяли методом нерадиоактивной количественной гибридизации NQH, белки в хорионе — с помощью панорамной масс-спектрометрии. При замершей беременности выявлено снижение уровня некоторых специфичных белков беременности — бета-1-гликопротеинов (PSG). Содержание рДНК было одинаково в клетках крови и в клетках децидуальной оболочки одного и того же женского организма. Замершая беременность ассоциирована с выраженным дисбалансом по содержанию рДНК в геноме эмбриона и геноме матери. В большинстве случаев геном эмбриона содержит достоверно меньше копий рДНК, чем геном матери и геномы других эмбрионов, развитие которых не прерывалось самопроизвольно. Таким образом, определение специфических белков в ворсинах хориона и числа копий рДНК в геномах потенциальных родителей с последующим моделированием числа копий рДНК у эмбриона может помочь в определении возможных причин бесплодия у супружеских пар и повысить качество пренатальной диагностики.

Ключевые слова: анэмбриония, децидуальная оболочка, замершая беременность, рДНК, тератогенный эффект, ЭКО, эмбрион, масс-спектрометрия

Финансирование: работа выполнена в рамках Программы фундаментальных научных исследований в Российской Федерации на долгосрочный период (2021–2030 годы) (№ 122030100170-5).

Благодарности: масс-спектрометрические измерения выполняли на оборудовании ЦКП «Протеом человека» Института биомедицинской химии (Россия).

Вклад авторов: равнозначный.

Соблюдение этических стандартов: исследование одобрено этическим комитетом РНИМУ им. Н. И. Пирогова (протокол № 228 от 17 апреля 2023 г.). Все обследованные подписали добровольное информированное согласие на участие в исследовании.

✉ **Для корреспонденции:** Петр Афанасьевич Клименко
ул. Новаторов, д. 3, г. Москва, 119421, Россия; klimenko_pa@rsmu.ru

Статья получена: 08.12.2025 **Статья принята к печати:** 19.01.2026 **Опубликована онлайн:** 28.01.2026

DOI: 10.24075/vrgmu.2026.002

Авторские права: © 2026 принадлежат авторам. **Лицензиат:** РНИМУ им. Н. И. Пирогова. Статья размещена в открытом доступе и распространяется на условиях лицензии Creative Commons Attribution (CC BY) (https://creativecommons.org/licenses/by/4.0/).

According to some data, spontaneous abortion in the first trimester most often results from natural selection, the number of embryos with chromosome abnormalities reaches 60–80% [1]. The rate of structural karyotype abnormalities in patients with recurrent pregnancy loss is 10 times higher than in the population: 2.4%. The standard embryo karyotyping involves testing for the Down syndrome, Patau syndrome, Edwards syndrome, Turner syndrome, Klinefelter syndrome. The patients having a history of two or more spontaneous abortions receive medical genetic counseling including the partners' cytogenetic testing with explanation of the genealogical and cytogenetic findings, assessment of the risk of giving birth to children with developmental abnormalities, clarification of the need for prenatal diagnosis (including testing of the chorion), and the use of donor cells in severe cases. Cytogenetic testing of the embryo, chorion, determination of translocations in parents are necessary in all stillbirth cases.

The chorionic villi sampling for prenatal testing involving collection of a tissue sample from the placenta for karyotyping and detection of specific genetic or biochemical abnormalities in an unborn child is most often used in obstetric practice [2]. According to the transcriptome analysis, 65% (n = 13,074) of all human proteins (n = 20,090) are expressed in the placenta, and 288 of these genes show expression that is increased relative to other tissue types. In contrast to conventional biochemical approaches involving tracing one specific protein or more, proteomics, specifically LC-MS/MS, represents an effective method to detect the altered protein expression, as well as proteins involved in the disease pathogenesis. In recent years, there have been great advances in identification of the differentially regulated proteins, biomarkers, protein modifications and polymorphisms in various human tissues, and the so-called missing proteins by mass spectrometry [3].

A missing protein is an unconfirmed genetic sequence, for which a protein has not yet been discovered [4]. According to the international Human Proteome Project (HUPO), there are currently 1343 missing proteins without any annotated functions predicted by the bioinformatics analysis or studied experimentally. The missing protein detection complexity can be due to not only their low abundance in many tissues, but also expression confined to several cell types within the human body.

The ribosomal genes that encode ribosomal RNAs (18S, 28S, and 5,8S rRNA) being part of ribosomes, the protein-synthesizing cytoplasmic organelles, are clustered in the ribosomal repeat (rDNA) represented in the genomes of eukaryotes by a large number of copies. The number of rDNA repeats in diploid human genomes varies between 200–711 copies [5]. Clusters of the rDNA tandem repeats of various size that are localized in short arms of five acrocentric chromosome pairs form the nucleolar organiser regions (NORs) of chromosomes. In humans, the rDNA copy number (R parameter) is determined by the combination of five pairs of parental acrocentric chromosomes. All rDNA copies in the cell are differentiated into potentially active and inactive. The number of active rDNA copies that is usually proportional to the number of inactive copies accounts for about 30–40% of the total copy number. The more rDNA copies there are in the genome, the more active copies there are, which are transcribed to ensure the rRNA quantity that is essential for ribosome biogenesis [6].

It has previously been shown that the ribosome biogenesis level, which depends on the number of rDNA copies in the genome, can affect conception and the course of pregnancy. The analysis of the share of non-viable zygotes in the samples of married couples with normal fertility, infertility, and miscarriage has shown that the loss of zygotes in the sample of healthy couples is significantly lower, than in the samples having reproductive problems. Therefore, the zygotic selection based on the dose of active rDNA copies in the genome can be one of the factors determining reproductive problems in some couples. In other words, very low and very high rDNA content in the embryonic genome can potentially hinder normal embryogenesis [7]. Another study has shown that the in vitro fertilization (IVF) procedure success depends on the total rDNA copy number in the woman's genome [8]. Women with the lower rDNA copy number had a lower chance of getting pregnant through IVF. One of the hypotheses explaining this fact assumes that women with the low rDNA copy number transmit the lower number to the embryo, which is insufficient for successful embryogenesis.

Thus, the level and presence or absence of specific proteomes in the chorion must correspond to a certain number of different DNA forms in the extracellular DNA.

The study aimed to identify uncommon proteins and determine rDNA in the maternal and fetal genomes during embryogenesis.

METHODS

The continuous prospective study of patients with miscarriage was conducted in May–July, 2023 at the Family Planning and Reproduction Center. Observations, in which we failed to collect al three biological media within the first 3 h, were excluded. Inclusion criteria: frozen pregnancy of unknown origin; teratogenic effect; abortion by the patient's free will. Exclusion criteria: other obstetric complications.

The study involved 45 patients, who were divided into three groups. A total of 25 patients (group I) were admitted to the hospital due to frozen pregnancy (5–13 weeks). Anembryonic pregnancy was reported in five of them, another 20 had frozen pregnancy of unknown origin. Furthermore, ultrasonography revealed discrepancies between the dead embryos' anthropometric data and gestational age (in early pregnancy there was no heartbeat, and at pregnancy periods over 7 weeks a decrease in the crown-rump length by 3–5 weeks was detected) in these patients. Five patients (group II) underwent pregnancy termination for medical reasons (teratogenic effects) after genetic counseling and the council at 13–21 weeks of pregnancy. The control group (group III) was represented by 15 healthy patients having no problems with their reproductive function, who were through artificial abortion by their own will at 8–11 weeks of pregnancy.

The chorionic and/or embryonic tissue (sample E) and decidual tissue (sample D) were collected from all the surveyed individuals during surgery. Moreover, blood was collected from the women's cubital vein before surgery (sample C).

Proteins of the chorion of patients with frozen pregnancy and patients post artificial abortion were tested by electrospray ionization tandem mass spectrometry (LS-MS/MS) as previously reported [9]. Preparation of chorionic villi samples for further proteomic analysis involved protein extraction using the lysis buffer based on the 2% SDS (sodium dodecyl sulfate), ultrasonic treatment, 1DE-gel concentration procedure for SDS removal [9]. Protein levels in the chorionic villi extracts were determined using bicinchoninic acid as a reference sample [10].

Reduction, alkylation with iodoacetamide, and in-gel tryptic digestion were performed as previously reported [11]. The peptide mixture was analyzed using the Ultimate 3000 nano-flow HPLC system (Dionex, USA) integrated with the Orbitrap Q Exactive HF mass spectrometer (Thermo Scientific, USA) and the Nanospray Flex ion source (Thermo Scientific, USA) [9].

Mass spectra in the ".raw" format were converted into appropriate mgf files using the ProteoWizard MS Convert v. 3.0.6867 software tool (http://proteowizard.sourceforge.net). Files were imported to the SearchGUI platform (v. 3.3.17) [12] and analyzed using the X!Tandem and MS-GF+ search algorithms applied to the SwissProt database (v. 2.22.2022, FASTA format) for the species Homo sapiens. The search was performed in the database of inverted and random amino acid sequences (decoy). The PeptideShaker integrator [13] was used to produce the Excel spreadsheet files with the protein identification results.

To determine the relative content of proteins identified in the chorion, the normalized spectral abundance factor (NSAF) showing high reproducibility was used [14].

DNA was isolated from the samples C, E, D by the extraction method involving the use of organic solvents. The solution containing 0.04 M EDTA, 2% sodium lauryl sarcosylate, and 150 μm/mL RNAse A (Sigma, USA) was added to the samples for 45 min at 37 °C, treated with proteinase K (200 μm/mL, Promega, USA) for 24 h at 37 °C, extracted using the equal volumes of the phenol/chloroform/isoamyl alcohol mixture (25 : 24 : 1), phenol and the chloroform/isoamyl alcohol mixture (24 : 1). DNA was precipitated by adding 1/10 volume of 3 M sodium acetate (pH 5.2) and 2.5 volumes of ice-cold ethanol. Phenol was stabilized with 8-hydroxyquinoline. DNA was collected by centrifugation at 10,000 G for 15 min at 4 °C, washed with 70% ethanol (v/v), dried, and dissolved in water.

Ribosomal gene copy number determination: the number of rDNA copies in DNA was determined by non-radioactive quantitative hybridization (NQH) [5]. To detect human rDNA (GenBank sample No. U13369), the mixture of probes for the rDNA oligo(18S) biotin-CTGTAATGATCCTTCCGCAGGTTCACCTAC and oligo(18S) biotin-TATCGGTCTCGTGCCGGTATTTAGCCTTAG was used. Denatured DNA was applied onto the filter (Optitran BA-S85, GE Healthcare, USA), 4–6 spots per sample. Standard genomic DNA samples (50 ng/ml) with the known rDNA content were applied onto the same filter to construct a calibration curve of signal intensity vs. rDNA copy number. The lambda phage DNA (50 ng/mL) was also applied onto the same filter to control the noise level. Then the filter was vacuum heated at 80 °C for 1.5 h. After the hybridization completion, the membrane filter was treated with the streptavidin-alkaline phosphatase conjugate (Sigma, USA) and placed in a solution of alkaline phosphatase substrates (bromo-chloro-indolyl-phosphate/nitro blue tetrazolium, BCIP/NBT). Then the filter was washed with water, dried in the dark, and scanned. The Imager 6 software allowing one to calculate the integrated intensity of signals from each point was used for rDNA quantification. Signals from all points corresponding to the same sample were summed up to calculate the mean and standard error for each sample.

No sample size calculation principles were used. Statistical analysis methods: descriptive statistics for quantitative variables are presented as the mean, median, and range of values. Pairwise comparison of samples was performed using the Mann–Whitney *U*-test (*p*). This test is best suited for our task due to small size of the samples used in the study. The test can be used to compare two groups, when there are at least three different trait values in each group. The StatPlus2007 software tool (http://www.analystsoft.com/) was used for calculation. The differences were considered significant at $p < 0.05$. The number of rDNA copies in the embryo's genome was used to predict frozen pregnancy in patients. Our results are preliminary and descriptive due to the fact that the sample was small.

RESULTS

Infertility has become a global health problem, with the number of people suffering from this condition growing every year. The IVF procedure holds great promise for infertility treatment. However, the early embryogenesis is complex, since a number of processes take place in this phase, including the transition from mother to zygote. In humans, the early embryonic development can be complicated by genomic errors that occur after fertilization. The nuclear abnormalities found in human embryos, especially those resulting from IVF, are due to DNA damage, aneuploidy, and decreased developmental potential. Transcription and expression of certain genes in the embryo are through a number of changes in the early embryonic development phase [15].

Comparative proteomic analysis

The multicopy genes that encode ribosomal rRNAs (rDNA) determine the ribosome biogenesis and, therefore, protein biosynthesis levels in the body, especially in early embryogenesis [16, 17]. The comparative proteomic analysis can provide new insights into biological pathways underlying the spontaneous abortion pathogenesis. That is why in the first phase of the study we assessed the human chorionic protein profile alterations associated with frozen pregnancy by panoramic mass spectrometry. Among proteins identified, pregnancy-specific glycoproteins were determined (PSG; Table 1). Human PSGs represent a group of molecules that are almost exclusively expressed by placental trophoblasts (chorionic villi) in pregnancy. Ten protein-encoding closely linked human PSG genes (PSG1–PSG9 and PSG11) form a subgroup of the carcinoembryonic antigen (CEA) gene family [18] (https://www.proteinatlas.org/humanproteome/tissue/placenta). CEA is an important tumor marker of colorectal and some other carcinomas [19]. We have also managed to identify all the CEA family subgroup members (Table 1). Furthermore, in individuals with frozen pregnancy, there was a significant decrease in the levels (estimated based on NSAF values) of such glycoproteins, as PSG3 and PSG2; glycoproteins PSG7 and PSG4 were not detected in the chorionic tissue. The decrease in PSG7 levels during fetal development can result in pregnancy loss [20, 21]. Thus, our data showing that low PSG levels are associated with poor pregnancy outcomes are consistent with the results of other authors [18].

Moreover, alpha-L-fucosidase, which plays an important role in cell adhesion during attachment and detachment of fetal membranes, was detected in samples of the chorion after abortion [22]. We also detected the decrease in expression of the reticulon-4 protein (RTN4), which is involved in apoptosis (GO: 0006915), in cases of embryo loss. The RTN4 deficiency can result in such phenotypes, as "abnormal trophoblast layer morphology", "fetal growth restriction", "reduced fetal size", and "embryonic lethality" [23].

In cases of embryo loss, PSG8, PSG7, PSG4 proteins were not determined in samples of the chorion; the pregnancy-specific beta-1-glycoprotein 6 (Q00889, PSG6) levels were low relative to the control (Table 1).

Furthermore, in cases of frozen pregnancy, we revealed the decreased levels of such proteins, as coactosin-like protein (*COTL1*), protein canopy homolog 2 (*CNPY2*), sideroflexin-3 (*SFXN3*), prohibitin-2 (PHB2), and hyaluronan and proteoglycan link protein 1 (HAPLN1), in the chorionic villi compared to the control samples of the chorion. For example, HAPLN1 is essential for production of the cartilaginous proteoglycan

Table 1. Pregnancy-specific glycoproteins (PSG) detected in human chorionic villi by panoramic mass spectrometry (LC-MS/MS)

##	Protein ID in the *UniProt database*	Gene	Protein	Biological process	NSAF value	
					Artificial abortion	Frozen pregnancy
1	Q00887	*PSG9*	Pregnancy-specific beta-1-glycoprotein 9	immune system process (GO:0002376)	0.0099	0.0051
2	Q9UQ74	*PSG8*	Pregnancy-specific beta-1-glycoprotein 8	immune system process (GO:0002376)	0.0053	undefined
3	Q13046	*PSG7*	Pregnancy-specific beta-1-glycoprotein 7	female pregnancy (GO:0022414)	0.0054	undefined
4	Q00889	*PSG6*	Pregnancy-specific beta-1-glycoprotein 6	immune system process (GO:0002376); female pregnancy (GO:0022414)	0.0051	0.0058
5	Q15238	*PSG5*	Pregnancy-specific beta-1-glycoprotein 5	cell adhesion (GO:0007155); female pregnancy (GO:0022414)	0.0129	0.0094
6	Q00888	*PSG4*	Pregnancy-specific beta-1-glycoprotein 4	immune system process (GO:0002376); female pregnancy (GO:0022414)	0.0159	undefined
7	Q16557	*PSG3*	Pregnancy-specific beta-1-glycoprotein 3	immune system process (GO:0002376); female pregnancy (GO:0022414)	0.0132	0.0079
8	P11465	*PSG2*	Pregnancy-specific beta-1-glycoprotein 2	cell adhesion (GO:0007155); female pregnancy (GO:0022414)	0.0146	0.0087
9	Q9UQ72	*PSG11*	Pregnancy-specific beta-1-glycoprotein 11	cell adhesion (GO:0007155); female pregnancy (GO:0022414)	0.0108	0.0089
10	P11464	*PSG1*	Pregnancy-specific beta-1-glycoprotein 1	immune system process (GO:0002376); female pregnancy (GO:0022414)	0.0072	0.0064

Note: NSAF — normalized spectral abundance factor reflecting protein content.

aggregates having a broad spectrum of biological functions. The lack of HAPLN1 results in perinatal mortality associated with severe chondrodysplasia [24] and heart malformations [25].

Thus, comparative proteomic analysis allowed us to determine the low abundance proteins specific for pregnancy development that are characterized by considerable alteration of their content (decrease and/or lack) during early embryogenesis in cases of spontaneous abortion.

Genetic testing

As is known, the body's level of protein biosynthesis is determined by ribosome biogenesis, the multicopy genes encoding ribosomal rRNA (rDNA), which represents one of the characteristics of adaptive capacity in humans. In this regard, in the next phase we determined rDNA in the maternal and fetal genomes during embryogenesis. Table 2 presents experimental

Table 2. Descriptive statistics for R parameter

Tissue type	Parameters	Group I (n = 25)	Group II (n = 5)	Group III (n = 15)
Maternal peripheral blood	Mean	417 ± 88	373 ± 183	425 ± 78
	Interval	322–629	191–713	314–612
	Median	398	442	412
Embryonic tissue	Mean	373 ± 183	363 ± 82	468 ±134
	Interval	191–713	242–436	295–723
	Median	261	401	478
Decidua	Mean	405 ± 92	434 ± 36	422 ± 70
	Interval	204–595	379–473	318–580
	Median	405	445	409

Note: the data are presented as the median (min–max); descriptive statistics for quantitative variables are presented as the mean and standard deviation — M (SD); sample C — blood from the patient's cubital vein; sample E — embryonic tissue; sample D — decidual tissue.

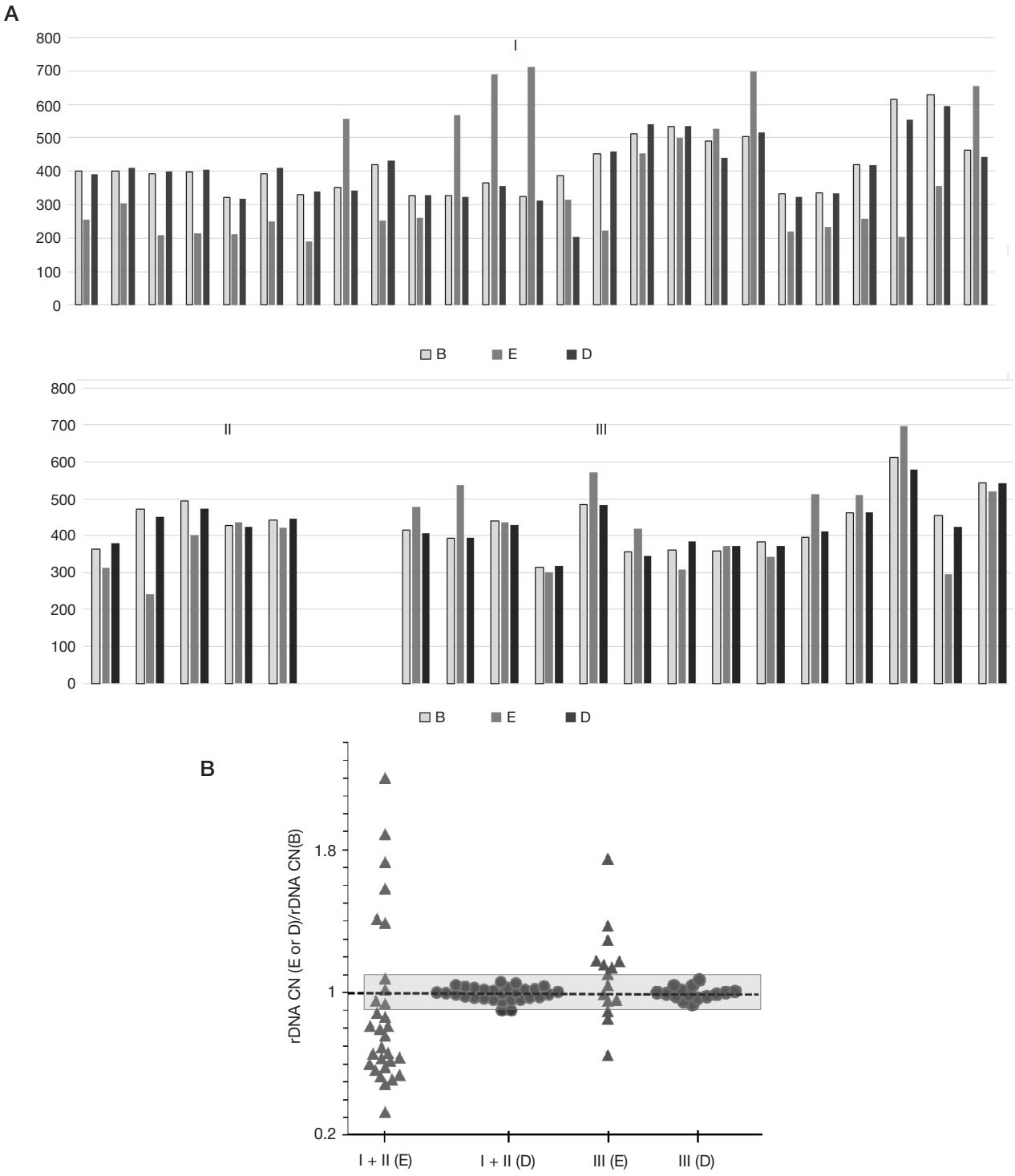

Fig. rDNA copy number in DNA isolated from three types of cells in groups I–III. **A**. The mean copy number in the DNA sample (n = 3) and the measurement error are provided. **B**. Alteration of rDNA copy number in embryonic and decidual tissues relative to rDNA levels in blood leukocytes

data that reflect the number of rDNA copies (R parameters) in DNA of blood leukocytes, decidua and the embryos' DNA.

Group I (Figure) — frozen pregnancy (No. 1–25) or suspected (visually) lack of the embryo (No. 20–25). Samples of the DNA isolated from blood cells and D tissue of the same women showed no differences in rDNA content ($p > 0.05$). This fact confirms the earlier reported data on equal rDNA levels in different tissues within the same body [26].

Embryonic genomes (tissue E) were dramatically different from maternal genomes (tissues C and D) based on the rDNA copy number. It is interesting to note that the differences were reported for five cases (No. 20–25), when the embryo could not be visually detected. It is likely that the cell division arrest occurred in early pregnancy. Among the maternal cells, there are most likely also cells from another organism. It is possible that the rDNA content in these cells is even lower.

As for the ratio of rDNA content in the embryo's genome and maternal cells, all embryos in group I split into two subgroups. In subgroup Ia (n = 20), the R (E) parameter was 1.4–3.3 times lower (mean — 1.7 times; $p < 0.001$), than R (C or D). In subgroup Ib (n = 5), the R (E) parameter was 1.7–2 times higher (mean — 1.8 times; p = 0.02), than R (C). Thus, the embryo development arrest is associated with either too low, or too high rDNA content compared to the woman's genome.

Group II — termination of pregnancy due to medical reasons (encephalocele, signs of congenital limb deformity, congenital CNS abnormality acrania, Edwards syndrome, and fusion of the pulmonary artery to aorta in the fetus). In this group, genomes of 4 embryos comprised more rDNA copies, than in group Ia (p = 0.01). The differences between groups IIC and IIE were non-significant. Only one embryonic DNA sample had lower rDNA content compared to the woman's leukocyte DNA.

As for groups with healthy and frozen pregnancy, the most significant results were obtained for the embryos only (Fig. 1), and the threshold number of rDNA repeats was 322. In our study, lower rDNA content values were associated with the embryos' death.

The analysis of the data reported allows us to draw the following conclusions

In cases of embryo loss, there are severe abnormalities of protein composition and the genes involved in pregnancy development in tissues of the chorion. Thus, low PSG levels were associated with poor pregnancy outcomes. In particular, in cases of frozen pregnancy no pregnancy-specific beta-1-glycoprotein 7 (PSG7), the decrease in the levels of which during fetal development can result in pregnancy loss, was found in the chorion.

We also detected downregulation of the reticulon-4 protein (RTN4) involved in apoptosis (GO: 0006915) in cases of embryo loss. The RTN4 deficiency can result in such phenotypes, as "abnormal trophoblast layer morphology", "fetal growth restriction", "reduced fetal size", and "embryonic lethality" [23].

The rDNA content is the same in blood cells and cells of the decidua of the same female body.

The threshold values of rDNA repeats in embryonic tissues (322) were determined, after the decrease of which pregnancy was terminated.

DISCUSSION

Frozen pregnancy is associated with severe imbalance of rDNA content in the embryonic and maternal genomes. In most cases, the embryo's genome comprises significantly less rDNA copies, than the maternal genome and genomes of other embryos, the development of which has not been not spontaneously interrupted. Very low rDNA content in the genome is likely to be associated with the low number of ribosomes, which is incapable of ensuring the protein synthesis level appropriate for the development of a particular embryo. It has been previously shown that the low rDNA copy number in the human genome (less than 300 copies) is associated with the lower life expectancy and dementia in the elderly [7, 27]. Cystic fibrosis, a monogenic disorder caused by the CFTR gene mutation, is associated with the larger rDNA copy number in the affected individual's genome. Schizophrenia, being a multifactorial disorder, is also associated with the increased rDNA content in the affected individual's genome [27, 28]. It is likely that low amounts of rDNA in the genome do not allow the genome with genetic abnormalities to be realized, and embryogenesis is interrupted at an early stage. Only five chromosomes in the human genome contain the rDNA encoding ribosomal RNA, of which the ribosome is assembled with the help of certain proteins. The ribosome provides molecular machinery for the synthesis of all proteins in our body [17, 29]. The very high rDNA content in the embryonic genome compared to maternal one also negatively affects embryogenesis. There are two possible explanations for this fact. First, high ribosome biogenesis levels resulting from the larger number of rDNA copies in the embryo's genome require a large amount of nutrients from the mother's body. If the maternal genome contains a low number of rDNA copies, it will not be able to fulfill the needs of the embryo. Second, genomes with the larger number of rDNA copies can contain mutations that block embryogenesis at the later stages, but allow for early embryo development. Genomes with low rDNA amounts and this genetic abnormality are rejected in early embryogenesis.

CONCLUSIONS

Determination of the *PSG8* (pregnancy-specific beta-1-glycoprotein 8), *PSG7* (putative pregnancy-specific beta-1-glycoprotein 7), *PSG6* (pregnancy-specific beta-1-glycoprotein 6), and *PSG4* (pregnancy-specific beta-1-glycoprotein 4) content be useful for prenatal prediction of pregnancy course. In most cases (16 surveyed individuals out of 20), frozen pregnancy is associated with the low rDNA content in the embryo's DNA relative to the control group (normal pregnancy). The low R parameter value shows that the cells are unable to ensure the ribosome biogenesis level appropriate for embryogenesis. Determination of specific proteins in the chorionic villi and rDNA copy number in the potential parents' genomes with subsequent modeling of the rDNA copy number in the embryo can help determine the cause of infertility in married couples and predict the ongoing pregnancy course.

References

1. Sidelnikova VM. Privychnaya poterya beremennosti. M.: Triada-H, 2002; 32 s. Russian.
2. Tarrade A, Lai Kuen R, Malassiné A, et al. Characterization of human villous and extravillous trophoblasts isolated from first trimester placenta. Lab Invest. 2001; 81 (9): 1199–211. Available from: https://doi.org/10.1038/labinvest.3780334.
3. Elguoshy A, Magdeldin S, Xu B, et al. Why are they missing? Bioinformatics characterization of missing human proteins. J Proteomics. 2016; 149: 7–14. Available from: https://doi.org/10.1016/j.jprot.2016.08.005.
4. Zhou L, Wong L, Wen Bin Goh W. Understanding missing proteins: a functional perspective. Drug Discov Today. 2018; 23 (3): 644–51. Available from: https://doi.org/10.1016/j.drudis.2017.11.011.
5. Malinovskaya E, Ershova E, Golimbet V, et al. Copy number of human ribosomal genes with aging: unchanged mean, but narrowed range and decreased variance in elderly group. Front Genet. 2018; 9: 306. Available from: https://doi.org/10.3389/fgene.2018.00306.
6. Lyapunova NA, Veiko NN. Ribosomnye geny v genome cheloveka: identifikaciya chetyrekh frakcij, ih lokalizaciya v yadryshke i metafaznyh hromosomah. Genetika. 2010; 46 (9): 1205–9.
7. Porohovnik LN, Egolina NA, Kosyakova NV, i dr. Zigoticheskij i embrional'nyj otbor po genomnoj doze aktivnyh ribosomnyh genov kak odin iz vozmozhnyh faktorov snizhennoj plodovitosti supruzheskih par. Medicinskaya genetika. 2012; 11 (6): 31–4. Russian.
8. Veiko N, Ershova E, Porokhovnik L, et al. Ribosomal, telomere, and mitochondrial repeat copy number variations in female genomes during ovarian stimulation and the prediction of in vitro fertilization outcome: a pilot study. Front Biosci (Schol Ed). 2023; 15 (3): 9. Available from: https://doi.org/10.31083/j.fbs1503009.
9. Shkrigunov T, Pogodin P, Zgoda V, et. al. Protocol for Increasing the Sensitivity of MS-Based Protein Detection in Human Chorionic Villi. Curr Issues Mol Biol. 2022; 44 (5): 2069–88. Available from:

https://doi.org/10.3390/cimb44050140.
10. Smith P, Krohn R, Hermanson G, et al. Measurement of Protein Using Bicinchoninic Acid Anal Biochem. 1985; 150 (1): 76–85. Available from: https://doi.org/10.1016/0003-2697(85)90442-7.
11. Shevchenko A, Tomas H, Havlis J, et al. In-gel digestion for mass spectrometric characterization of proteins and proteomes. Nat Protoc. 2006; 1 (6): 2856–60. Available from: https://doi.org/10.1038/nprot.2006.468.
12. Vaudel M, Barsnes H, Berven F, et al. SearchGUI: An open-source graphical user interface for simultaneous OMSSA and X!Tandem searches. Proteomics. 2011; 11 (5): 996–9. Available from: https://doi.org/10.1002/pmic.201000595.
13. Vaudel M, Burkhart J, Zahedi R, et al. PeptideShaker enables reanalysis of MS-derived proteomics data sets. Nat Biotechnol. 2015; 33 (1): 22–4. Available from: https://doi.org/10.1038/nbt.3109.
14. Neilson K, Keighley T, Pascovici D, et al. Label-free quantitative shotgun proteomics using normalized spectral abundance factors. Methods Mol Biol. 2013; 1002: 205–22. Available from: https://doi.org/10.1007/978-1-62703-360-2_17.
15. Godini R, Fallahi H. Dynamics changes in the transcription factors during early human embryonic development. J Cell Physiol. 2019; 234 (5): 6489–502. Available from: https://doi.org/10.1002/jcp.27386.
16. Porohovnik LN, Veiko NN, Ershova ES, i dr. Kopijnost' ribosomnoj DNK (rDNK) v genomah zhenshchin kak faktor uspeshnosti EKO i nalichiya oslozhnenij beremennosti. Medicinskaya genetika. 2019; 18 (11): 14–25. Available from: https://doi.org/10.25557/2073-7998.2019.11.14-25. Russian.
17. Liao C, Pang N, Liu Z, et al. Transient inhibition of rDNA transcription in donor cells improves ribosome biogenesis and preimplantation development of embryos derived from somatic cell nuclear transfer. FASEB J. 2020; 34 (6): 8283–95. Available from: https://doi.org/10.1096/fj.202000025RR.
18. Hammarström S. The carcinoembryonic antigen (CEA) family: structures, suggested functions and expression in normal and malignant tissues. Semin Cancer Biol. 1999; 9 (2): 67–81. Available from: https://doi.org/10.1006/scbi.1998.0119.
19. An Online Catalog of Human Genes and Genetic Disorders: PREGNANCY-SPECIFIC BETA-1-GLYCOPROTEIN 11; PSG11. Available from: https://omim.org/entry/176401.
20. Su X, Zhang J, Yang W, et al. Identification of the Prognosis-Related lncRNAs and Genes in Gastric Cancer. Front Genet. 2020; 11: 22. Available from: https://doi.org/10.3389/fgene.2020.00027.
21. Khan W, Hammarström S. Identification of a new carcinoembryonic antigen (CEA) family member in human fetal liver--cloning and sequence determination of pregnancy-specific glycoprotein 7. Biochem Biophys Res Commun. 1990; 168 (1): 214–25. Available from: https://doi.org/10.1016/0006-291x(90)91696-p.
22. Jamioł M, Wawrzykowski J, Mojsym W, et al. Activity of selected glycosidases and availability of their substrates in bovine placenta during pregnancy and parturition with and without retained foetal membranes. Reprod Domest Anim. 2020; 55 (9): 1093–102. Available from: https://doi.org/10.1111/rda.13747.
23. Sui L, An L, Tan K, et al. Dynamic Proteomic Profiles of In Vivo- and In Vitro-Produced Mouse Postimplantation Extraembryonic Tissues and Placentas. Biol Reprod. 2014; 91 (155): 1–16. Available from: https://doi.org/10.1095/biolreprod.114.124248.
24. Watanabe N, Kato T, Fujita A, et al. Cooperation between mDia1 and ROCK in Rho-induced actin reorganization. Nat Cell Biol. 1999; 1 (3): 136–43. Available from: https://doi.org/10.1038/11056.
25. Wirrig E, Snarr B, Chintalapudi M, et al. Cartilage link protein 1 (Crtl1), an extracellular matrix component playing an important role in heart development. Dev Biol. 2007; 310 (2): 291–303. Available from: https://doi.org/10.1016/j.ydbio.2007.07.041.
26. Veiko N, Ershova S, Veiko R, et al. Mild cognitive impairment is associated with low copy number of ribosomal genes in the genomes of elderly people. Front Genet. 2022; 13: 967448. Available from: https://doi.org/10.3389/fgene.2022.967448.
27. Ershova E, Malinovskaya E, Golimbet V, et al. Copy number variations of satellite III (1q12) and ribosomal repeats in health and schizophrenia. Schizophr Res. 2020; 223: 199–212. Available from: https://doi.org/10.1016/j.schres.2020.07.022.
28. Kondrateva E, Ershova E, Nikolaeva E, i dr. Rezul'taty izucheniya kompleksa ribosomnyh genov cheloveka pri mukoviscidoze. Pul'monologiya. 2023; 33 (1): 7–16. Available from: https://doi.org/10.18093/0869-0189-2023-33-1-7-16.
29. Sun Y, Hu X, Qiu D, et al. rDNA Transcription in Developmental Diseases and Stem Cells. Stem Cell Rev Rep. 2023; 19 (4): 839–52. Available from: https://doi.org/10.1007/s12015-023-10504-6.

Литература

1. Сидельникова В. М. Привычная потеря беременности. М.: Триада-Х, 2002; 32 с.
2. Tarrade A, Lai Kuen R, Malassiné A, et al. Characterization of human villous and extravillous trophoblasts isolated from first trimester placenta. Lab Invest. 2001; 81 (9): 1199–211. Available from: https://doi.org/10.1038/labinvest.3780334.
3. Elguoshy A, Magdeldin S, Xu B, et al. Why are they missing? Bioinformatics characterization of missing human proteins. J Proteomics. 2016; 149: 7–14. Available from: https://doi.org/10.1016/j.jprot.2016.08.005.
4. Zhou L, Wong L, Wen Bin Goh W. Understanding missing proteins: a functional perspective. Drug Discov Today. 2018; 23 (3): 644–51. Available from: https://doi.org/10.1016/j.drudis.2017.11.011.
5. Malinovskaya E, Ershova E, Golimbet V, et al. Copy number of human ribosomal genes with aging: unchanged mean, but narrowed range and decreased variance in elderly group. Front Genet. 2018; 9: 306. Available from: https://doi.org/10.3389/fgene.2018.00306.
6. Ляпунова Н. А., Вейко Н. Н. Рибосомные гены в геноме человека: идентификация четырех фракций, их локализация в ядрышке и метафазных хромосомах. Генетика. 2010; 46 (9): 1205–9.
7. Пороховник Л. Н., Еголина Н. А., Косякова Н. В., и др. Зиготический и эмбриональный отбор по геномной дозе активных рибосомных генов как один из возможных факторов сниженной плодовитости супружеских пар. Медицинская генетика. 2012; 11 (6): 31–4.
8. Veiko N, Ershova E, Porokhovnik L, et al. Ribosomal, telomere, and mitochondrial repeat copy number variations in female genomes during ovarian stimulation and the prediction of in vitro fertilization outcome: a pilot study. Front Biosci (Schol Ed). 2023; 15 (3): 9. Available from: https://doi.org/10.31083/j.fbs1503009.
9. Shkrigunov T, Pogodin P, Zgoda V, et. al. Protocol for Increasing the Sensitivity of MS-Based Protein Detection in Human Chorionic Villi. Curr Issues Mol Biol. 2022; 44 (5): 2069–88. Available from: https://doi.org/10.3390/cimb44050140.
10. Smith P, Krohn R, Hermanson G, et al. Measurement of Protein Using Bicinchoninic Acid Anal Biochem. 1985; 150 (1): 76–85. Available from: https://doi.org/10.1016/0003-2697(85)90442-7.
11. Shevchenko A, Tomas H, Havlis J, et al. In-gel digestion for mass spectrometric characterization of proteins and proteomes. Nat Protoc. 2006; 1 (6): 2856–60. Available from: https://doi.org/10.1038/nprot.2006.468.
12. Vaudel M, Barsnes H, Berven F, et al. SearchGUI: An open-source graphical user interface for simultaneous OMSSA and X!Tandem searches. Proteomics. 2011; 11 (5): 996–9. Available from: https://doi.org/10.1002/pmic.201000595.
13. Vaudel M, Burkhart J, Zahedi R, et al. PeptideShaker enables reanalysis of MS-derived proteomics data sets. Nat Biotechnol. 2015; 33 (1): 22–4. Available from: https://doi.org/10.1038/nbt.3109.
14. Neilson K, Keighley T, Pascovici D, et al. Label-free quantitative shotgun proteomics using normalized spectral abundance factors. Methods Mol Biol. 2013; 1002: 205–22. Available from: https://doi.org/10.1007/978-1-62703-360-2_17.
15. Godini R, Fallahi H. Dynamics changes in the transcription factors during early human embryonic development. J Cell Physiol. 2019; 234 (5): 6489–502. Available from: https://doi.org/10.1002/jcp.27386.
16. Пороховник Л. Н., Вейко Н. Н., Ершова Е. С., и др. Копийность рибосомной ДНК (рДНК) в геномах женщин как фактор успешности ЭКО и наличия осложнений беременности. Медицинская генетика. 2019; 18 (11): 14–25. Available from:

https://doi.org/10.25557/2073-7998.2019.11.14-25.
17. Liao C, Pang N, Liu Z, et al. Transient inhibition of rDNA transcription in donor cells improves ribosome biogenesis and preimplantation development of embryos derived from somatic cell nuclear transfer. FASEB J. 2020; 34 (6): 8283–95. Available from: https://doi.org/10.1096/fj.202000025RR.
18. Hammarström S. The carcinoembryonic antigen (CEA) family: structures, suggested functions and expression in normal and malignant tissues. Semin Cancer Biol. 1999; 9 (2): 67–81. Available from: https://doi.org/10.1006/scbi.1998.0119.
19. An Online Catalog of Human Genes and Genetic Disorders: PREGNANCY-SPECIFIC BETA-1-GLYCOPROTEIN 11; PSG11. Available from: https://omim.org/entry/176401.
20. Su X, Zhang J, Yang W, et al. Identification of the Prognosis-Related lncRNAs and Genes in Gastric Cancer. Front Genet. 2020; 11: 22. Available from: https://doi.org/10.3389/fgene.2020.00027.
21. Khan W, Hammarström S. Identification of a new carcinoembryonic antigen (CEA) family member in human fetal liver--cloning and sequence determination of pregnancy-specific glycoprotein 7. Biochem Biophys Res Commun. 1990; 168 (1): 214–25. Available from: https://doi.org/10.1016/0006-291x(90)91696-p.
22. Jamioł M, Wawrzykowski J, Mojsym W, et al. Activity of selected glycosidases and availability of their substrates in bovine placenta during pregnancy and parturition with and without retained foetal membranes. Reprod Domest Anim. 2020; 55 (9): 1093–102. Available from: https://doi.org/10.1111/rda.13747.
23. Sui L, An L, Tan K, et al. Dynamic Proteomic Profiles of In Vivo- and In Vitro-Produced Mouse Postimplantation Extraembryonic Tissues and Placentas. Biol Reprod. 2014; 91 (155): 1–16. Available from: https://doi.org/10.1095/biolreprod.114.124248.
24. Watanabe N, Kato T, Fujita A, et al. Cooperation between mDia1 and ROCK in Rho-induced actin reorganization. Nat Cell Biol. 1999; 1 (3): 136–43. Available from: https://doi.org/10.1038/11056.
25. Wirrig E, Snarr B, Chintalapudi M, et al. Cartilage link protein 1 (Crtl1), an extracellular matrix component playing an important role in heart development. Dev Biol. 2007; 310 (2): 291–303. Available from: https://doi.org/10.1016/j.ydbio.2007.07.041.
26. Veiko N, Ershova S, Veiko R, et al. Mild cognitive impairment is associated with low copy number of ribosomal genes in the genomes of elderly people. Front Genet. 2022; 13: 967448. Available from: https://doi.org/10.3389/fgene.2022.967448.
27. Ershova E, Malinovskaya E, Golimbet V, et al. Copy number variations of satellite III (1q12) and ribosomal repeats in health and schizophrenia. Schizophr Res. 2020; 223: 199–212. Available from: https://doi.org/10.1016/j.schres.2020.07.022.
28. Кондратьева Е., Ершова Е., Николаева Е., и др. Результаты изучения комплекса рибосомных генов человека при муковисцидозе. Пульмонология. 2023; 33 (1): 7–16. Available from: https://doi.org/10.18093/0869-0189-2023-33-1-7-16.
29. Sun Y, Hu X, Qiu D, et al. rDNA Transcription in Developmental Diseases and Stem Cells. Stem Cell Rev Rep. 2023; 19 (4): 839–52. Available from: https://doi.org/10.1007/s12015-023-10504-6.

CYP1A2 PHARMACOGENETIC MARKERS AS CLINICAL PREGNANCY PREDICTORS IN THE IN VITRO FERTILIZATION PROGRAMS FOR ANOVULATORY INFERTILITY

Lapshtaeva AV[1]✉, Sychev IV[2], Adamchik AI[3], Puzakova DV[1], Marmuleva VS[4], Sychev DA[2,5]

[1] National Research Mordovia State University, Saransk, Russia
[2] Petrovsky Russian Scientific Center of Surgery, Moscow, Russia
[3] Mordovian Republican Central Clinical Hospital, Saransk, Russia
[4] Ivanovo State Medical University, Ivanovo, Russia
[5] Russian Medical Academy of Continuous Professional Education, Moscow, Russia

Anovulatory infertility remains a significant medical and social issue requiring the development of new approaches to personalized patient management in assisted reproductive technology programs. Pharmacogenetic testing of hormone metabolism gene polymorphisms can contribute to optimization of ovarian stimulation protocols and higher in vitro fertilization (IVF) efficacy. The study aimed to assess a possible association of polymorphic variants of CYP isoenzyme genes (*CYP1A1, CYP1A2*, *CYP17A1*, *CYP19A1*) with the IVF program clinical efficacy in patients with anovulatory infertility. A total of 18 polymorphisms of the *CYP1A1*, *CYP1A2*, *CYP17A1*, and *CYP19A1* genes were analyzed by genotyping on the Illumina iScan platform. The *CYP1A2* T/T rs2470890 and A/A rs762551 genotype carrier state is associated with the increased likelihood of getting pregnant (OR = 3.824; 95% CI: 1.150–12.713, p = 0.023 and OR = 4.030; 95% CI: 1.372–11.839, p = 0.009, respectively). As for other studied polymoprhisms, including rs1048943, rs1800031, rs4646903, rs2606345 (gene *CYP1A1*), rs2069514 (gene *CYP1A2*), rs743572, rs104894136 (gene *CYP17A1*), rs10046, rs936306, rs700518, rs749292, rs1062033, rs2470152, rs28757157, rs6493497, rs7176005 (*CYP19A1*), no significant differences in the abundance of genotypes between comparison groups were revealed (p > 0.05). The pilot study data obtained suggest the potential role of the *CYP1A2* gene rs2470890 and rs762551 variants in modulation of the individual response to treatment and the IVF program efficacy in patients with anovulatory infertility.

Keywords: anovulatory infertility, in vitro fertilization, cytochrome P450, pharmacogenetics, *CYP1A2*, rs2470890, rs762551

Author contribution: Sychev DA, Lapshtaeva AV — study concept and design, study management, manuscript writing and approval; Sychev IV, Marmuleva VS — statistical analysis, database work; Puzakova DV — technical editing; Lapshtaeva AV, Adamchik AI, Puzakova DV — search for literature, manuscript writing; Lapshtaeva AV, Adamchik AI — clinical and biological material collection.

Compliance with ethical standards: the study was approved by the ethics committee of the National Research Ogarev Mordovia State University (protocol no. 116 dated 12 May 2023). All the subject submitted the informed consent to take part in the study.

✉ **Correspondence should be addressed:** Anna V. Lapshtaeva
Bolshevistskaya, 68, Saransk, 430005, Russia; av_lapshtaeva@mail.ru

Received: 25.12.2025 **Accepted:** 12.01.2026 **Published online:** 22.01.2026

DOI: 10.24075/brsmu.2026.001

Copyright: © 2026 by the authors. **Licensee:** Pirogov University. This article is an open access article distributed under the terms and conditions of the Creative Commons Attribution (CC BY) license (https://creativecommons.org/licenses/by/4.0/).

ФАРМАКОГЕНЕТИЧЕСКИЕ МАРКЕРЫ *CYP1A2* КАК ПРЕДИКТОРЫ КЛИНИЧЕСКОЙ БЕРЕМЕННОСТИ В ПРОГРАММАХ ЭКСТРАКОРПОРАЛЬНОГО ОПЛОДОТВОРЕНИЯ ПРИ АНОВУЛЯТОРНОМ БЕСПЛОДИИ

А. В. Лапштаева[1]✉, И. В. Сычев[2], А. И. Адамчик[3], Д. В. Пузакова[1], В. С. Мармулева[4], Д. А. Сычев[2,5]

[1] Национальный исследовательский Мордовский государственный университет имени Н. П. Огарёва, Саранск, Россия
[2] Российский научный центр хирургии имени Б. В. Петровского, Москва, Россия
[3] Мордовская республиканская центральная клиническая больница, Саранск, Россия
[4] Ивановский государственный медицинский университет, Иваново, Россия
[5] Российская медицинская академия непрерывного профессионального образования, Москва, Россия

Ановуляторное бесплодие остается значительной медико-социальной проблемой, требующей разработки новых подходов к персонализированному ведению пациентов в программах вспомогательных репродуктивных технологий. Фармакогенетическое тестирование полиморфизмов генов метаболизма гормонов может способствовать оптимизации протоколов овариальной стимуляции и повышению эффективности экстракорпорального оплодотворения (ЭКО). Целью исследования было оценить возможную ассоциацию между полиморфными вариантами генов изоферментов CYP (*CYP1A1*, *CYP1A2*, *CYP17A1*, *CYP19A1*) и клинической эффективностью программ ЭКО у пациенток с ановуляторным бесплодием. Проведен анализ 18 полиморфизмов генов *CYP1A1*, *CYP1A2*, *CYP17A1* и *CYP19A1* с использованием генотипирования на платформе Illumina iScan. Носительство генотипов T/T rs2470890 и A/A rs762551 гена *CYP1A2* ассоциировано с увеличением вероятности наступления беременности (OR = 3,824; 95% CI: 1,150–12,713, p = 0,023 и OR = 4,030; 95% CI: 1,372–11,839, p = 0,009 соответственно). Для остальных исследованных полиморфизмов, включая rs1048943, rs1800031, rs4646903, rs2606345 (ген *CYP1A1*), rs2069514 (ген *CYP1A2*), rs743572, rs104894136 (ген *CYP17A1*), rs10046, rs936306, rs700518, rs749292, rs1062033, rs2470152, rs28757157, rs6493497, rs7176005 (*CYP19A1*), статистически достоверных различий в частоте встречаемости генотипов между группами сравнения выявлено не было (p > 0,05). Полученные данные пилотного исследования указывают на потенциальную роль генетических вариантов гена *CYP1A2* rs2470890 и rs762551 в модуляции индивидуального ответа на терапию и эффективности программ ЭКО у пациенток с ановуляторным бесплодием.

Ключевые слова: ановуляторное бесплодие, экстракорпоральное оплодотворение, цитохром P450, фармакогенетика, *CYP1A2*, rs2470890, rs762551

Вклад авторов: Д. А. Сычев, А. В. Лапштаева — концепция и дизайн исследования, организация исследования, подготовка и утверждение рукописи; И. В. Сычев, В. С. Мармулева — статистический анализ, работа с базой данных; Д. В. Пузакова — техническое редактирование; А. В. Лапштаева, А. И. Адамчик, Д. В. Пузакова — поиск литературы, подготовка рукописи; А. В. Лапштаева, А. И. Адамчик — сбор клинического и биологического материала.

Соблюдение этических стандартов: исследование одобрено локальным этическим комитетом ФГБОУ ВО «МГУ им. Н. П. Огарева» (протокол № 116 от 12 мая 2023 г.). Все участники исследования подписали добровольное согласие на участие в исследовании.

✉ **Для корреспонденции:** Анна Васильевна Лапштаева
ул. Большевистская, д. 68, г. Саранск, 430005, Россия; av_lapshtaeva@mail.ru

Статья получена: 25.12.2025 **Статья принята к печати:** 12.01.2026 **Опубликована онлайн:** 22.01.2026

DOI: 10.24075/vrgmu.2026.001

Авторские права: © 2026 принадлежат авторам. **Лицензиат:** РНИМУ им. Н. И. Пирогова. Статья размещена в открытом доступе и распространяется на условиях лицензии Creative Commons Attribution (CC BY) (https://creativecommons.org/licenses/by/4.0/).

Anovulatory infertility representing a reproductive dysfunction resulting from the lack of ovulation occupies one of the leading positions in the structure of female infertility. Its relevance is due to not only high prevalence (which is 25–30% of all female infertility cases according to the data provided by different authors), but also complex pathogenesis, diversity of clinical forms and pronounced effects on the patient's overall health that are far beyond the reproductive dysfunction [1].

The disorder pathogenesis is multilevel and polyetiological. Regardless of the primary lesion severity (hypothalamus, pituitary gland, ovaries, or peripheral endocrine glands), the pathological cascade finally results in the deep disintegration of the hypothalamic-pituitary-ovarian axis leading to the impaired dominant follicle growth, dominance, and rupture. The basis is dysregulation of the gonadotropin-releasing hormone (GnRH) secretion circadian rhythm, which entails impaired synthesis and pulsatile secretion of the follicle-stimulating hormone (FSH) and luteinizing hormone and, therefore, blocked folliculogenesis and ovulation [1, 2].

Etiotropic therapy for anovulatory infertility is aimed at restoring the ovulatory function of the ovaries by the hormonal stimulation classified into indirect (anti-estrogen) and direct (gonadotropic) based on the application point. However, despite the existence of effective controlled ovarian stimulation protocols, there are still serious problems related to not only treatment resistance, high risk of complications, such as ovarian hyperstimulation syndrome and multiple pregnancy, but also psychological discomfort in the patient and her partner due to the treatment protocol duration and cyclical nature [3–5].

The today's reproductive medicine pays considerable attention to the search for genetic markers allowing one to predict the response to ovulation stimulation and the IVF program efficacy. In the context of anovulatory infertility, genetic studies are focused on polymorphisms of the genes involved in regulation of folliculogenesis, steroidogenesis, insulin metabolism, and gonadotropin sensitivity [6–8].

Biotransformation of a significant number of endogenous steroids, xenobiotics, and drugs is mediated by the cytochrome P450 (CYP) family enzymes classified as heme-based monooxygenases [9]. In the reproductive function regulation process, a special role is given to the CYP isoforms that are localized in the steroid-producing tissues: adrenal cortex, ovaries, and placenta. The main function of estradiol 2-hydroxylation in the liver is implemented by the CYP1A2 isoform, while in the extrahepatic tissues similar catalytic activity is shown by CYP1A1 [10–12]. CYP17A1 (17α-hydroxylase/17,20-lyase) is the key enzyme catalyzing two successive phases: 17-α-hydroxylation of progesterone and pregnenolone and the side chain cleavage (17,20-lyase activity) yielding androgens (dehydroepiandrosterone and androstenedione). CYP19A1 (aromatase) catalyzes the conversion of androgens (testosterone and androstenedione) into estrogens (estradiol and estrone) [13]. Abnormal functioning of specific isoforms leads to profound steroidogenesis dysfunction manifested by either deficiency of estrogens necessary for ovulation, or excess androgens, which block the follicle growth and maturation.

High CYP enzyme genetic polymorphism rate results in a broad spectrum of enzyme activity alterations, which have a significant effect on the xenobiotic metabolism, risk of side effects and regulation of physiological processes [14, 15]. The authors had earlier identified the associations of some CYP polymorphisms allowing one to predict the response to ovulation stimulation and the IVF efficacy [16, 17].

The study aimed to assess a possible association of polymorphic variants of the CYP isoenzyme genes (*CYP1A1*, *CYP1A2*, *CYP17A1*, *CYP19A1*) with the IVF program clinical efficacy in patients with anovulatory infertility.

METHODS

The study involved 176 females diagnosed with anovulatory infertility (ICD-10 code N97) in accordance with the criteria of European and Russian clinical guidelines. These patients requested an IVF program at the assisted reproductive technology department of the Perinatal Center, Mordovian Republican Central Clinical Hospital (Saransk), between May 2023 and December 2024. All the study participants were in their early fertile age, 25–35 years (29.4 ± 3.7 years); they were of Caucasian origin, were born and lived in the Volga Federal District of Russia. All the patients were through the IVF program, involving the use of their own oocytes and embryo transfer; the program involved the use of the GnRH antagonists (subcutaneous ganirelix, cetrorelix 0.25 mg/day), recombinant gonadotropins (subcutaneous follitropin alfa, starting dose 150–225 IU/day with subsequent adjustment), and choriogonadotropin alfa (subcutaneous ovitrelle 250 μg) within the framework of the short superovulation stimulation protocol. The prescribed assessment and treatment were conducted in accordance with the National clinical guidelines on treatment of female infertility and assisted reproductive technology/intrauterine insemination.

A total of 60 women were selected for enrollment based on the inclusion criteria. Inclusion criteria: women aged 25–35 years; infertility due to the lack of ovulation; normal ovarian reserve; no endometrial abnormality based on the ultrasonography, hysteroscopy data; normal karyotype in both partners. Exclusion criteria: extragenital and genital abnormalities, due to which there were contraindications for the basic IVF program; patient's voluntary refusal to take part in the study at any stage.

The fact of getting pregnant (pregnancy was diagnosed by determining serum concentrations of the human chorionic gonadotropin β-subunit 14 days after the embryo transfer to the uterine cavity) was considered as a major outcome in the women assessed; the test was considered to be positive, when the levels were above 30 IU/L (biochemical pregnancy). Ultrasonographic diagnosis of clinical pregnancy to determine the number of fertilized eggs in the uterine cavity was performed 21 days after the embryo transfer. On day 31, physicians of appropriate specialty performed ultrasonography in order to detect fetal heartbeat. Women were divided into groups based on the major IVF program outcome considering their enthicity, demographic and medical history data: group 1 (index group) consisted of women, who got pregnant after one try and had no history of IVF attempts (n = 30); group 2 (comparison group), who failed to get pregnant and had a history of three unsiccessful IVF attempts (n = 30).

On the day of enrollment, each patient underwent additional venous blood collection: 6 mL of blood were collected by venipuncture from the cubital vein in the morning in the fasting state into the disposable sterile EDTA vacuum tube for further genotyping. Biomaterial was frozen at a temperature of –20 °C, transported to the laboratory, and then stored at –70 °C. DNA was isolated from blood using a magnetic sorbent and reagents by Genotek (Russia) in the Allsheng Auto-Pure 96 system (China). When performing the whole-genome testing, sample preparation and scanning were accomplished using the iScan system (Illumina, USA) in accordance with the Infinium HTS Assay Guide protocol [18]. The Infinium Global Screening Array-24 v3.0 kit was used (USA). In this study a total of

18 single nucleotide polymorphisms (SNPs) were analyzed, which, in the authors' opinion developed based on the literature review, could have predictive potential: rs1048943, rs1800031, rs2606345, rs4646903 (*CYP1A1*), rs762551, rs2069514, rs2470890 (*CYP1A2*), rs743572, rs104894136 (*CYP17A1*), rs10046, rs936306, rs700518, rs749292, rs1062033, rs2470152, rs28757157, rs6493497, rs7176005 (*CYP19A1*).

Statistical data processing was performed using the StatSoft Statistica 12.5 software package. The quantitative trait distribution was tested for normality using the Shapiro–Wilk test. The normally distributed quantitative indicators were presented as the mean and standard deviation (M (±SD). Comparison of two independent groups based on quantitative traits was performed using the Student's *t*-test. Qualitative traits (genotype and allele frequencies) were compared using the Pearson's chi-squared test (χ^2) or Fischer's exact test (when the expected frequencies in the contingency table cells were below 5). The genotype distribution consistency with the Hardy–Weinberg principle (HWE) was tested in the control group using the χ^2 test. The strength of associations between genotypes and the IVF program outcomes was assessed by calculating the odds ratio (OR) and 95% confidence interval (95% CI). When testing statistical hypotheses, the critical significance level (p) was set at 0.05. Considering the limited sample size (n = 60) and the need to exclude false positives typical for asymptotic tests (chi-squared test), significance of the associations revealed was verified using the permutation test. The Monte Carlo permutation test involving generation of 10,000 random phenotype permutations with the preserved genotype-based structure of the sample was used. This approach is considered to be a gold standard of genetic testing in small samples, since it does not depend on the data distribution pattern and allows one to accurately calculate the error probability empirical value (p-perm). The empirical levels $p < 0.05$ were considered significant.

RESULTS

The groups were matched for age, infertility duration, fact of having obesity, basal FSH and estradiol levels, anti-Müllerian hormone (AMH) levels, and the number of antral follicles ($p > 0.05$) (Table 1). We believe that the differences in the response to ovulation stimulation and IVF efficacy can be due to genetic differences in *CYP1A1*, *CYP1A2*, *CYP17A1*, *CYP19A1*.

Comparative analysis of the distribution of frequencies of genotypes with polymorphisms of these genes in the groups of patients with beneficial and adverse IVF outcomes revealed polymorphic variants significantly correlated to the successful implantation and the fact of getting pregnant (Table 2). The distribution of genotypes in the control group was compliant with the Hardy–Weinberg equilibrium ($p > 0.05$)

Thus, in the *CYP1A2* gene, the rs2470890 polymorphism T/T genotype carrier state is associated with the 3.8-fold increased likelihood of successful IVF (OR = 3.824; 95% CI: 1.150–12.713, p = 0.023). In contrast, the C/C genotype was far less abundant in the group with beneficial outcomes, representing the risk factor of unsuccessful attempts (OR = 0.167; 95% CI: 0.033–0.853, p = 0.016). We also determined a significant association between the *CYP1A2* rs762551 polymorphism A/A genotype and positive IVF outcomes: the genotype carrier state increases the likelihood of getting pregnant 4-fold (OR = 4.030; 95% CI: 1.372–11.839, p = 0.009) relative to the carrier state for other genotypes. At the same time, the C/C genotype of this locus showed a downward trend of frequency in the group with beneficial outcomes (OR = 0.167; 95% CI: 0.033–0.853, p = 0.016), which can indicate its unfavorable prognostic value.

As for other studied polymorphisms, including rs1048943, rs4646903, rs2606345 (gene *CYP1A1*), rs2069514 (gene *CYP1A2*), rs743572 (gene *CYP17A1*), and a number of loci of the gene *CYP19A1* (rs936306, rs28757157, rs749292, rs10046, rs700518, rs1062033, rs2470152, rs6493497, rs7176005), no significant differences in the abundance of genotypes between comparison groups were revealed ($p > 0.05$). As for polymorphisms rs1800031 (gene *CYP1A1*) and rs104894136 (gene *CYP17A1*), associations could not be analyzed due to the sample monomorphism.

Primary analysis involving the use of standard parametric tests revealed significant differences in the distribution of genotypes across the *CYP1A2* loci. To confirm the fact that the results were resistant to the small sample effect, a permutation test was performed. For the rs762551 polymorphism (genotype A/A), the empirical significance value obtained based on the 10,000 resampling, confirmed the non-random nature of the association (p-perm = 0.012, OR = 4.03). A similar result was reported for the rs2470890 polymorphism (genotype T/T): the empirical p-value also retained statistical significance (p-perm = 0.025, OR = 3.82). Thus, the use of permutation analysis confirmed the fact that high likelihood of getting pregnant in carriers of these genotypes is not a statistical "artifact" associated with the sample size, but reflects a real biological pattern.

DISCUSSION

In this study, to assess possible associations of polymorphic variants of the cytochrome P450 isoenzyme-encoding genes (*CYP1A1*, *CYP1A2*, *CYP17A1*, *CYP19A1*) with the IVF program clinical efficacy in patients with anovulatory infertility, the analysis of the distribution of frequencies of 18 SNP genotypes was conducted. The data obtained suggest that two polymorphisms are associated with beneficial IVF program outcomes: rs2470890 and rs762551.

The two SNPs located in the intronic region of the gene *CYP1A2* encoding the enzyme that is responsible for 2-hydroxylation of estradiol in the liver can alter the activity of CYP1A2, which affects the estrogen metabolism, thereby affecting the women's responsiveness to ovarian stimulation in IVF programs. The rs2470890 and rs762551 association with the CYP1A2 protein expression was illustrated by other estrogen-dependent conditions [12, 19]. The A allele of the rs762551 polymorphism (*CYP1A2*) is associated with the increased enzyme inducibility and, therefore, with the higher rate of the estrogen and xenobiotic metabolism [20].

At first glance, the accelerated estradiol metabolism can be considered as a negative factor reducing the hormone levels. However, in the context of controlled ovarian stimulation, during which estradiol levels often reach supraphysiological values, high CYP1A2 activity can play a protective role. We assume that the effective estrogen biotransformation reported in carriers of the rs762551 (A/A) and rs2470890 (T/T) genotypes prevents the endometrium overexposure to high doses of exogenous and endogenous hormones. There is evidence that excess estradiol can reduce endometrial receptivity and disrupt synchronizarion of the embryo development and endometrial readiness, thereby shifting the "implantation window" [21–23].

The controlled ovarian stimulation protocol that precedes IVF is based on administration of supraphysiological exogenous gonadotropin doses aimed at inducing multiple folliculogenesis. Multifollicular development results in hypersecretion of estradiol,

Table 1. Major diagnostic criteria of the surveyed women's ovulatory potential

Indicators	Group 1 (n = 30)	Group 2 (n = 30)	χ^2	p
Age				
25–30	43.3% (13 individuals)	50% (15 individuals)	0,268	0.605
31–35	56.7% (17 individuals)	50% (15 individuals)		
Obesity				
Yes	23.3% (7 individuals)	40% (12 individuals)	1,926	0.166
No	76.7% (23 individuals)	60% (18 individuals)		
AMH				
Below 1.0 ng/mL	13.3% (4 individuals)	40% (9 individuals)	–	0.114*
1.0–3.5 ng/mL	73.4% (22 individuals)	60% (18 individuals)	1,274	0.274
Over 3.5 ng/mL	13.3% (4 individuals)	10% (3 individuals)	–	0.688*
Basal FSH				
Below 10 IU/L	50% (15 individuals)	43,3% (13 individuals)	0,268	0.605
Over 10 IU/L	50% (15 individuals)	56,7% (17 individuals)		
Basal estradiol				
Below 40 pg/mL	63.3% (19 individuals)	70% (21 individuals)	0,300	0.584
Over 40 pg/mL	36.7% (11 individuals)	30% (9 individuals)		
Antral follicle counts				
Below 5	–	10% (3 individuals)	–	–**
5–12	80% (24 individuals)	80% (24 individuals)	0	1000
Over 12	20% (6 individuals)	10% (3 individuals)	–	0.275*

Note: * — p is compliant with Fischer's exact test; ** — not calculated due to the lack of cases in one of the groups.

the levels of which are significantly higher than the natural ovarian cycle indicators. The resulting excessive steroid load has a modulatory effect on the endometrial maturation, causing the "implantation window" shift. The phenomenon pathogenesis is based on the complex of structural, transcriptional, and immunoregulatory changes in the endometrium, which eventually determines its receptive status [22].

At the molecular level, supraphysiological estradiol concentrations induced by ovarian stimulation has a modulatory effect on the transcriptome activity of the genes associated with endometrial receptivity. Suppression of the progesterone receptor expression accompanied by dysregulation of the genes that are cucial for successful embryo implantation, such as Cox1, Lif, Ptgs2, and Hegfl, is reported as one of the key mechanisms [24–26]. Furthermore, hyperestrogenism typical for the stimulated cycle results in suppression of expression of the Hoxa11 and Cdh1 factors, which also adversely affects the endometrium receptive properties. In parallel, the impaired spatiotemporal expression of the estrogen and progesterone receptors is observed, which suggests systemic alteration of the endocrine signaling in the endometrium under the exposure to exogenous gonadotropins [23, 27].

Thus, the genetically determined active metabolism can contribute to maintaining the hormonal balance more favorable in terms of the embryo implantation, which is in line with the clinical results we have obtained.

The lack of significant differences in the distribution of genotypes across the groups of women, who got pregnant and failed to get pregnant, for the *CYP17A1* and *CYP19A1* steroidogenesis genes can indicate that in the context of exogenous gonadotropin stimulation the one's own estrogen production variability the plays a less important role, than their systemic metabolism and CYP1A2-mediated clearance.

This study has a number of limitations. First, these are related to the small sample size (n = 60), which is typical for pilot projects. It is well known, that genetic testing in small groups is associated with the risk of false positives (type I error). However, the permutation testing method we have used (10,000 permutations) allows one to reliably filter out random findings. The fact that the associations of the *CYP1A2* polymorphism (rs762551 and rs2470890) were still significant when applying the permutation control, in combination with the high odds ratio (OR > 3.8), suggests reliability of the data obtained, regardless of the pilot study design limitations. Second, the impact of the concomitant therapy and other clinical factors potentially modulating the effect of the drugs used for controlled ovarian stimulation was not assessed in this study. Nevertheless, the patterns revealed (high odds ratio: OR > 3.0) suggest a significant clinical effect of the studied loci.

The data obtained justify the feasibility of further research focused on the *CYP1A2* polymorphisms as potential biomarkers for IVF protocol personalization.

CONCLUSIONS

The pilot study conducted revealed significant associations between the *CYP1A2* gene polymorphisms and IVF outcomes in women with anovulatory infertility. The data obtained suggest that the CYP1A2 rs2470890 T/T homozygous genotype and rs762551 A/A homozygous genotype carrier state is associated with the more than 3-fold increased chance of getting pregnant after IVF (OR = 3.824 and OR = 4.030, respectively). These associations that reach the statistical significance level (p = 0.023 and p = 0.009) are characterized by relatively narrow confidence intervals, which indicates sufficient reliability of the patterns revealed in the current sample.

The lack of significant differences in the distribution of genotypes across other 16 studied polymorphisms of the cytochrome P450 family genes (*CYP1A1*, *CYP17A1* и *CYP19A1*) does not eliminate their potential role in regulation of the endocrine processes coupled with the controlled ovarian stimulation. It is likely that the influence of these polymorphisms

Table 2. Distribution of some polymorphisms of the CYP system genes in women with anovulatory infertility

Gene	Polymorphism	Genotypes	Group 1 ($n = 30$)	Group 2 ($n = 30$)	χ^2 (chi-squared test)	OR	95% CI	p
CYP1A1	rs1048943	T/T	28	28	0	–	–	1.00
		T/C	2	2		–	–	
	rs1800031	A/A	30	30	–	–	–	–
	rs4646903	A/A	25	26	–	0.769	0.185–3.198	0.718**
		A/G	5	4		1.300	0.313–5.404	
	rs2606345	A/A	16	19	0.617	0.662	0.236–1.858	0.433
		C/A	12	9	0.659	1.556	0.534–4.532	0.417
		C/C	2	2	0	–*	–	1.00
CYP1A2	rs2470890	C/C	2	9	–	0.167	0.033–0.853	0.016**
		C/T	15	16	0.067	0.875	0.318–2.410	0.797
		T/T	13	5	5.079	3.824	1.150–12.713	0.023
	rs2069514	G/G	28	29	–	–*	–	0.50**
		G/A	2	1		–*	–	
	rs762551	A/A	19	9	6.696	4.030	1.372–11.839	0.009
		C/A	9	12	0.659	0.643	0.211–1.873	0.417
		C/C	2	9	–	0.167	0.033–0.853	0.016**
CYP17A1	rs743572	G/G	6	9	0.800	0.583	0.178–1.913	0.372
		G/A	15	14	0.067	1.143	0.415–3.148	0.797
		A/A	9	7	0.341	1.408	0.445–4.453	0.560
	rs104894136	G/G	30	30	–	–	–	–
CYP19A1	rs10046	A/A	10	9	0.077	1.167	0.393–3.467	0.782
		A/G	14	14	0	–	–	1.00
		G/G	6	7	0.098	0.821	0.240–2.814	0.755
	rs936306	C/C	16	15	0.067	1.143	0.415–3.148	0.797
		T/T	4	2	–	2.154	0.363–12.764	0.386**
		T/C	10	13	0.635	0.654	0.229–1.864	0.426
	rs700518	C/C	10	9	0.077	1.167	0.393–3.467	0.782
		T/T	7	7	0	–	–	1.000
		T/C	13	14	0.067	0.874	0.316–2.418	0.796
	rs749292	A/A	6	10	1.364	0.500	0.155–1.616	0.243
		G/A	15	11	1.086	1.147	0.411–3.204	0.298
		G/G	9	9	0	–	–	1.000
	rs1062033	C/C	8	7	0.089	1.195	0.371–3.853	0.766
		G/C	13	12	0.069	1.147	0.411–3.204	0.794
		G/G	9	11	0.300	0.740	0.252–2.175	0.584
	rs2470152	A/A	8	6	0.373	1.455	0.435–4.860	0.542
		G/A	16	14	0.267	1.306	0.474–3.602	0.606
		G/G	6	10	1.364	0.500	0.155–1.616	0.243
	rs28757157	C/C	19	21	0.300	0.740	0.252–2.175	0.584
		T/T	3	3	0	–	–	1 000
		T/C	8	6	0.373	1.455	0.435–4.860	0.542
	rs6493497	G/G	21	20	0.077	1.167	0.393–3.467	0.782
		G/A	9	10		0.857	0.228–2.547	
	rs7176005	C/C	21	20	0.077	1.167	0.393–3.467	0.782
		C/T	9	10		0.857	0.228–2.547	

Note: * — not calculated due to the lack of cases in one of the groups или of the critically low number of observations; ** — p is compliant with Fischer's exact test.

on IVF outcomes is either of more complex nature requiring the analysis of genotype-genotype interactions, or is manifested at the level of other mechanisms not covered by simple association analysis.

The reported association of *CYP1A2* polymorphisms with the IVF success can result from the crucial role of this enzyme in metabolism of estrogens and other hormonal substrates that determine the effectiveness of ovarian stimulation. The differences in the CYP1A2 enzyme activity depending on the genotype can affect the circulating hormone levels, oocyte quality, and endometrial receptivity, being valuable predictors of the assisted reproductive technology success.

The data obtained open the prospects for the development of molecular genetic tests allowing for preliminary patient stratification based on the IVF success likelyhood. Integration of the information about *CYP1A2* genotypes into predictive models might contribute to personalization of the controlled ovarian stimulation protocols, gonadotropin dosing optimization, and improvement of the assisted reproductive technology efficacy. However, the *CYP1A2* genotyping introduction into clinical practice requires additional prospective trials, pharmacogenetic analysis, and the development of evidence-based clinical guidelines.

Thus, the study representing an important step towards understanding the fertility molecular genetic underpinnings can provide the basis for the development of innovative approaches to personalized management of patients with unovulatory infertility in the assisted reproductive technology programs.

References

1. Anvarova ShA, Shukurov FI, Tulametova ShA. Innovacionnye metody reshenija problemy zhenskogo besplodija, associirovannogo s jendokrinnymi narushenijami. Akusherstvo, ginekologija i reprodukcija. 2024; 18 (5): 706–19. DOI: 10.17749/2313-7347/ob.gyn.rep.2024.514.
2. Chervonnova NA, Jahina AJu, Baryshnikova EV, Jahin DI, Jamashkina EI. Funkcija jendokrinnoj sistemy u zhenshhin s besplodiem. Medicinskij alfavit. 2024; 19: 38–42. DOI: 10.33667/2078-5631-2024-19-38-42.
3. Ammar IMM, Abdou AM. Effect of Ubiquinol supplementation on ovulation induction in Clomiphene Citrate resistance. Middle East Fertil Soc J. 2021; 26 (22). DOI: 10.1186/s43043-021-00070-7.
4. Ganer Herman H, Mizrachi Y, Horowitz E, Weissman A, Sabban B, Gluck O, et al. Obstetric outcomes following ovarian hyperstimulation syndrome in IVF — a comparison with uncomplicated fresh and frozen transfer cycles. BMC Pregnancy Childbirth. 2022; 22 (22): 573. DOI: 10.1186/s12884-022-04903-9.
5. Liu S, Mo M, Xiao S, Li L, Hu X, Hong L, et al. Pregnancy outcomes of women with polycystic ovary syndrome for the first in vitro fertilization treatment: a retrospective cohort study with 7678 patients. Front. Endocrinol. 2020; 11. DOI: 10.3389/fendo.2020.575337.
6. Conforti A, Santi D, Allegra A, Mignini Renzini M, Marino A, Brigante C, et al. Impact of gonadotropin genetic profile and ovarian reserve on controlled ovarian stimulation: data from prospective cohort of the GENOCS trial. Front Endocrinol (Lausanne). 2025; 22 (16). DOI: 10.3389/fendo.2025.1601803.
7. Xu Y, Zhang Z, Wang R, Xue S, Ying Q, Jin L. Roles of estrogen and its receptors in polycystic ovary syndrome. Front Cell Dev Biol. 2024; 19 (12). DOI: 10.3389/fcell.2024.1395331. PMID: 38961865; PMCID: PMC11219844.
8. Lysova AN, Hamoshina MB, Zarubina EG. Geneticheskie aspekty anovuljatornogo besplodija. Vestnik novyh medicinskih tehnologij. 2025; 32 (1): 102–6. DOI: 10.24412/1609-2163-2025-1-102-106.
9. Yang S, Wang L, Wu J, Liu T, Pei S, Zhou Q, et al. Recent Advances in Structure, Biofunction, Detection, and Disease Therapeutic Targeting of Cytochrome P450. Chembiochem. 2025; 26 (14): e202500278. DOI: 10.1002/cbic.202500278.
10. You Y, Huang J, Zhu X, Sheng H, Liu Y. Cytochrome P450 (CYP) 1 enzymes in acute lung injury: from molecular insights to therapeutic implications. Redox Rep. 2025; 30 (1): 2550807. DOI: 10.1080/13510002.2025.2550807.
11. Chagaj NB, Mkrtumjan AM. Metabolizm jestrogenov, prizhiznennye narushenija processov metilirovanija i rak molochnoj zhelezy. Problemy jendokrinologii. 2019; 65 (3): 161–73.
12. Bai X, Xie J, Sun S, Zhang X, Jiang Y, Pang D. The associations of genetic polymorphisms in CYP1A2 and CYP3A4 with clinical outcomes of breast cancer patients in northern China. Oncotarget. 2017; 8 (24): 38367-38377. DOI: 10.18632/oncotarget.16359.
13. Heidarzadehpilehrood R, Pirhoushiaran M, Abdollahzadeh R, Binti Osman M, Sakinah M, Nordin N, et al. A Review on CYP11A1, CYP17A1, and CYP19A1 Polymorphism Studies: Candidate Susceptibility Genes for Polycystic Ovary Syndrome (PCOS) and Infertility. Genes (Basel). 2022; 13 (2): 302. DOI: 10.3390/genes13020302.
14. Mondal S, Shrivastava P, Mehra R. Computing pathogenicity of mutations in human cytochrome P450 superfamily. Biochim Biophys Acta Proteins Proteom. 2025; 1873 (4): 141078. DOI: 10.1016/j.bbapap.2025.141078.
15. Esteves F, Rueff J, Kranendonk M. The central role of cytochrome P450 in xenobiotic metabolism — a brief review on a fascinating enzyme family. J Xenobiot. 2021; 11 (3): 94–114. DOI: 10.3390/jox11030007.
16. Lazaros LA, Hatzi EG, Xita NV, Makrydimas GV, Kaponis AI, Takenaka A, et al. Aromatase (CYP19) gene variants influence ovarian response to standard gonadotrophin stimulation. J Assist Reprod Genet. 2012; 29 (2): 203–209. DOI: 10.1007/s10815-011-9673-y.
17. Song D, Huang XL, Hong L, Yu JM, Zhang ZF, Zhang HQ, et al. Sequence variants in FSHR and CYP19A1 genes and the ovarian response to controlled ovarian stimulation. Fertil Steril. 2019; 112 (4): 749–757. DOI: 10.1016/j.fertnstert.2019.05.017.
18. ILLUMINA. Infinium HTS Assay: Reference Guide. Document # 15045738 v04. November 2019. Режим доступа: https://support.illumina.com/content/dam/illumina-support/documents/documentation/chemistry_documentation/infinium_assays/infinium-hts/infinium-hts-assay-reference-guide-15045738-04.pdf (дата обращения: 22.12.2025).
19. Kublinskij KS, Novickij VV, Urazova OI. Allel'nyj polimorfizm genov fermentov metabolizma jestrogenov pri genital'nom jendometrioze. Patogenez. 2015; 13 (3): 41–44.
20. Alalawy AI, Sakran MI, Alzuaibr FM, Alotaibi MA, Elshazli RM. Unraveling the molecular significance of CYP1A2 (rs762551; c.-9-154 C>A) genetic variant on breast carcinoma susceptibility: Insights from case-control study and meta-analysis. Pathol Res Pract. 2024; 261: 155501. DOI: 10.1016/j.prp.2024.155501.
21. Parisi F, Fenizia C, Introini A, Zavatta A, Scaccabarozzi C, Biasin M, et al. The pathophysiological role of estrogens in the initial stages of pregnancy: molecular mechanisms and clinical implications for pregnancy outcome from the periconceptional period to end of the first trimester. Hum Reprod Update. 2023; 29 (2): 699–720. DOI: 10.1093/humupd/dmad016.
22. Bourdon M, Maignien C, Ouazana M, Kefelian F, Marcellin L, Patrat C, et al. Oestradiol and reproductive outcomes in ART: when too much of a good thing hurts. Reprod Biomed Online. 2025; 51 (6): 105131. DOI: 10.1016/j.rbmo.2025.105131.
23. Ojosnegros S, Seriola A, Godeau AL, Veiga A. Embryo implantation in the laboratory: an update on current techniques. Hum Reprod Update. 2021; 27 (3): 501–530. DOI :10.1093/humupd/dmaa054
24. Ma WG, Song H, Das SK, Paria BC, Dey SK. Estrogen is a critical determinant that specifies the duration of the window of uterine receptivity for implantation. Proc Natl Acad Sci USA. 2003; 100 (5): 2963–8. DOI:10.1073/pnas.0530162100 (2003).
25. Simon C, Domínguez F, Valbuena D, Pellicer A. The role of estrogen in uterine receptivity and blastocyst implantation. Trends Endocrinol Metab. 2003; 14 (5): 197–9. DOI: 10.1016/s1043-2760(03)00084-5.
26. Muter J, Lynch VJ, McCoy RC, Brosens JJ. Human embryo implantation. Development. 2023; 150 (10): dev201507. DOI: 10.1242/dev.201507.
27. Ezoe K, Daikoku T, Yabuuchi A, Murata N, Kawano H, Abe T, et al. Ovarian stimulation using human chorionic gonadotrophin impairs blastocyst implantation and decidualization by altering ovarian hormone levels and downstream signaling in mice. Mol Hum Reprod. 2014; 20 (11): 1101–16. DOI:10.1093/molehr/gau065.

Литература

1. Анварова Ш. А., Шукуров Ф. И., Туламетова Ш.А. Инновационные методы решения проблемы женского бесплодия, ассоциированного с эндокринными нарушениями. Акушерство, гинекология и репродукция. 2024; 18 (5): 706–719. DOI: 10.17749/2313-7347/ob.gyn.rep.2024.514.
2. Червоннова Н. А., Яхина А. Ю., Барышникова Е. В., Яхин Д. И., Ямашкина Е. И. Функция эндокринной системы у женщин с бесплодием. Медицинский алфавит. 2024; 19: 38–42. DOI: 10.33667/2078-5631-2024-19-38-42.
3. Ammar IMM, Abdou AM. Effect of Ubiquinol supplementation on ovulation induction in Clomiphene Citrate resistance. Middle East Fertil Soc J. 2021; 26 (22). DOI: 10.1186/s43043-021-00070-7.
4. Ganer Herman H, Mizrachi Y, Horowitz E, Weissman A, Sabban B, Gluck O, et al. Obstetric outcomes following ovarian hyperstimulation syndrome in IVF — a comparison with uncomplicated fresh and frozen transfer cycles. BMC Pregnancy Childbirth. 2022; 22 (22): 573. DOI: 10.1186/s12884-022-04903-9.
5. Liu S, Mo M, Xiao S, Li L, Hu X, Hong L, et al. Pregnancy outcomes of women with polycystic ovary syndrome for the first in vitro fertilization treatment: a retrospective cohort study with 7678 patients. Front. Endocrinol. 2020; 11. DOI: 10.3389/fendo.2020.575337.
6. Conforti A, Santi D, Allegra A, Mignini Renzini M, Marino A, Brigante C, et al. Impact of gonadotropin genetic profile and ovarian reserve on controlled ovarian stimulation: data from prospective cohort of the GENOCS trial. Front Endocrinol (Lausanne). 2025; 22 (16). DOI: 10.3389/fendo.2025.1601803.
7. Xu Y, Zhang Z, Wang R, Xue S, Ying Q, Jin L. Roles of estrogen and its receptors in polycystic ovary syndrome. Front Cell Dev Biol. 2024; 19 (12). DOI: 10.3389/fcell.2024.1395331. PMID: 38961865; PMCID: PMC11219844.
8. Лысова А. Н., Хамошина М. Б., Зарубина Е. Г. Генетические аспекты ановуляторного бесплодия. Вестник новых медицинских технологий. 2025; 32 (1): 102–106. DOI: 10.24412/1609-2163-2025-1-102-106.
9. Yang S, Wang L, Wu J, Liu T, Pei S, Zhou Q, et al. Recent Advances in Structure, Biofunction, Detection, and Disease Therapeutic Targeting of Cytochrome P450. Chembiochem. 2025; 26 (14): e202500278. DOI: 10.1002/cbic.202500278.
10. You Y, Huang J, Zhu X, Sheng H, Liu Y. Cytochrome P450 (CYP) 1 enzymes in acute lung injury: from molecular insights to therapeutic implications. Redox Rep. 2025; 30 (1): 2550807. DOI: 10.1080/13510002.2025.2550807.
11. Чагай Н. Б., Мкртумян А. М. Метаболизм эстрогенов, прижизненные нарушения процессов метилирования и рак молочной железы. Проблемы эндокринологии. 2019; 65 (3): 161–173.
12. Bai X, Xie J, Sun S, Zhang X, Jiang Y, Pang D. The associations of genetic polymorphisms in CYP1A2 and CYP3A4 with clinical outcomes of breast cancer patients in northern China. Oncotarget. 2017; 8 (24): 38367-38377. DOI: 10.18632/oncotarget.16359.
13. Heidarzadehpilehrood R, Pirhoushiaran M, Abdollahzadeh R, Binti Osman M, Sakinah M, Nordin N, et al. A Review on CYP11A1, CYP17A1, and CYP19A1 Polymorphism Studies: Candidate Susceptibility Genes for Polycystic Ovary Syndrome (PCOS) and Infertility. Genes (Basel). 2022; 13 (2): 302. DOI: 10.3390/genes13020302.
14. Mondal S, Shrivastava P, Mehra R. Computing pathogenicity of mutations in human cytochrome P450 superfamily. Biochim Biophys Acta Proteins Proteom. 2025; 1873 (4): 141078. DOI: 10.1016/j.bbapap.2025.141078.
15. Esteves F, Rueff J, Kranendonk M. The central role of cytochrome P450 in xenobiotic metabolism — a brief review on a fascinating enzyme family. J Xenobiot. 2021; 11 (3): 94–114. DOI: 10.3390/jox11030007.
16. Lazaros LA, Hatzi EG, Xita NV, Makrydimas GV, Kaponis AI, Takenaka A, et al. Aromatase (CYP19) gene variants influence ovarian response to standard gonadotrophin stimulation. J Assist Reprod Genet. 2012; 29 (2): 203–209. DOI: 10.1007/s10815-011-9673-y.
17. Song D, Huang XL, Hong L, Yu JM, Zhang ZF, Zhang HQ, et al. Sequence variants in FSHR and CYP19A1 genes and the ovarian response to controlled ovarian stimulation. Fertil Steril. 2019; 112 (4): 749–757. DOI: 10.1016/j.fertnstert.2019.05.017.
18. ILLUMINA. Infinium HTS Assay: Reference Guide. Document # 15045738 v04. [Электронный ресурс]. — November 2019. — Режим доступа: https://support.illumina.com/content/dam/illumina-support/documents/documentation/chemistry_documentation/infinium_assays/infinium-hts/infinium-hts-assay-reference-guide-15045738-04.pdf (дата обращения: 22.12.2025).
19. Кублинский К. С., Новицкий В. В., Уразова О. И. Аллельный полиморфизм генов ферментов метаболизма эстрогенов при генитальном эндометриозе. Патогенез. 2015; 13 (3): 41–44.
20. Alalawy AI, Sakran MI, Alzuaibr FM, Alotaibi MA, Elshazli RM. Unraveling the molecular significance of CYP1A2 (rs762551; c.-9-154 C>A) genetic variant on breast carcinoma susceptibility: Insights from case-control study and meta-analysis. Pathol Res Pract. 2024; 261: 155501. DOI: 10.1016/j.prp.2024.155501.
21. Parisi F, Fenizia C, Introini A, Zavatta A, Scaccabarozzi C, Biasin M, et al. The pathophysiological role of estrogens in the initial stages of pregnancy: molecular mechanisms and clinical implications for pregnancy outcome from the periconceptional period to end of the first trimester. Hum Reprod Update. 2023; 29 (2): 699–720. DOI: 10.1093/humupd/dmad016.
22. Bourdon M, Maignien C, Ouazana M, Kefelian F, Marcellin L, Patrat C, et al. Oestradiol and reproductive outcomes in ART: when too much of a good thing hurts. Reprod Biomed Online. 2025; 51 (6): 105131. DOI: 10.1016/j.rbmo.2025.105131.
23. Ojosnegros S, Seriola A, Godeau AL, Veiga A. Embryo implantation in the laboratory: an update on current techniques. Hum Reprod Update. 2021; 27 (3): 501–530. DOI :10.1093/humupd/dmaa054
24. Ma WG, Song H, Das SK, Paria BC, Dey SK. Estrogen is a critical determinant that specifies the duration of the window of uterine receptivity for implantation. Proc Natl Acad Sci USA. 2003; 100 (5): 2963–8. DOI:10.1073/pnas.0530162100 (2003).
25. Simon C, Domínguez F, Valbuena D, Pellicer A. The role of estrogen in uterine receptivity and blastocyst implantation. Trends Endocrinol Metab. 2003; 14 (5): 197–9. DOI: 10.1016/s1043-2760(03)00084-5.
26. Muter J, Lynch VJ, McCoy RC, Brosens JJ. Human embryo implantation. Development. 2023; 150 (10): dev201507. DOI: 10.1242/dev.201507.
27. Ezoe K, Daikoku T, Yabuuchi A, Murata N, Kawano H, Abe T, et al. Ovarian stimulation using human chorionic gonadotrophin impairs blastocyst implantation and decidualization by altering ovarian hormone levels and downstream signaling in mice. Mol Hum Reprod. 2014; 20 (11): 1101–16. DOI:10.1093/molehr/gau065.

OPTIMAL HAEE SYNTHETIC PEPTIDE THERAPEUTIC DOSE WITH REPEATED ADMINISTRATION TO APP/PS1 MICE

Kozin SA[1], Lysikova EA[2], Yakovlev RYu[3], Mukhina KA[1], Soloveva AE[2], Shmigol TA[2], Makarov AA[1], Mitkevich VA[1]✉

[1] Engelhardt Institute of Molecular Biology, Russian Academy of Sciences, Moscow, Russia
[2] Pirogov Russian National Research Medical University, Moscow, Russia
[3] Scientific Centre RTA LLC, Moscow, Russia

High efficacy of the synthetic Ac-His-Ala-Glu-Glu-NH_2 (HAEE) peptide in suppression of the congophilic amyloid plaque formation was earlier shown in the animal model of Alzheimer's disease. The study conducted as part of the pre-clinical trial aimed to determine the optimal therapeutic dose of this peptide when used as an anti-amyloid agent for treatment of this disorder. The APP/PS1 transgenic mice randomized into four experimental groups and one control group (eight males and eight females per group) were used as model animals. Mice of experimental groups 1, 2, 3, and 4 twice a week throughout eight weeks received subcutaneous injections of drugs with the following HAEE dosage: 0.18 mg/kg, 0.30 mg/kg, 1.50 mg/kg, 3.00 mg/kg. Mice of the control group were administered saline. The Congo red stain was used to determine amyloid plaques in the hippocampus of all animals. Quantification of such plaques showed a significant ($p < 0.001$) decrease in the number of plaques in mice of experimental groups (the average plaque number per brain slice was 7.5 ± 2.1, 3.2 ± 0.9, 3.1 ± 0.6, and 3.3 ± 0.7 in mice of groups 1, 2, 3, and 4, respectively) compared to control mice (15.7 ± 4.6). Since the number of plaques in groups 2, 3, and 4 did not change significantly, the minimal HAEE dose, with which the lowest number of amyloid plaques is observed in the studied mice, is 0.3 mg/kg. This is roughly equivalent to the dose of 1.75 mg in terms of one adult human. Thus, the optimal therapeutic HAEE dose for clinical trials has been experimentally substantiated.

Keywords: Alzheimer's disease, amyloid-beta, amyloid plaques, HAEE peptide, preclinical trials, APP/PS1 transgenic mice, histochemical staining, Congo red, therapeutic dose, disease-modifying therapy

Funding: the study was supported by the Ministry of Health of the Russian Federation, topic: Pharmaceutical Development and Preclinical Trials of the Peptide Drug for Treatment of Alzheimer's Disease, 125022602911-9.

Acknowledgements: the authors would like to express their gratitude to E.V. Myachin, Chairman of the VSE Cooperative (Moscow, Russia), for providing the HAEE lyophilized synthetic peptide.

Author contribution: Kozin SA — study design, literature review, manuscript writing; Lysikova EA — experimental research involving APP/PS1 mice, проведение transcardial perfusion, histochemical analysis; Yakovlev RYu — analysis of the input HAEE synthetic peptide samples; Mukhina KA, Soloveva AE, Shmigol TA — experimental research involving APP/PS1 mice, preparation of brain slices, fluorescence microscopy image acquisition and analysis; Makarov AA, Mitkevich VA — study design, manuscript writing.

Compliance with ethical standards: the study was approved by the Ethics Committee of the Engelhardt Institute of Molecular Biology RAS (protocol No. 3 dated 11 September 2025) and conducted in accordance with guidelines for working with laboratory animals.

✉ **Correspondence should be addressed:** Vladimir A. Mitkevich
Vavilova, 32, Moscow, 119991; mitkevich@eimb.ru

Received: 09.12.2025 **Accepted:** 19.01.2026 **Published online:** 04.02.2026

DOI: 10.24075/brsmu.2026.006

Copyright: © 2026 by the authors. **Licensee:** Pirogov University. This article is an open access article distributed under the terms and conditions of the Creative Commons Attribution (CC BY) license (https://creativecommons.org/licenses/by/4.0/).

ОПТИМАЛЬНАЯ ТЕРАПЕВТИЧЕСКАЯ ДОЗА СИНТЕТИЧЕСКОГО ПЕПТИДА HAEE ПРИ МНОГОКРАТНОМ ВВЕДЕНИИ МЫШАМ ЛИНИИ APP/PS1

С. А. Козин[1], Е. А. Лысикова[2], Р. Ю. Яковлев[3], К. А. Мухина[1], А. Е. Соловьёва[2], Т. А. Шмиголь[2], А. А. Макаров[1], В. А. Митькевич[1]✉

[1] Институт молекулярной биологии имени В. А. Энгельгардта Москва, Россия
[2] Российский национальный исследовательский медицинский университет имени Н. И. Пирогова, Москва, Россия
[3] Общество с ограниченной ответственностью «Научный центр РТА», Москва Россия

Ранее в исследованной на животных модели болезни Альцгеймера была показана высокая эффективность использования синтетического пептида Ac-His-Ala-Glu-Glu-NH2 (HAEE) для подавления образования конгофильных амилоидных бляшек. Целью настоящей работы, выполненной в рамках доклинического исследования, было установить оптимальную терапевтическую дозу этого пептида при его использовании в качестве антиамилоидного средства в терапии данного заболевания. В качестве модельных животных были использованы трансгенные мыши линии APP/PS1, случайным образом распределенные по четырем экспериментальным группам и одной контрольной (по восемь самцов и восемь самок в каждой группе). Мышам из экспериментальных групп 1, 2, 3 и 4 дважды в неделю в течение девяти недель делали подкожные инъекции препаратов со следующими дозировками HAEE: 0,18 мг/кг, 0,30 мг/кг, 1,50 мг/кг, 3,00 мг/кг. Мышам из контрольной группы вводили физиологический раствор. В гиппокампе всех животных окрашиванием красителем Конго красный определяли амилоидные бляшки. Анализ количества таких бляшек показал достоверное ($p < 0,001$) уменьшение их числа у мышей из экспериментальных групп (среднее число бляшек на один срез мозга составляло 7,5 ± 2,1, 3,2 ± 0,9, 3,1 ± 0,6 и 3,3 ± 0,7 для мышей из групп 1, 2, 3 и 4 соответственно) по сравнению с мышами из контрольной группы (15,7 ± 4,6). Так как число бляшек в группах 2, 3 и 4 достоверно не изменялось, минимальная доза HAEE, при которой наблюдается наименьшее число амилоидных бляшек у исследованных мышей, составляет 0,3 мг/кг, что приблизительно соответствует дозе 1,75 мг в пересчете на одного взрослого человека. Таким образом, экспериментально обосновано оптимальное значение терапевтической дозы HAEE для клинических исследований.

Ключевые слова: болезнь Альцгеймера, бета-амилоид, амилоидные бляшки, пептид HAEE, доклинические испытания, трансгенные мыши линии APP/PS1, гистохимическое окрашивание, Конго красный, терапевтическая доза, болезнь-модифицирующая терапия

Финансирование: при поддержке Министерства здравоохранения Российской Федерации, тема: Фармацевтическая разработка и доклинические исследования лекарственного средства пептидной структуры для лечения болезни Альцгеймера, 125022602911-9.

Благодарности: Е. В. Мячину, председателю кооператива «ВСЕ» (Москва, Россия), за предоставление лиофилизированного синтетического пептида HAEE.

Вклад авторов: С. А. Козин — дизайн исследования, обзор литературы, подготовка рукописи; Е. А. Лысикова — экспериментальные исследования на мышах линии APP/PS1, проведение транскардиальной перфузии, гистохимический анализ; Р. Ю. Яковлев — входной анализ образцов синтетического пептида HAEE; К. А. Мухина, А. Е. Соловьёва, Т. А. Шмиголь — экспериментальные исследования на мышах линии APP/PS1, приготовление срезов мозга, получение изображений на флуоресцентном микроскопе и анализ; А. А. Макаров, В. А. Митькевич — дизайн исследования, подготовка рукописи.

Соблюдение этических стандартов: исследование одобрено этическим комитетом ИМБ им. В. А. Энгельгардта РАН (протокол № 3 от 11 сентября 2025 г.) и проведено в соответствии с правилами работы с лабораторными животными.

✉ **Для корреспонденции:** Владимир Александрович Митькевич
ул. Вавилова, д. 32, г. Москва, 119991; mitkevich@eimb.ru

Статья получена: 09.12.2025 **Статья принята к печати:** 19.01.2026 **Опубликована онлайн:** 04.02.2026

DOI: 10.24075/vrgmu.2026.006

Авторские права: © 2026 принадлежат авторам. **Лицензиат:** РНИМУ им. Н. И. Пирогова. Статья размещена в открытом доступе и распространяется на условиях лицензии Creative Commons Attribution (CC BY) (https://creativecommons.org/licenses/by/4.0/).

Alzheimer's disease (AD) is the most prevalent neurodegenerative disorder and the most common cause of dementia in the elderly all over the world [1]. According to statistical data, the number of patients with AD in Russia is 1.5–2 million [2].

The presence of extracellular fibrillary aggregates, or amyloid plaques, showing a characteristic signal when Congo red stained is one of the main pathological features of AD [3]. The aggregated amyloid-beta (Aβ) species are the main components of amyloid plaques [4]. Amyloid-beta is a short polypeptide (37–43 amino acid residues), the low nanomolar concentrations of which are found in human blood and cerebrospinal fluid [5]. However, during the AD pathogenesis cerebral amyloidosis starts to develop in the brain for unknown reasons, due to which monomeric Aβ molecules are first converted into soluble oligomers and then accumulate in various parts of the brain as amyloid plaques, but especially and primarily in the hippocampus [6]. The first amyloid plaques in brain tissues are formed 10–20 years before the onset of AD clinical manifestations, but it is Aβ aggregation that initiates further AD-associated disease processes, including tau-protein hyperphosphorylation and neurodegeneration [4]. Therefore, the search for candidate drugs for amyloid plaque disruption and/or amyloid plaque formation prevention represents the key strategy of the development of disease-modifying therapy for AD [7].

To date, three anti-Aβ antibodies, aducanumab, lecanemab, and donanemab, have been legally registered in the USA [8–10] for initial treatment of the early-stage AD, including patients having mild cognitive impairment or mild dementia due to Alzheimer's disease with the diagnosis confirmed based on Aβ using positron emission tomography of amyloid or cerebrospinal fluid biomarkers. These novel disease-modifying treatment methods act by decreasing the amount of amyloid plaques in the brain and demonstrate clinical benefits of anti-amyloid therapy [11].

However, due to dangerous side effects of antibodies [12], the development of drug candidates from the class of low molecular weight compounds, involving peptides and peptidomimetics, as molecular agents that target specific binding to various regions of the Aβ amino acid sequence, is being continued [13].

The Ac-His-Ala-Glu-Glu-NH2 (HAEE) synthetic peptide (PubChem CID: 56971578) has been developed as a potential disease-modifying drug for AD therapy [14], which effectively passes from blood into the brain tissue crossing the blood-brain barrier [15]. The drug target of HAEE is the 11-Glu-Val-His-His-14 (EVHH) Aβ fragment that forms an intermolecular complex stabilized by complementary ionic interactions with HAEE (review in [16]). The EVHH fragment was selected as a drug target due to the fact that it represents an Aβ molecular determinant, which has a rigid conformation of the main polypeptide chain and controls the Aβ binding to the α4β2 subtype nicotinic acetylcholine receptor, as well as all the Aβ zinc-dependent interactions [17, 18]. Considering crucial role of all the above interactions in the AD pathogenesis, it was expected that blocking the EVHH fragment by HAEE should inhibit amyloid plaque formation *in vivo*. Indeed, high anti-amyloid efficacy of HAEE was reported in pilot experiments involving the use of transgenic animals (APP/PS1 mice and CL2120 nematodes) as AD models (review in [18]).

Thus, the mechanism of the HAEE anti-amyloid effect is based on disruption of the zinc-dependent intermolecular interfaces in the amyloid-beta oligomers and aggregates, as well as in the complexes formed by Aβ and subtype α4β2 nicotinic acetylcholine receptors via selective HAEE binding with the 11-Glu-Val-His-His-14 amino acid sequence fragment of amyloid-beta, leading to reduction of the amount of amyloid-beta aggregates in the model animal's body.

The study aimed to determine the HAEE optimal therapeutic dose for effective inhibition of amyloid plaque formation in the hippocampus of APP/PS1 mice within the framework of the pre-clinical trial of the HAEE-based drug as a potential anti-amyloid drug for treatment of AD.

METHODS

Laboratory animals

The experiments involved APPswe/PS1dE9/Blg transgenic mice [19]. This lineage was obtained by crossing the B6;C3-Tg(APPswe,PSEN1dE9)85Dbo/Mmjax transgenic mice (#034829-JAX, JAX, Maine, USA) also referred to as APP/PS1 with the C57Bl6J wild type mice of the C57Bl6J/ChG lineage (Institute of Physiologically Active Compounds, Chernogolovka, Russia). The APP/PS1 transgenic mice are acknowledged AD models [18]. Since the age of 4–6 months these animals show typical cognitive signs of the AD-like disorder; there is a considerable amount of congophilic amyloid plaques in specific brain regions, including hippocampus and brain cortex [20]. Experimental animals were kept in the pathogen-free vivarium (Engelhardt Institute of Molecular Biology, Moscow, Russia) under the conditions, including standard diet, ad libitum access to food and water, daylight lasting 12 h, ambient temperature between +22 and +24 °C, and relative humidity 50–65%. Breeding and control genotyping of bloodstock were performed as previously reported [19].

Experimental groups of animals

In this study, the experiments involved the total of 40 male and 40 female APP/PS1 transgenic mice. The animals were randomized into five groups, 8 males and 8 females per group (Table). The age of each animal at the time of the first injection and euthanasia was 5 and 7 months, respectively. Mice of group 1 (controls) were subcutaneously administered the isotonic 0.9% sodium chloride solution (normal saline). Mice of groups 2–5 were administered the HAEE synthetic peptide solution at a dose of 0.18 mg/kg, 0.30 mg/kg, 1.50 mg/kg, and 3.00 mg/kg, respectively. The 7-months-old mice were euthanized.

Reagents

All the chemical compounds and solvents used in the study were of and HPLC or higher grade, these were purchased from Sigma-Aldrich (St. Louis, Missouri, USA), unless otherwise specified. Medicinal product "Ac-His-Ala-Glu-Glu-NH2 Tetrapeptide, solution for subcutaneous administration", 3.5 mg/mL (Pharmsynthez, Russia). The HAEE peptide structure was confirmed by NMR spectroscopy and tandem mass spectrometry.

Preparation of the synthetic HAEE-based drugs for injection

The HAEE-based drug with the baseline concentration of 3.5 mg/mL was diluted with the sterile isotonic 0.9% sodium chloride solution to achieve the working peptide concentration ensuring the desired HAEE-based drug dose (for example, 0.30 mg/kg) per 125 μL of the diluted solution. The total volume of a single injection sample was 150 μL for all the HAEE doses

Table. Inhibition of the congophilic amyloid plaque formation in the hippocampal areas CA1, CA2, CA3 and the dentate gyrus in transgenic APP/PS1 mice receiving repeated subcutaneous injections of the drugs based on the Ac-His-Ala-Glu-Glu-NH2 (HAEE) synthetic peptide prepared in 125 μL of normal saline and differing in the dose of the administered peptide

Transgenic APP/PS1 mice				Injection (HAEE drug prepared in 125 μL of normal saline)	Brain sections	Congophilic amyloid plaque (CAP) counts per brain section	Significance
Group	Number of animals	Age at first injection (months)	Age at euthanasia (months)	Dose (mg/kg) of the administered HAEE synthetic peptide / total number of injections	Total number	Hyppocampal areas CA1, CA2, CA3 and the dentate gyrus (mean ± SEM)	Relative to controls (group No. 1)
No. 1, control	16	5	7	0 / 17	160	15.7 ± 4.6	–
No. 2	16	5	7	0.18 / 17	160	7.5 ± 2.1	$p < 0.001$
No. 3	16	5	7	0.30 / 17	160	3.2 ± 0.9	$p < 0.001$
No. 4	16	5	7	1.50 / 17	160	3.1 ± 0.6	$p < 0.001$
No. 5	16	5	7	3.00 / 17	160	3.3 ± 0.7	$p < 0.001$

used in the study. Each animal was administered 125 μL of the sample.

Administration of test drugs to experimental animals

Transgenic mice of five experimental groups were administered test drugs (normal saline or samples with different HAEE peptide doses) twice a week throughout 9 weeks via subcutaneous injection of appropriate drugs in accordance with the existing requirements for and approaches to drug dose adjustment in laboratory animals [21]. The frequency and total number of injections administered to mice of the experimental groups throughout the study, as well as information on the HAEE dosage in the injection samples for each experimental group are provided in the Table.

Preparing histological sections of the brain

Transcardial perfusion with the 4% paraformaldehyde solution in phosphate-buffered saline was performed in animals after the terminal anesthesia with Avertin (Sigma Aldrich, Germany). The dissected brain was fixed in the 4% paraformaldehyde solution in phosphate-buffered saline for 12–16 h. Tissues were dehydrated in the solutions with increasing ethanol concentrations: 75% — 1 h, three 95% changes 5 min each, 100% — 15 min, 100% — 45 min, ethanol-chloroform (1 : 1) — 30 min, chloroform — 1 h, chloroform — 12–16 h. Brain specimens were paraffin soaked at 60 °C in three consecutive paraffin changes, with 1 h incubation in each. Embedding tissues in paraffin blocks was accomplished using the Leica EG1160 system (Leica Microsystems, Germany). The 8 μm serial brain sections were obtained using the Leica RM2265 microtome (Leica Microsystems, Germany) and mounted on the poly-L-lysine coated glass slides. Sections was deparaffinized in xylene — two changes 10 min each, rehydrated in ethanol: 100% — 5 min, 90% — 5 min, 75% — 5 min, water — 10 min, stained with 0.5% alcohol solution of Congo red dye — 5 min, differentiated in the 0.2% KOH solution in 80% ethanol; slices were washed with deionized water for 10 min. The Immu-Mount medium (Thermo Scientific) was used to mount coverslips.

Identification of congofilic amyloid plaques in the hyppocampal areas CA1, CA2, CA3 and dentate gyrus by histochemistry method

The sections obtained covering the area of the brain from 0.48 to 1.92 mm relative to the midline in lateral stereotaxic coordinates were used for congophilic amyloid plaque quantification in the hyppocampus [22]. Every 15th section was assessed, which resulted in 10 sections per animal. Since the Congo red dye is capable of forming a fluorescent complex with amyloid fibrils being part of amyloid plaques, detection of congophilic amyloid plaques was performed using the

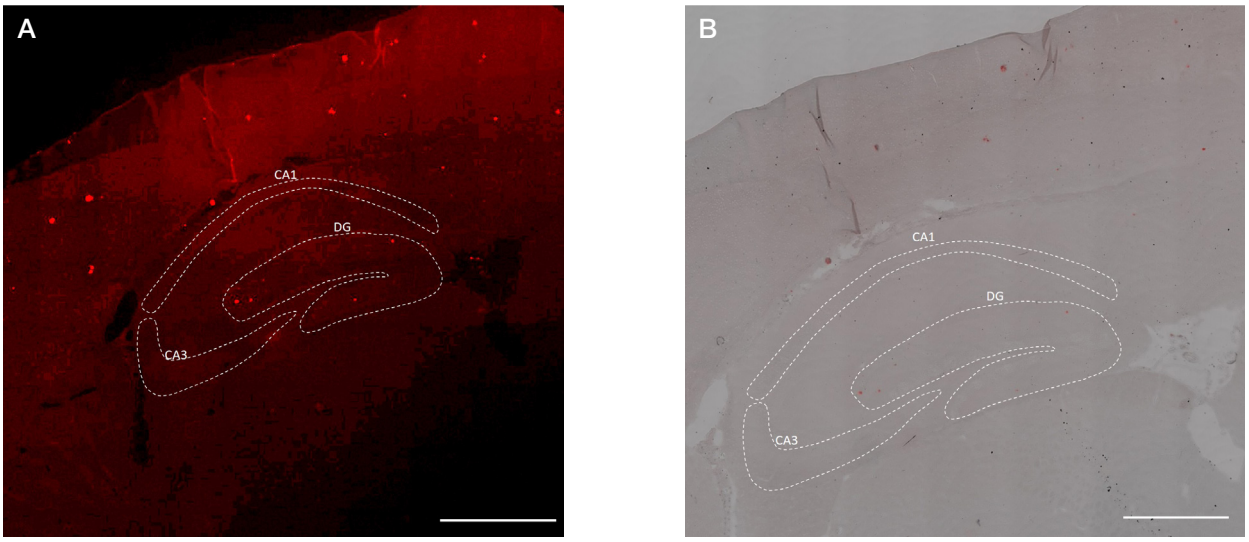

Fig. Congophilic amyloid plaques in the typical brain section from the intact transgenic APP/PS1 mouse aged five months. **A**. Fluorescence signal after Congo red staining. **B**. Combined Congo red fluorescence and transmitted light microscopy images. The *dotted line* indicates the CA1, CA3 areas and the DG (dentate gyrus). Scale — 500 μm

LSM880 confocal microscope (Carl Zeiss, Germany) by mosaic scanning of individual hyppocampal areas at 10× magnification in the spectral range with peak excitation at 596 nm and emission at 620 nm (Fig. 1A). To identify anatomic structures of the brain, the resulting fluorescence image was combined with the transmitted light microscopy image (Fig. 1B). All visible congophilic amyloid plaques of any size were counted manually. Mean values and standard deviations of congophilic amyloid plaque counts per section were calculated for each group of mice (Table).

Statistical analysis methods

The data were presented as mean values for at least three independent amyloid plaque counts ± standard error of the mean (SEM). The Shapiro–Wilk test was used to test the distribution for normality. Pairwise comparison of the studied groups was performed using the Mann–Whitney *U*-test. The significance level was 99.9% ($p < 0.001$). Statistical analysis was performed using the STATISTICA 8.0 software package (StatSoft Inc., USA).

RESULTS

Fig. 1 presents a typical image of the Congo red stained brain section from an intact 5-months-old APP/PS1 mouse. Congophilic amyloid plaques (CAP) that could be seen in the brain of the 7-months-old experimental animals of all five experimental groups after injections showed similar localization and size distribution in the brain parenchyma. However, plaque quantification revealed significant intergroup differences.

The data on the CAP counts in the hippocampal areas CA1, CA2, CA3 and the dentate gyrus of the 7-months-old APP/PS1 transgenic mice of experimental groups 1–5 are provided in the Table. In control animals of group 1 not exposed to the HAEE peptide, the CAP count is 15.7 ± 4.6, which is consistent with the literature data on the intact 7-months-old APP/PS1 transgenic mice [23, 24].

In mice of group 2, which were repeatedly administered the HAEE initial dose (0.18 mg/kg), the CAP count was 7.5 ± 2.1, i.e. it decreased twice compared to control mice. In mice of group 3, which received HAEE at a dose of 0.30 mg/kg, the CAP counts decreased considerably (more than twice) compared to mice of group 2 and were almost 5 times lower compared to controls. The further 5- and 10-fold HAEE dose increase relative to the dose of 0.30 mg/kg did not lead to any changes in the CAP counts in animals of groups 4 and 5 compared to mice of group 3.

Thus, in this study it was found for the first time that the dose of 0.30 mg/kg was optimal for CAP formation inhibition in male and female APP/PS1 transgenic mice with the repeated subcutaneous administration of the HAEE synthetic peptide.

DISCUSSION

In this study, we provide and analyze the experimental data on the congophilic amyloid plaque counts in the sections of the isolated brain areas of transgenic mice, i.e. amyloid plaques identified using Congo red stain only. This classic visualization method, that is specific for fibrillary amyloid plaques representing the main neuro-morphological sign of amyloidosis associated with the Alzheimer's disease pathogenesis, does not take into account the possible presence of soluble amyloid-beta aggregates and oligomers in brain tissues.

The HAEE peptide capability of suppressing amyloid plaque formation in APP/PS1 transgenic mice, that are widely used as the AD animal model (review in [18]), has been already shown in a few papers. Such a capability was first demonstrated in 2015 [24] on an example of a limited sample of male and female animals ($n = 6$ and $n = 7$ in the control and experimental groups, respectively). Experimental animals received intravenous injections of the HAEE peptide at a dose of 1.13 mg/kg twice a month throughout 5 months, since the age of 2 months (each animal received a total of nine injections). As a result, the 7-months-old transgenic mice exposed to the HAEE peptide showed the decrease in congophilic amyloid plaque counts in the hyppocampal areas CA1, CA2, CA3 and the dentate gyrus by 60% compared to control animals. Then, male APP/PS1 transgenic mice received intravenous injections of a dose of 0.05 mg/kg monthly throughout 5 months, since the age of 2 months (each animal received a total of six injections) [25]. In the hippocampus of 8-months-old mice administered the HAEE-based drugs, the congophilic amyloid plaque count (24.7 ± 3.4 per section) turned out to be 22% lower compared to control animals (31.7 ± 4.9 per section). Finally, it has recently been shown that both intraperitoneal and intranasal injections of the synthetic HAEE at a dose of 50 mg/kg to male APP/PS1 transgenic mice every 48 h throughout 1.5 months, since the age of 6 months, resulted in the decrease in the amyloid load on brain tissues in the injected animals compared to control animals. The load assessed based on the area of the apparent surface of amyloid plaques in the hyppocapus decreased 4.7- and 3.5-fold with the use of intraperitoneal and intranasal administration routes, respectively [26].

Thus, the efficacy of using the synthetic HAEE to suppress amyloid plaque formation in the hippocampus of APP/PS1 transgenic mice has been earlier reported for both males and females with the use of intravenous, intraperitoneal, and intranasal administration routes. Treatment of mice with HAEE was started at the age of both 2 months, when these animals had no amyloid inclusions in the brain, and 6 months, when there were at least five congophilic amyloid plaques in the hyppocampus [23]; the administration period changed from 1.5 to five months, and the intervals between injections were 2–30 days.

In the above studies, the dose also varied between 0.05 and 50 mg/kg with various administration rates. All these differences in experimental procedures made it impossible to draw a conclusion, which dose (0.05 mg/kg, 1.13 mg/kg or 50.00 mg/kg) was the most appropriate as a therapeutic dose for clinical trials. It is clear that the dose of 50.00 mg/kg is safe, but redundant. At the same time, the dose of 0.05 mg/kg seems to be less effective, than the dose of 1.13 mg/kg.

Despite variability of the above experimental protocols, it seems entirely reasonable to use the data on the changes in congophilic amyloid plaque counts in the hyppocampal areas CA1, CA2, CA3 and the dentate gyrus of APP/PS1 transgenic mice counted by the method [24], previously reported as reliable criterion for assessment of the HAEE peptide anti-amyloid efficacy.

It is well known, that up to the age of seven months there are no significant sex differences in the development of cerebral amyloidosis in APP/PS1 transgenic mice [27], therefore, in this study, subcutaneous injections were administered to 5-months-old animals of both sexes, and brain harvesting for histochemical analysis was performed in 7-months-old mice. Injections were administered twice a week for nine weeks. The following four synthetic HAEE doses were selected for testing: 0.18 mg/kg; 0.30 mg/kg; 1.50 mg/kg; 3.00 mg/kg. Testing showed that under exposure to HAEE the CAP counts of the injected mice decreased considerably compared to control

animals with all the studied doses. However, the CAP counts were roughly the same when using the doses of 0.30 mg/kg, 1.50 mg/kg, and 3.00 mg/kg. The fact that the 5- and 10-fold increase of the dose of 0.30 mg/kg caused no therapeutic effect enhancement (i.e. no CAP count decrease) suggests that when other experimental conditions are the same (period and rate of injections, age of mice at the time of the first injection), the dose of 0.30 mg/kg is necessary and sufficient for optimal suppression of amyloid plaque formation in the studied animal model of AD. The dose of 0.30 mg/kg is roughly equivalent to the dose of 1.75 mg in terms of an adult human.

It is well known, that in 5-months-old APP/PS1 transgenic mice, amyloid plaques are formed within 24 h [28], after which the plaques are in dynamic equilibrium with soluble Aβ oligomers, and some of these oligomers initiate formation of new amyloid plaques due to their structural and functional features [29]. Recently, it has been found in animal models that the HAEE anti-amyloid effect mechanism is based on the peptide capability of effectively passing from blood to brain tissues through the blood-brain barrier and binding the Aβ molecules that are present both in the form of soluble monomers and oligomers, and as part of insoluble amyloid plaques, which ensures rapid removal of excess Aβ molecules from the brain [18, 30].

The findings that the dose increase over 0.30 mg/kg does not result in the HAEE peptide anti-amyloid effect enhancement suggest the limited number of drug targets for HAEE, i.e. this dose is enough for the HAEE molecules to “brush” the already formed amyloid plaques from the neuronal surface and prevent the soluble Aβ oligomer formation.

CONCLUSIONS

The study made it possible to define the value of 0.30 mg/kg as the optimal Ac-His-Ala-Glu-Glu-NH2 (HAEE) synthetic peptide dose for cerebral amyloidosis inhibition in male and female APP/PS1 transgenic mice. This mouse lineage is widely used as model animals to study the Alzheimer's disease pathogenesis all over the world. That is why the research results obtained using this model are considered as highly reliable in terms of translation into clinical practice. Thus, the findings represent a scientific foundation for the use of repeated subcutaneous injections of the HAEE synthetic peptide prepared in 0.5 mL of normal saline at a dose of 1.75 mg for phase 1 clinical trial. Certainly, the efficacy of the HAEE peptide as an anti-amyloid agent for disease-modifying therapy of AD can be proven in further clinical trials only, and the results obtained represent an essential element of successful clinical trials.

References

1. Livingston G, et al. Dementia prevention, intervention, and care: 2020 report of the Lancet Commission. The Lancet. 2020; 396 (10248): 413–46.
2. Mihajlova NM. Organizaciya vnebol'nichnoj gerontopsihiatricheskoj pomoshchi pri demencii i kognitivnom snizhenii. CHast' 1: Demograficheskie sdvigi, sozdanie kliniki pamyati i Al'cgejmerovskih centrov. ZHurnal nevrologii i psihiatrii im. S. S. Korsakova. 2017; 117 (6): 111–19. Russian.
3. Jagust W, et al. “Alzheimer's disease” is neither “Alzheimer's clinical syndrome” nor “dementia”. Alzheimer's & Dementia: The Journal of the Alzheimer's Association. 2019; 15 (1): 153–7.
4. Hampel H, et al. The Amyloid-β Pathway in Alzheimer’s Disease. Molecular Psychiatry. 2021; 26 (10): 5481–03.
5. Roher AE, et al. Amyloid beta peptides in human plasma and tissues and their significance for Alzheimer's disease. Alzheimers Dement. 2009; 5 (1): 18–29.
6. Long JM, Holtzman DM. Alzheimer Disease: An Update on Pathobiology and Treatment Strategies. Cell. 2019; 179 (2): 312–39.
7. Cummings JL, et al. Alzheimer's disease drug development pipeline: 2025. Alzheimer's & Dementia: Translational Research & Clinical Interventions. 2025; 11 (2): e70098.
8. Budd Haeberlein S, et al. Two Randomized Phase 3 Studies of Aducanumab in Early Alzheimer’s Disease. The Journal of Prevention of Alzheimer's Disease. 2022; 9 (2): 197–210.
9. Mintun MA, et al. Donanemab in Early Alzheimer's Disease. N Engl J Med. 2021; 384 (18): 1691–704.
10. van Dyck CH, et al. Lecanemab in Early Alzheimer's Disease. N Engl J Med. 2023; 388 (1): 9–21.
11. Hardy J, Mummery C. An anti-amyloid therapy works for Alzheimer’s disease: why has it taken so long and what is next? Brain. 2023; 146 (4): 1240–2.
12. Kepp KP, et al. The amyloid cascade hypothesis: an updated critical review. Brain. 2023; 146 (10): 3969–90.
13. Wang C, et al. Advances in Alzheimer’s Disease-Associated Aβ Therapy Based on Peptide. International Journal of Molecular Sciences. 2023; 24 (17): 13110.
14. Kozin SA, i dr. Peptid Ac-His-Ala-Glu-Glu-NH2 i ego proizvodnye, prednaznachennye dlya vosstanovleniya deficita endogennogo komponenta krovi cheloveka. Patent RF №2826728. Oficial'nyj byulleten' Federal'noj sluzhby po intellektual'noj sobstvennosti (Rospatent) №26–2024, 11/09/2024-20/09/2024, 2024. Russian.
15. Ivanova AV, et al. Comparative pharmacokinetics and biodistribution of HAEE and HASS peptides. Bulletin of RSMU. 2025 (4): 45–50.
16. Kozin SA. Rol' vzaimodejstvij cinka i beta-amiloida v patogeneze bolezni Al'cgejmera. Uspekhi biologicheskoj himii. 2023; 63: 149–74. Russian.
17. Nikolskij KS, i dr. Issledovanie interfejsa svyazyvaniya beta-amiloida s kandidatnym markerom nejrodegenerativnyh zabolevanij. Matematicheskaya biologiya i bioinformatika. 2025; 20 (1): 212–35. Russian.
18. Kozin SA, et al. Switching On/Off Amyloid Plaque Formation in Transgenic Animal Models of Alzheimer’s Disease. International Journal of Molecular Sciences. 2024; 25 (1): 72.
19. Lysikova EA, i dr. Liniya transgennyh myshej APPswe/PS1dE9/Blg dlya modelirovaniya cerebral'nogo amiloidoza pri bolezni Al'cgejmera. Molekulyarnaya biologiya. 2023; 57 (1): 85–94. Russian.
20. Jankowsky JL, et al. Co-expression of multiple transgenes in mouse CNS: a comparison of strategies. Biomol Eng. 2001; 17 (6): 157–65.
21. Rybakova AV, i dr. Sushchestvuyushchie trebovaniya i podhody k dozirovaniyu lekarstvennyh sredstv laboratornym zhivotnym. Vedomosti Nauchnogo centra ekspertizy sredstv medicinskogo primeneniya. 2018; 8 (4): 207–17. Russian.
22. Paxinos G, Franklin KBJ. Paxinos and Franklin’s the Mouse Brain in Stereotaxic Coordinates. 4th ed. Elsevier Academic Press, 2013.
23. Garcia-Alloza M, et al., Characterization of amyloid deposition in the APPswe/PS1dE9 mouse model of Alzheimer disease. Neurobiology of Disease. 2006; 24 (3): 516–24.
24. Tsvetkov PO, et al. Peripherally Applied Synthetic Tetrapeptides HAEE and RADD Slow Down the Development of Cerebral β-Amyloidosis in AβPP/PS1 Transgenic Mice. J Alzheimers Dis. 2015; 46 (4): 849–53.
25. Kozin SA. Cinkovyj kompleks peptida HAEE dlya lecheniya nejrodegenerativnyh zabolevanij. Patent RF №2784319. Oficial'nyj byulleten' Federal'noj sluzhby po intellektual'noj sobstvennosti (Rospatent), № 33–2022, 21/11/2022-27/11/2022, 2022. Russian.
26. Patrakhanov E. Effectiveness of the tetrapeptide HAEE: an innovative approach to Alzheimer’s treatment in experimentation. Research Results in Pharmacology. 2024; 10 (4): 107–11.

27. Kuzubova E, et al. Sex-Dependent Phenotypic and Histomorphometric Biomarkers in the APPswe/PS1dE9/Blg Mouse Model of Alzheimer's Disease. Brain Sciences. 2025; 15 (11): 1237.
28. Meyer-Luehmann M, et al. Rapid appearance and local toxicity of amyloid-beta plaques in a mouse model of Alzheimer's disease. Nature. 2008; 451 (7179): 720–4.
29. Nirmalraj PN, Bhattacharya S, Thompson D. Accelerated Alzheimer's Aβ-42 secondary nucleation chronologically visualized on fibril surfaces. Science Advances. 2024; 10 (43): eadp5059.
30. Mukhina KA, et al. The Tetrapeptide HAEE Promotes Amyloid-Beta Clearance from the Brain. International Journal of Molecular Sciences. 2025; 26 (23): 11591.

Литература

1. Livingston G, et al. Dementia prevention, intervention, and care: 2020 report of the Lancet Commission. The Lancet. 2020; 396 (10248): 413–46.
2. Михайлова Н. М. Организация внебольничной геронтопсихиатрической помощи при деменции и когнитивном снижении. Часть 1: Демографические сдвиги, создание клиники памяти и Альцгеймеровских центров. Журнал неврологии и психиатрии им. С. С. Корсакова. 2017; 117 (6): 111–19.
3. Jagust W, et al. "Alzheimer's disease" is neither "Alzheimer's clinical syndrome" nor "dementia". Alzheimer's & Dementia: The Journal of the Alzheimer's Association. 2019; 15 (1): 153–7.
4. Hampel H, et al. The Amyloid-β Pathway in Alzheimer's Disease. Molecular Psychiatry. 2021; 26 (10): 5481–03.
5. Roher AE, et al. Amyloid beta peptides in human plasma and tissues and their significance for Alzheimer's disease. Alzheimers Dement. 2009; 5 (1): 18–29.
6. Long JM, Holtzman DM. Alzheimer Disease: An Update on Pathobiology and Treatment Strategies. Cell. 2019; 179 (2): 312–39.
7. Cummings JL, et al. Alzheimer's disease drug development pipeline: 2025. Alzheimer's & Dementia: Translational Research & Clinical Interventions. 2025; 11 (2): e70098.
8. Budd Haeberlein S, et al. Two Randomized Phase 3 Studies of Aducanumab in Early Alzheimer's Disease. The Journal of Prevention of Alzheimer's Disease. 2022; 9 (2): 197–210.
9. Mintun MA, et al. Donanemab in Early Alzheimer's Disease. N Engl J Med. 2021; 384 (18): 1691–704.
10. van Dyck CH, et al. Lecanemab in Early Alzheimer's Disease. N Engl J Med. 2023; 388 (1): 9–21.
11. Hardy J, Mummery C. An anti-amyloid therapy works for Alzheimer's disease: why has it taken so long and what is next? Brain. 2023; 146 (4): 1240–2.
12. Kepp KP, et al. The amyloid cascade hypothesis: an updated critical review. Brain. 2023; 146 (10): 3969–90.
13. Wang C, et al. Advances in Alzheimer's Disease-Associated Aβ Therapy Based on Peptide. International Journal of Molecular Sciences. 2023; 24 (17): 13110.
14. Козин С. А., и др. Пептид Ac-His-Ala-Glu-Glu-NH2 и его производные, предназначенные для восстановления дефицита эндогенного компонента крови человека. Патент РФ №2826728. Официальный бюллетень Федеральной службы по интеллектуальной собственности (Роспатент) №26–2024, 11/09/2024-20/09/2024, 2024.
15. Иванова А. В., et al. Сравнительная фармакокинетика и биораспределение пептидов HAEE и HASS. Вестник РГМУ. 2025 (4): 50–56.
16. Козин С. А. Роль взаимодействий цинка и бета-амилоида в патогенезе болезни Альцгеймера. Успехи биологической химии. 2023; 63: 149–74.
17. Никольский К. С., и др. Исследование интерфейса связывания бета-амилоида с кандидатным маркером нейродегенеративных заболеваний. Математическая биология и биоинформатика. 2025; 20 (1): 212–35.
18. Kozin SA, et al. Switching On/Off Amyloid Plaque Formation in Transgenic Animal Models of Alzheimer's Disease. International Journal of Molecular Sciences. 2024; 25 (1): 72.
19. Лысикова Е. А., и др. Линия трансгенных мышей APPswe/PS1dE9/Blg для моделирования церебрального амилоидоза при болезни Альцгеймера. Молекулярная биология. 2023; 57 (1): 85–94.
20. Jankowsky JL, et al. Co-expression of multiple transgenes in mouse CNS: a comparison of strategies. Biomol Eng. 2001; 17 (6): 157–65.
21. Рыбакова А. В., и др. Существующие требования и подходы к дозированию лекарственных средств лабораторным животным. Ведомости Научного центра экспертизы средств медицинского применения. 2018; 8 (4): 207–17.
22. Paxinos G, Franklin KBJ. Paxinos and Franklin's the Mouse Brain in Stereotaxic Coordinates. 4th ed. Elsevier Academic Press, 2013.
23. Garcia-Alloza M, et al., Characterization of amyloid deposition in the APPswe/PS1dE9 mouse model of Alzheimer disease. Neurobiology of Disease. 2006; 24 (3): 516–24.
24. Tsvetkov PO, et al. Peripherally Applied Synthetic Tetrapeptides HAEE and RADD Slow Down the Development of Cerebral β-Amyloidosis in AβPP/PS1 Transgenic Mice. J Alzheimers Dis. 2015; 46 (4): 849–53.
25. Козин С. А. Цинковый комплекс пептида HAEE для лечения нейродегенеративных заболеваний. Патент РФ №2784319. Официальный бюллетень Федеральной службы по интеллектуальной собственности (Роспатент) № 33–2022, 21/11/2022-27/11/2022, 2022.
26. Patrakhanov E. Effectiveness of the tetrapeptide HAEE: an innovative approach to Alzheimer's treatment in experimentation. Research Results in Pharmacology. 2024; 10 (4): 107–11.
27. Kuzubova E, et al. Sex-Dependent Phenotypic and Histomorphometric Biomarkers in the APPswe/PS1dE9/Blg Mouse Model of Alzheimer's Disease. Brain Sciences. 2025; 15 (11): 1237.
28. Meyer-Luehmann M, et al. Rapid appearance and local toxicity of amyloid-beta plaques in a mouse model of Alzheimer's disease. Nature. 2008; 451 (7179): 720–4.
29. Nirmalraj PN, Bhattacharya S, Thompson D. Accelerated Alzheimer's Aβ-42 secondary nucleation chronologically visualized on fibril surfaces. Science Advances. 2024; 10 (43): eadp5059.
30. Mukhina KA, et al. The Tetrapeptide HAEE Promotes Amyloid-Beta Clearance from the Brain. International Journal of Molecular Sciences. 2025; 26 (23): 11591.

ASSESSING FUNCTIONAL ACTIVITY OF MICROGLIA AND MACROPHAGES IN BARRIER-ASSOCIATED BRAIN AREAS OF SPONTANEOUSLY HYPERTENSIVE RATS

Razenkova VA✉, Korzhevskii DE

Institute of Experimental Medicine, Saint Petersburg, Russia

The cerebrovascular disorder associated with arterial hypertension results in neuroinflammation, in which microglia and macrophages of the brain are actively involved. The study aimed to assess functional activity and immunophenotype of microglia and macrophages in the areas of brain barriers in spontaneously hypertensive rats (SHR). Specimens of the brain of male Wistar rats and SHR (age 3–4 months, n = 10) were used. The study involved the use of immunohistochemistry analysis and confocal laser microscopy. The presence of M2 activation (CD206) and phagocytic activity (CD68) markers in the population of microglia and macrophages was assessed. It was shown that the CD206 protein was present in perivascular cells, the counts of which were considerably increased in SHR (40.69 ± 4.87 cells per 1 mm^2 vs. 28.73 ± 1.39 in Wistar rats; t-test, p = 0.0007). The quantitative analysis conducted allowed us to identify the upward trend of the share of phagocytic cells in the brain of SHR compared to Wistar rats. No changes in the CD68 protein distribution were found in SHR, therefore, activation of microglia and macrophages is not accompanied by the phagocytic activity increase. The findings suggest alternative activation of brain macrophages in neuroinflammation caused by arterial hypertension.

Keywords: neuroinflammation, microglia, macrophages, spontaneously hypertensive rats, immunohistochemistry

Funding: the study received financil support from the Russian Science Foundation, project No. 24-15-00032, https://rscf.ru/en/project/24-15-00032/

Author contribution: Razenkova VA — setting up immunohistochemistry reactions, interpretation of results, image manipulation, manuscript writing; Korzhevskii DE — concept, study planning, literature review, manuscript editing.

Compliance with ethical standards: the study approved by the Ethics Committee of the Institute of Experimental Medicine (protocol No. 2/24 dated 25 April 2024) was conducted in accordance with provisions of the Declaration of Helsinki (2013)

✉ **Correspondence should be addressed:** Valeria A. Razenkova
Akademika Pavlova, 12, Saint Petersburg, 197376, Russia; valeriya.raz@yandex.ru

Received: 04.02.2026 **Accepted:** 21.02.2026 **Published online:** 28.02.2026

DOI: 10.24075/brsmu.2026.008

Copyright: © 2026 by the authors. **Licensee:** Pirogov University. This article is an open access article distributed under the terms and conditions of the Creative Commons Attribution (CC BY) license (https://creativecommons.org/licenses/by/4.0/).

ОЦЕНКА ФУНКЦИОНАЛЬНОЙ АКТИВНОСТИ МИКРОГЛИИ И МАКРОФАГОВ В АССОЦИИРОВАННЫХ С БАРЬЕРАМИ ОБЛАСТЯХ ГОЛОВНОГО МОЗГА СПОНТАННО-ГИПЕРТЕНЗИВНЫХ КРЫС

В. А. Разенкова✉, Д. Э. Коржевский

Институт экспериментальной медицины, Санкт-Петербург, Россия

Нарушение мозгового кровотока при артериальной гипертензии приводит к развитию нейровоспаления, активными участниками которого являются микроглия и макрофаги головного мозга. Целью работы было изучение функциональной активности и иммунофенотипа микроглии и макрофагов в области барьеров головного мозга спонтанно-гипертензивных крыс (SHR). Использовали материал головного мозга крыс-самцов Вистар и SHR (возраст 3–4 месяца, n = 10). Работа выполнена с применением методов иммуногистохимического анализа и конфокальной лазерной микроскопии. Оценивали наличие маркера М2 активации (CD206) и фагоцитарной активности (CD68) в популяции микроглии и макрофагов. Показано, что белок CD206 присутствует в периваскулярных клетках, число которых значительно увеличено у крыс SHR (40,69 ± 4,87 клеток на 1 мм^2 против 28,73 ± 1,39 у крыс Вистар; t-test, p = 0,0007). Проведенный количественный анализ позволил выявить тенденцию увеличения доли фагоцитирующих клеток в головном мозге у крыс SHR по сравнению с крысами Вистар. Изменений в распределении белка CD68 у крыс SHR не выявлено, следовательно, активация микроглии и макрофагов не сопровождается усилением фагоцитарной активности. Полученные результаты свидетельствуют об альтернативной активации макрофагов головного мозга при нейровоспалении, вызванном артериальной гипертензией.

Ключевые слова: нейровоспаление, микроглия, макрофаги, спонтанно-гипертензивные крысы, иммуногистохимия

Финансирование: исследование выполнено при финансовой поддержке Российского Научного Фонда, проект № 24-15-00032, https://rscf.ru/project/24-15-00032/

Вклад авторов: В. А. Разенкова — постановка иммуногистохимических реакций, интерпретация результатов, работа с изображениями, подготовка рукописи; Д. Э. Коржевский — концепция, планирование исследования, анализ литературы, редактирование текста рукописи.

Соблюдение этических стандартов: исследование одобрено этическим комитетом ФГБНУ «ИЭМ» (протокол № 2/24 от 25 апреля 2024 г.), проведено в соответствии с положениями Хельсинкской декларации (2013 г.)

✉ **Для корреспонденции:** Валерия Алексеевна Разенкова
ул. Академика Павлова, д. 12, г. Санкт-Петербург, 197376, Россия; valeriya.raz@yandex.ru

Статья получена: 04.02.2026 **Статья принята к печати:** 21.02.2026 **Опубликована онлайн:** 28.02.2026

DOI: 10.24075/vrgmu.2026.008

Авторские права: © 2026 принадлежат авторам. **Лицензиат:** РНИМУ им. Н. И. Пирогова. Статья размещена в открытом доступе и распространяется на условиях лицензии Creative Commons Attribution (CC BY) (https://creativecommons.org/licenses/by/4.0/).

Macrophages of the brain represent a multicomponent diverse cell population. These include microglia of the brain's nervous tissue, macrophages of the meninges, perivascular areas, and choroid plexus, as well as the monocyte-derived macrophages migrating from the vascular bed into the nervous tissue in various disorders [1]. Such population diversity, regional specificity, as well as high plasticity of microglia and macrophages determine the versatility of their morphological and functional characteristics. In the last decade, numerous studies focused on the origin and morphofunctional heterogeneity of

these immune system cells were conducted. Thus, several border-assosiated microglia and macrophage subtypes under physiological conditions and in neuroinflammation associated with various CNS disorders were described [2–4].

In particular, microglia is involved in regulation of blood flow through cerebral blood vessels and preservation of the blood-brain barrier (BBB) integrity. It has been shown that when inflammation is triggered microglia phagocytizes the astrocyte terminal processes, disrupting the BBB integrity [5], while selective microgliocyte elimination results in microvascular dysfunction [6]. Perivascular macrophages are capable of presenting exogenous antigens by MHC class II. Therefore, these represent T-cell infiltration sites in autoimmune disorders, Alzheimer's and Parkinson's diseases [7]. Epiplexus macrophages of the brain's choroid plexus, or Kolmer cells, limit the amount of peripheral blood molecules, as well as pathogens and lymphocytes, entering the cerebrospinal fluid under the conditions of invasion and tissue damage [8]. Perivascular and epiplexus macrophages generate more reactive oxygen species in response to the increase in blood or cerebrospinal fluid levels of certain compounds, which can aggravate the disease [9]. In contrast, some data demonstrate that perivascular and meningeal macrophages contribute to β-amyloid clearance in Alzheimer's disease or cerebral amyloid angiopathy [10]. Taken together, the data suggest that the contribution of macrophages to neuroinflammation depends on numerous factors, which opens large-scale prospects for modulation of their activity, and, consequently, the use of this approach for therapeutic purposes.

However, it is difficult to clearly delineate microglia and macrophage subtypes in the CNS due to limited specificity of most marker proteins, such as CD11b, F4/80, CX3CR1, CD45, and Iba-1 [11]. Immunophenotypic characteristics of epiplexus macrophages match the characteristics of other mononuclear phagocytes comprising the MHC II, CD11b, CD68, and Iba-1 marker proteins [12]. In addition, when culturing cells *ex vivo*, microgliocytes lose their characteristic features (morphological traits, genetic and epigenetic markers), and become virtually indistinguishable from macrophages [13]. In this regard, immunophenotyping of the CNS microglia and macrophages in vivo seems possible only in conjunction with morphological assessment.

Several experimental models simulating pathological features of certain diseases are currently used to study manifestations of neuroinflammation [14]. Thus, arterial hypertension, which is considered a serious health problem for people worldwide [15] and can be a neuroinflammation pathology model, is associated with impaired inflammation regulation. Spontaneusly hypertensive rats (SHR) are used for standardized hypertension. The research shows that in SHR the cerebral blood flow impairment associated with chronic hypertension leads to inflammation, which can result in neurodegeneration [16]. The results of the study focused on the brain immune system characteristics in arterial hypertension show that microglia of SHR shows morphological signs of activation [17–19]. Preliminary data were also obtained that made it possible to predict the type of polarization of activated microglial cells in SHR [20].

Disruption of the blood-brain and blood-cerebrospinal fluid barriers [16, 21] resulting from the decreased elasticity of cerebral blood vessels caused by remodeling of their cellular layers is a typical manifestation of arterial hypertension reported for SHR. Thus, the response of microglia and macrophages to systemic and local pro-inflammatory stimuli turns out to be most pronounced in the zones of the blood-brain, blood-cerebrospinal fluid, and cerebrospinal fluid-brain barriers. Nevertheless, morphofunctional state of the brain's immune cells in the zones of barriers in this disorder is still poorly understood.

The study aimed to assess functional activity and immunophenotype of microglia and macrophages in the subependymal zone of the lateral and third ventricles, as well as in the choroid plexus of the SHR brain.

METHODS

Brain specimens of male Wistar rats and SHR with the body weight of 250–300 g (age 3–4 months, n = 10) fixed in zinc-ethanol-formaldehyde and paraffin-embedded in accordance with the standard method were used for immunophenotyping of microglia and macrophages in normotensive and hypertensive animals. When forming groups of animals with arterial hypertension, SHR with the average systolic blood pressure equal to or above 200 mHg were selected. Blood pressure of SHR was measured before biomaterial collection using the Systola noninvasive blood pressure measurement system (Neurobotics, Russia).

Identification of microglia and macrophages in brain sections was performed using antibodies against the Iba-1 protein (ab5076, Abcam, UK and ET-1705-78, Huabio, China), CD68 lysosomal glycoprotein (GB113109, Servicebio, China), and CD206 mannose receptor (HA722892, Huabio, China).

Reagents from the UltraVision Quanto Detection System HRP (TL-060-QHL, Fisher Scientific, USA), anti-Goat HRP-DAB Cell & Tissue Staining Kit (CTS008, R&D Systems, USA), Mouse and Rabbit Specific HRP/DAB IHC Detection Kit (ab236466, Abcam, UK) were used as secondary reagents. The 3'3-diaminobenzidine chromogen from the Stable DAB/Plus kit (Diagnostic BioSystems, USA) was used for the monoenzyme reaction product visualization. For immunofluorescence, the sections incubated in secondary antibodies were treated with the Cy2 fluorochrome-conjugated streptavidin (016-220-084, Jackson ImmunoResearch, USA) and the solution of the Cy3 fluorochrome-conjugated goat anti-horseradish peroxidase antibody (123-165-021, Jackson ImmunoResearch, USA).

The resulting preparations were assessed using the Leica DM750 microscope (Germany) and the LSM800 confocal laser microscope equipped with the Airyscan system. Immunomorphological analysis of microglia and macrophages was performed in the barrier zones adjacent to brain centers: ependyma of the lateral and third ventricles (in the area of striatum and mediobasal hypothalamus, respectively), pia mater, lateral ventricular choroid plexus. The expert, who performed morphological and quantitative assessment of the preparations obtained, was blinded in terms of information about the test objects.

Quantification involved enumeration of cells in three fields of view for each preparation using the ×10 and ×20 lens magnification, then standardization based on the scale length of 1 mm^2 was applied (the number of values used to calculate the mean for each case was 6). The percentage of cells containing two markers (Iba-1 and CD68) was calculated by dividing the Iba-1^+/$CD68^+$ cell counts by the Iba-1^+ cell counts. To analyze the images, the ImageJ2 program in the FIJI extension was used (https://imagej.net/software/fiji/). The Coloc2 (https://imagej.net/plugins/coloc-2) and Colocalization Finder (http://rsb.info.nih.gov/ij/plugins/colocalization-finder.html) were used to assess co-localization of the studied markers. Pearson's correlation coefficients were determined for various brain areas of Wistar rats and SHR: subependymal zone of the lateral and

Table 1. Systolic blood pressure in SHR

Rat No.	Systolic blood pressure, mmHg			
	First measurement	Second measurement	Third measurement	Mean
1	211	201	229	214
2	215	203	207	208
3	200	222	235	219
4	251	235	240	242
5	208	209	210	209

third ventricles, choroid plexus. Statistical processing was performed in GraphPad Prism 8 (GraphPad Software, USA). The samples were tested for normality using the Shapiro–Wilk test for small samples. The distribution was considered normal at $p > 0.05$. One-way and two-way ANOVA was used to compare the data, with subsequent comparison of the group using the post-hoc Tukey's test and the Kruskal–Wallis test involving the use of the post-hoc Dunn's test. The data were provided as the mean ± standard deviation. The differences were considered significant at $p < 0.05$.

RESULTS

The results of blood pressure measurement in the SHR selected for the study are provided in Table 1.

Immunohistochemical staining of CD206 in brain sections of Wistar and SHR revealed perivascular cells (in the nervous tissue of the brain and the choroid plexus) and cells of the pia mater (Fig. 1). No cells staining positive for CD206 were reported in the nervous tissue of the brain. The average $CD206^+$ cell counts per 1 mm^2 higher in rats with genetically determined arterial hypertension (*t*-test, $p = 0.0007$), these were 40.69 ± 4.87 cells (vs. 28.73 ± 1.39 in Wistar rats).

The use of double immunohistochemical staining made it possible to identify microglia and macrophages ($Iba\text{-}1^+$) containing the CD68 protein (Fig. 2). These are found in all the studied barrier zones (subependymal zone of the lateral and third ventricles, choroid plexus) and have specific morphological features. Near the ependyma of the lateral and third ventricles these represent typical dendritic subependymal microgliocytes of the basket-like and spindle-like morphotype. The $CD68^+$ granule distribution in the cytoplasm of these cells corresponds to general ideas about the localization of lysosomes. Cells of the choroid plexus are characterized by the sparsely-branched or spindle-like morphotype, and their $CD68^+$ granules are also distributed in the areas of lysosome localization. We should also mention the cells associated with neither ependyma, nor choroid plexus, but distributed freely in the ventricular lumen. Such cells were usually found in the preparations from SHR. The CD68 protein granules in the intraventricular cells occupied almost the entire cytoplasm, concealing the nucleus (Fig. 2a).

The differences in the quantitative distribution of $Iba\text{-}1^+$/$CD68^+$ microgliocytes and macrophages in various barrier zones of the brain turn out to be region-specific, which is confirmed by the analysis of variance ($F = 117.4$, $p < 0.0001$). Thus, it has been shown that the highest percentage of

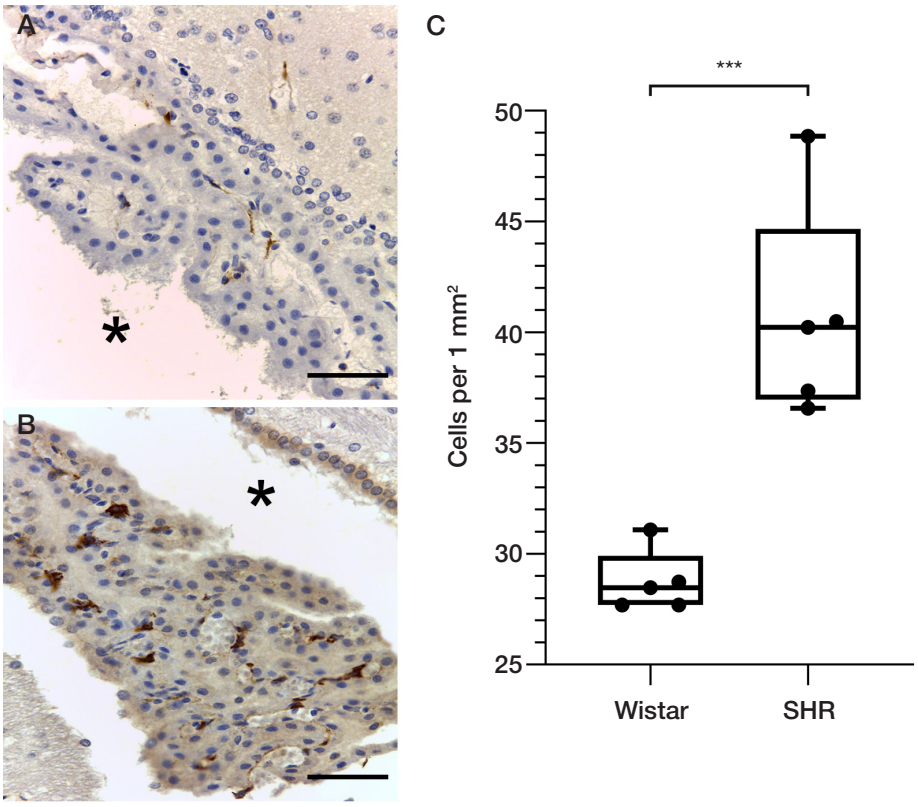

Fig. 1. CD206 in the choroid plexus of the brain of Wistar rats **(A)**, SHR **(B)**. Immunohistochemical staining of CD206 with hematoxylin staining of nuclei. The lateral ventricular cavity is marked by an asterisk. **C**. Difference between $CD206^+$ counts in rats of different lineages, *p*-value < 0.01. The line inside the box plot represents the median (Me). The scale bar is 50 μm

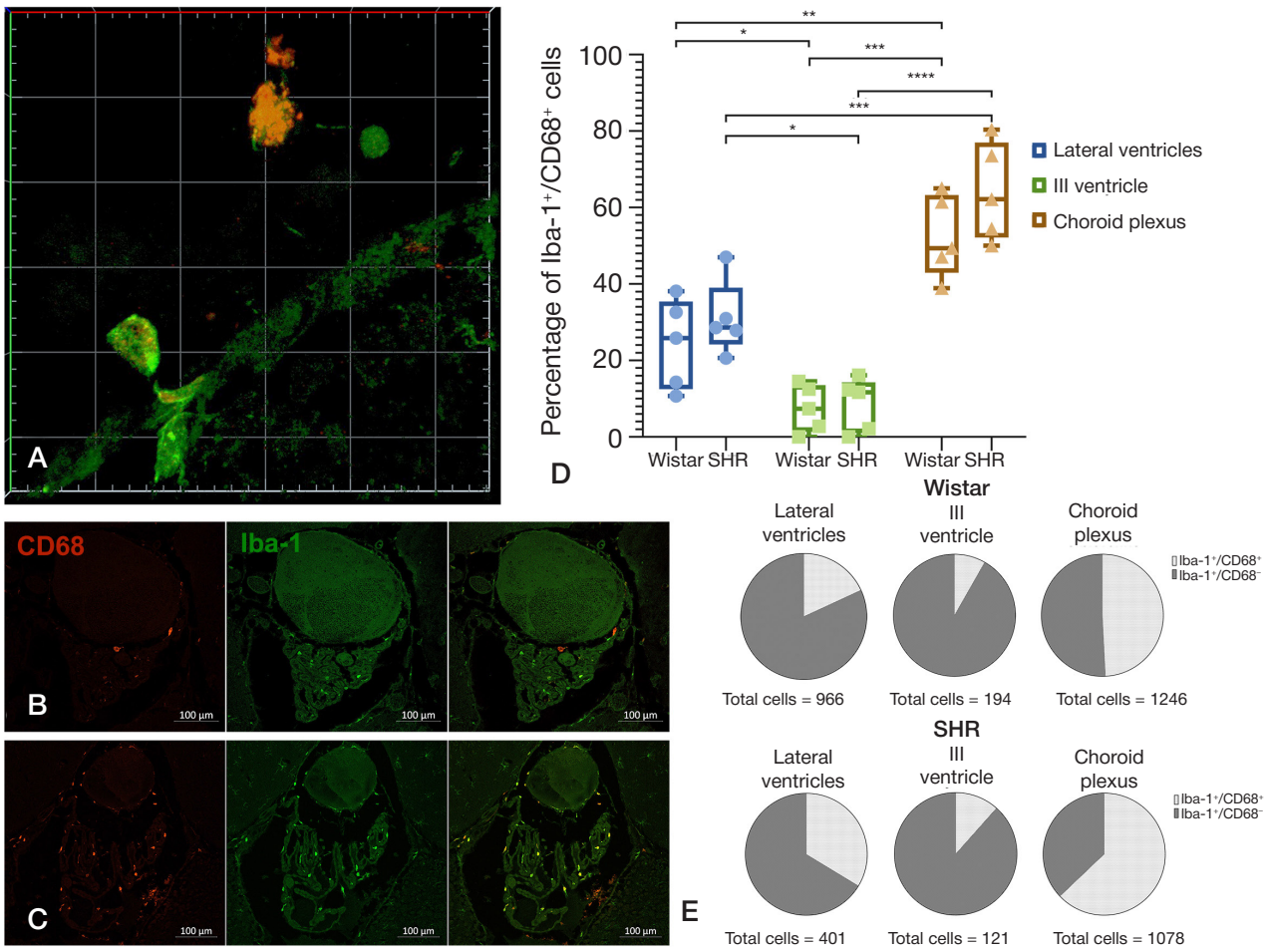

Fig. 2. Quantitative analysis results. Double immunohistochemical CD68 (*red channel*) and Iba-1 (*green channel*) stain. **A**–**C**. Overall view of subependymal microglia of the lateral **(A)** and third (**B**, **C**) ventricles. **A**. Subependymal and intraventricular microglia of SHR, 3D reconstruction of a series of optic slices, measuring grid cell size 10 × 10 μm, Wistar rats **(B)**, SHR **(C)**. **D**, **E**. Comparison results for the percentage of the cells staining positive for two markers, box plot **(D)** and pie chart **(E)**. *P*-value: * — < 0.05; ** — < 0.01; *** — < 0.001. The line inside the box plot represents the median (Me)

Iba-1$^+$/CD68$^+$ cells is observed in the choroid plexus. In the subependymal zone of the lateral and third ventricles, the content of double-immunopositive cells is not so high (Table 2). Quantification revealed no significant differences between the groups of normotensive and hypertensive rats ($F = 2.19$, $p = 0.16$). However, the data of the SHR sample are slightly displaced relative to the Wistar rat sample (Fig. 2D, E) toward the increase in the percentage of the cells staining positive for two markers.

The analysis of co-localization (Fig. 3) yielded the average correlation values for each area in both groups (Wistar rats and SHR; Table 3). In all the cases, the correlation criterion accepts the values that are enough for co-localization to be considered non-random (the criterion values are different from zero). However, no apparent displacement of values associated with arterial hypertension was reported (two-way ANOVA, $F = 0.56$, $p = 0.48$). Furthermore, there were also no significant differences in the level of correlation of the Iba-1 and CD68 revealed when analyzing different areas of interest (two-way ANOVA, $F = 3.45$, $p = 0.06$).

DISCUSSION

Macrophages play a special role in maintaining tissue homeostasis, neutralization of pathogens and aberrant cells, as well as initiation and modulation of adaptive immunity due to their phagocytic activity, capacity for efferocytosis and antigen presentation. The decades of research focused on physiological and cytochemical features of macrophages of various organs in inflammation made it possible to reveal two major functional states designated as M1 and M2 polarization types [22]. Later the scientific community gradually moved away from the rigid dichotomy concept and concluded that the macrophage functional states represented a wide range of phenotypes, from the pro-inflammatory M1 to the reparative M2 [23, 24]. Further division into subtypes made it possible to more accurately characterize the role of these cell populations in inflammation and develop individual therapeutic strategies for treatment of various disorders [25].

It is assumed that the brain's microglia shows similar polarization features during activation [26], which enables

Table 2. Percentage of Iba-1$^+$/CD68$^+$ cells in various brain areas of Wistar rats and SHR. The data are provided as the mean ± standard deviation

Area	Wistar	SHR
Subependymal zone of the lateral ventricles	24.31 ± 11.68	30.99 ± 9.727
Subependymal zone of the III ventricle	7.435 ± 6.178	8.442 ± 6.987
Choroid plexus	52.34 ± 10.72	64.09 ± 12.75

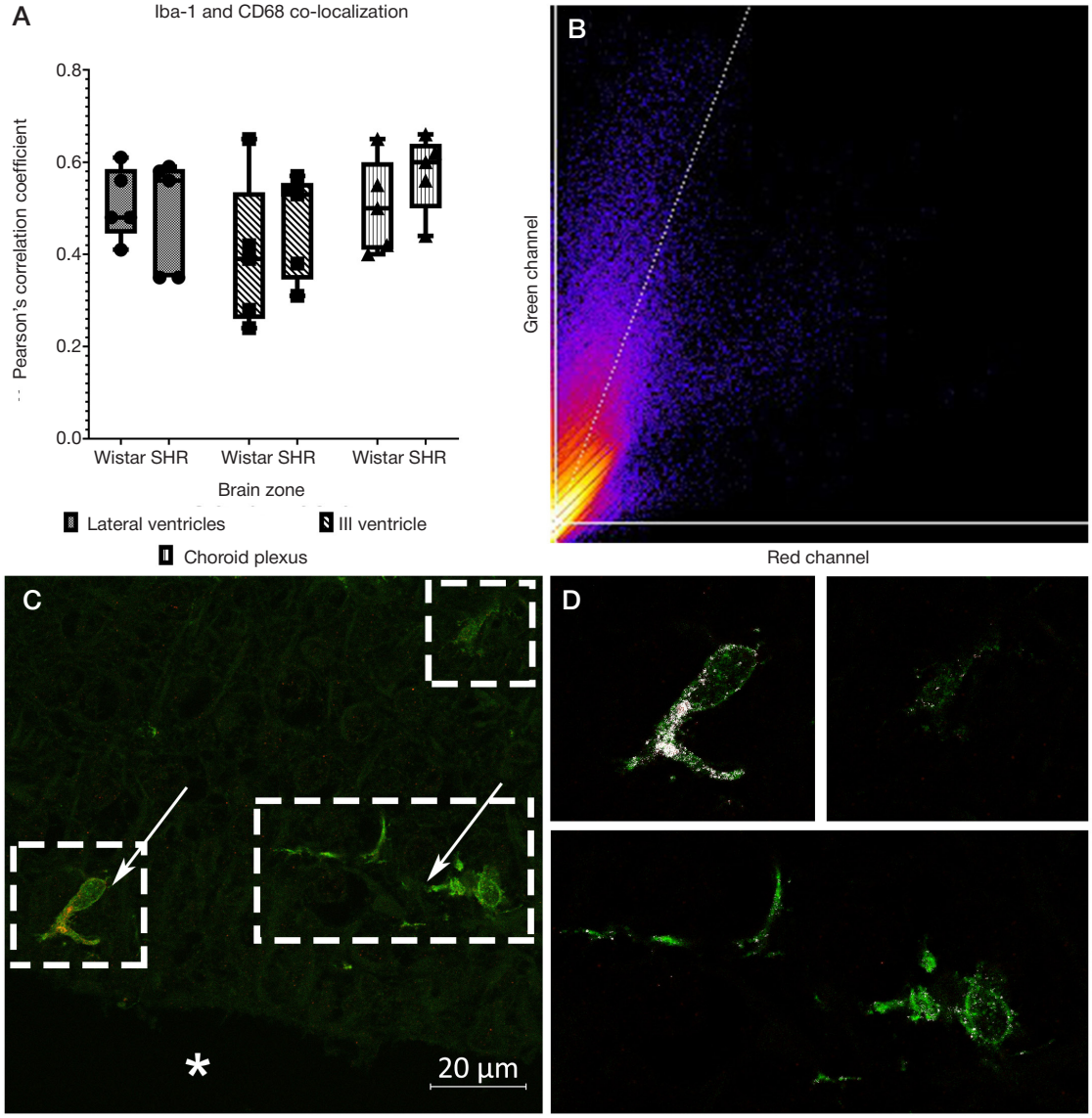

Fig. 3. Co-localization analysis results. Double immunohistochemical Iba-1 (*green channel*) and CD68 (*red channel*) stain. **A**. Pearson's correlation coefficients in various brain areas of Wistar rats and SHR. **B**. Correlation diagram of two channels. **C**. Microglia of the third ventricular floor. **D**. Co-localization of Iba-1 and CD68. Sites of marker co-localization are highlighted in *white* in Fig. **D**. Arrows point at microglia, *frames* show the areas presented in Fig. **D**, the ventricular cavity is marked by an *asterisk*. The line inside the box plot represents the median (Me)

the use of the existing paradigm for comparative studies and extrapolation of the results obtained for various organs. However, microgliocytes differ from other macrophages in both histogenesis and a number of structural characteristics [2, 27]. In this case, it is necessary to use a differentiated approach to assessment of microglia and macrophages considering their features.

The earlier reported study showed that microglia of the rats with genetically determined arterial hypertension could show increased phagocytic activity [11]. In this study, a hypothesis was tested about the possibility of M2a polarization of the brain's microglia in SHR.

It is well known that the activated M2a macrophages are capable of endocytosis, these stimulate cellular growth and tissue regeneration [25]. In laboratory rodents, the most typical M2a subtype marker proteins include CD206, Fizz1, Ym1/2, and arginase 1 [28]. The CD206 mannose receptor was selected for assessment of functional activity of the brain's immune cells based on the characteristics of the proposed markers [29] and the results of the screening immunohistochemistry testing involving the use of various antibodies.

The immunohistochemistry staining results obtained and subsequent quantification show a significant increase in $CD206^+$ cell number in SHR, which may indicate a shift towards M2a polarization type. This allows us to provide further directions in the field of immunophenotyping of microglia and macrophages of the SHR CNS, for example, by multiplex immunohistochemistry involving the use of the broad antibody panel against proteins specific for the M2a phenotype.

Table 3. Pearson's correlation coefficient in various brain areas of Wistar and SHR rats. The data are provided as the mean ± standard deviation

Area	Wistar	SHR
Subependymal zone of the lateral ventricles	0.51 ± 0.08	0.49 ± 0.12
Subependymal zone of the III ventricle	0.4 ± 0.16	0.47 ± 0.11
Choroid plexus	0.5 ± 0.1	0.58 ± 0.08

Identification of the role of macrophages in arterial hypertension attracts the researchers' attention. It is noted that SHR have the increased levels of intestinal CD11b$^+$ cells inhibiting the release of pro-inflammatory cytokines. However, the SHR levels of pro-inflammatory cytokines are also increased compared to the control group [30]. In contrast, it is noted that M1 macrophages predominate in the abdominal cavity by month 4, but the difference in the quantity of the M1- and M2-polarized cells becomes smaller as early as by month 6 [31]. The authors assume that macrophages of different organs will also acquire different immunophenotypes, i.e. M1 can predominate in one organ and M2 can predominate in another one. This can be due to the fact that tissue-resident macrophages can attract the immune cells arriving to the tissues from different sources, which, in turn, are influenced by the region-specific microenvironment. Apparently, in arterial hypertension, the nervous tissue microenvironment reinforces the need for at least CD206 expression increase and at most M2a polarization of the brain's macrophages.

However, localization of those is limited to perivascular spaces, pia mater, and the choroid plexus. The cells staining positive for CD206 specifically in the brain's nervous tissue were reported in none of the studied cases.

The lack of CD206 marker in dendritic microglia and the fact of finding CD206 in typical macrophages only can indicate differences in the expression profiles of activation markers in microgliocytes and macrophages. Nevertheless, the results of certain studies are likely to be in conflict with this assumption. In one of the recent reports focused on functional heterogeneity of the CNS glial cells, the authors admit the possibility of existence of the CD206$^+$ microglia population [13]. The original research results obtained by flow cytometry show that some human P2Y12$^+$ cells can have low CD206 protein levels [32]. Another study reported simultaneous CD32 and CD206 expression in microgliocytes under combined exposure to electromagnetic field and the TNFα neuroinflammation inducer [33]. The authors interpret the emergence of such a combination of markers in favor of tissue restoration in response to damaging effects. In rodents, the emergence of CD206$^+$ microglia was reported in spinal cord injuries [34] and during early postnatal development [35]. Considering the fact that the above studies involved cell cultures and the use of flow cytometry, these data are not strictly comparable with immunohistochemistry assessment results.

The presence of CD206 in the rat brain's microglia detected by immunohistochemistry was, for example, reported in the paper focused on the effect of quercetin on activation of the brain's immune cells [36]. Co-localization of Iba-1 and CD206 proteins is clearly visible in the brain sections acquired after the exposure to quercetin having anti-inflammatory and antioxidant effects and presumably contributing to type M2 microglia activation. However, in ischemic/reperfusion damage, the microglial response to antiCD206 antibodies was rather weak, and there was no immunohistochemical response in the control group. In contrast, in mice with the Alzheimer's disease-associated neuroinflammation [37], no CD206 and Iba-1 co-localization was revealed. In this regard, the authors conclude that the CD206$^+$ macrophages and Iba-1$^+$ microglial cells represent different populations. Furthermore, the use of antibodies against marker proteins of macrophages (such as CD206 and Iba-1) also does not give us all information about the origin of the cells found in brain sections. That is why it seems difficult to perfectly distinguish microglia, microglia-like cells, and macrophages that infiltrate the brain. Thus, the hypothesis about the possibility or impossibility of the CD206 mannose receptor expression by microglia in rats with various nervous system states needs further verification.

The quantitative analysis results obtained in this study allowed us to determine readiness for phagocytosis of microglia cells and macrophages based on the presence of functional lysosomes that are detectable due to the presence of macrosialin (CD68), the transmembrane glycoprotein of lysosomes and phagosomes [38].

When assessing co-localization of the Iba-1 and CD68 proteins, it was hypothesized that the Iba-1$^+$/CD68$^+$ microglia reported in the vicinity of brain barriers in SHR was in active state. The Pearson's correlation coefficient was selected to compare Iba-1 and CD68 protein co-localization levels due to the ease of interpretation of values. Its values vary from –1 to 1, where "–1" indicates a complete negative, "1" a complete positive, and "0" a random correlation [39]. In both Wistar rats and SHR, co-localization of proteins in all the studied zones was non-random (the spread in mean values was 0.4–0.6). However, the quantification performed suggests the lack of significant differences in Iba-1 and CD68 protein co-localization levels.

One more methodological approach involved quantitative assessment of the percentage of cells staining positive for two markers relative to the general population of Iba-1$^+$ cells in the choroid plexus, as well as near the ependyma of the lateral and third ventricles. It was noted that the largest percentage of Iba-1$^+$/CD68$^+$ cells was typical for the brain's choroid plexus, where a specific macrophage population (Kolmer cells) was localized [40]. The nature of these cells is still a matter of debate, but their function is associated with active phagocytosis. The least percentage of double immunopositive cells is reported for the subependymal zone of the third ventricle in the area of hypothalamus, which is likely to result from the presence of specific glial cells (tanycytes) in the ependyma. Tanycytes ensure bidirectional transport of bioactive molecules between cerebrospinal fluid and blood [41]. The subependymal zone of the lateral ventricles, which does not have such a lining, occupies an intermediate position.

Despite the fact that the analysis of variance revealed no significant differences between the percentage of cells staining positive for Iba-1 and CD68 in different rat strain, the analysis of descriptive statistics shows that the data of the SHR sample are displaced relative to the Wistar rat sample towards the increase in the counts of such cells. In particular, the median, as well as minimum and maximum values can be higher (Fig. 2). The findings suggest heterogeneity of the studied SHR group, regardless of the selection performed based on blood pressure. Larger samples should be used for further research.

The data obtained suggest that rats with arterial hypertension can show activation of phagocytic activity of microglia and macrophages in the zones of the blood-brain, blood-cerebrospinal fluid, and cerebrospinal fluid-brain barriers. Furthermore, considering the co-localization analysis results, it is necessary to emphasize that it is probably the number, but not the functional activity level of cells that changes.

CONCLUSIONS

Neuroinflammation caused by arterial hypertension in SHR results in polarization shift towards M2 variant in macrophages of the pia mater, choroid plexus, and perivascular spaces. The population affiliation of the brain's CD206$^+$ cells remains unclear and should be clarified through further research using double immunohistochemical labeling. Activation of microglia and macrophages in SHR is apparently not accompanied by the

increase in the phagocytic activity of these cells. The identified trend towards the increase in the percentage of Iba-1$^+$/CD68$^+$ cells in the SHR brain compared to the Wistar rat brain can result from intrapopulation differences; it can also be a sign of the increase in the percentage of active phagocytes. Further research is required to test these hypetheses.

References

1. Silvin A, Qian J, Ginhoux F. Brain macrophage development, diversity and dysregulation in health and disease. Cell Mol Immunol. 2023; 20: 1277–89.
2. Li Q, Barres BA. Microglia and macrophages in brain homeostasis and disease. Nat Rev Immunol. 2017; 18 (4): 225–42.
3. Brioschi S, Zhou Y, Colonna M. Brain macrophages in development, homeostasis and disease. J Immunol [Internet]. 2020 Jan 15 [cited 2026 Jan 15]; 204 (2): 294. Available from: https://pmc.ncbi.nlm.nih.gov/articles/PMC7034672/.
4. Mrdjen D, Pavlovic A, Hartmann FJ, Schreiner B, Utz SG, Leung BP, et al. High-dimensional single-cell mapping of central nervous system immune cells reveals distinct myeloid subsets in health, aging, and disease. Immunity [Internet]. 2018 Feb 20 [cited 2026 Jan 15]; 48 (2): 380–95.e6. Available from: https://www.sciencedirect.com/science/article/pii/S1074761318300323?via%3Dihub.
5. Haruwaka K, Ikegami A, Tachibana Y, Ohno N, Konishi H, Hashimoto A, et al. Dual microglia effects on blood brain barrier permeability induced by systemic inflammation. Nat Commun. 2019; 10 (1): 5816.
6. Bisht K, Okojie KA, Sharma K, Lentferink DH, Sun Y-Y, Chen H-R, et al. Capillary-associated microglia regulate vascular structure and function through PANX1-P2RY12 coupling in mice. Nat Commun. 2021; 12 (1): 5289.
7. Taketomi T, Tsuruta F. Towards an understanding of microglia and border-associated macrophages. Biology (Basel). 2023 Aug 5; 12 (8): 1091.
8. Engelhardt B, Vajkoczy P, Weller RO. The movers and shapers in immune privilege of the CNS. Nat Immunol. 2017; 18 (2): 123–31.
9. Vara-Pérez M, Movahedi K. Border-associated macrophages as gatekeepers of brain homeostasis and immunity. Immunity. 2025; 58 (5): 1085–100.
10. Greenberg SM, Bacskai BJ, Hernandez-Guillamon M, Pruzin J, Sperling R, van Veluw SJ. Cerebral amyloid angiopathy and Alzheimer disease — one peptide, two pathways. Nat Rev Neurol. 2020; 16 (1): 30–42.
11. Amici SA, Dong J, Guerau-de-Arellano M. Molecular mechanisms modulating the phenotype of macrophages and microglia. Front Immunol. 2017; 8: 1520.
12. Wan Y, Hua Y, Garton HJL, Novakovic N, Keep RF, Xi G. Activation of epiplexus macrophages in hydrocephalus caused by subarachnoid hemorrhage and thrombin. CNS Neurosci Ther. 2019; 25 (10): 1134–41.
13. Kotova MM, Apukhtin KV, Nikitin VS, Kalueff AV. On functional heterogeneity of micro- and astroglia. Russian Journal of Physiology. 2024; 110 (11): 1824–45. Russian.
14. Tamura Y, Yamato M, Kataoka Y. Animal models for neuroinflammation and potential treatment methods. Front Neurol [Internet]. 2022 Jun 27 [cited 2026 Jan 15]; 13: 890217. Available from: www.frontiersin.org.
15. Guzik TJ, Nosalski R, Maffia P, Drummond GR. Immune and inflammatory mechanisms in hypertension. Nat Rev Cardiol. 2024 Jun; 21 (6): 396–416.
16. Fang Z, Shen G, Amin N, Lou C, Wang C, Fang M. Effects of neuroinflammation and autophagy on the structure of the blood–brain barrier in ADHD model. Neuroscience. 2023; 530: 17–25.
17. Cohen EM, Mohammed S, Kavurma M, Nedoboy PE, Cartland S, Farnham MMJ, et al. Microglia in the RVLM of SHR have reduced P2Y12R and CX3CR1 expression, shorter processes, and lower cell density. Auton Neurosci Basic Clin. 2019; 216: 9–16.
18. Guselnikova VV, Razenkova VA, Sufieva DA, Korzhevskii DE. Activation of microglia in the brain of spontaneously hypertensive rats. Bulletin of RSMU. 2023; (3): 49–55.
19. Kulikova PV, Guselnikova VV. Morphological characterization of glial cells in the Substantia nigra of spontaneously hypertensive SHR rats. Medical academic journal. 2024; 24 (2): 93–9. Russian.
20. Razenkova VA, Kirik OV., Korzhevskii DE. Microglia immunophenotyping in paraffin sections of the brain. Cell Tissue Biol. 2025; 19 (6): 597–604.
21. Gonzalez-Marrero I, Hernández-Abad LG, Castañeyra-Ruiz L, Carmona-Calero EM, Castañeyra-Perdomo A. Changes in the choroid plexuses and brain barriers associated with high blood pressure and ageing. Neurol (English Ed). 2022; 37 (5): 371–82.
22. Mills CD, Kincaid K, Alt JM, Heilman MJ, Hill AM. M-1/M-2 macrophages and the Th1/Th2 paradigm. J Immunol. 2000; 164 (12): 6166–173.
23. Mosser DM, Edwards JP. Exploring the full spectrum of macrophage activation. Nat Rev Immunol. 2008; 8 (12): 958.
24. Xue J, Schmidt S V., Sander J, Draffehn A, Krebs W, Quester I, et al. Transcriptome-based network analysis reveals a spectrum model of human macrophage activation. Immunity. 2014; 40 (2): 274–88.
25. Ji Y, Li X, Yao X, Sun J, Yi J, Shen Y, et al. Macrophage polarization: molecular mechanisms, disease implications, and targeted therapeutic strategies. Front Immunol. 2025 Dec 12; 16: 1732718.
26. Orihuela R, McPherson CA, Harry GJ. Microglial M1/M2 polarization and metabolic states. Br J Pharmacol. 2016; 173 (4): 649–65.
27. Prinz M, Erny D, Hagemeyer N. Ontogeny and homeostasis of CNS myeloid cells. Nat Immunol. 2017; 18 (4): 385–92.
28. Martinez FO, Gordon S. The M1 and M2 paradigm of macrophage activation: time for reassessment. F1000Prime Rep. 2014; 6:13.
29. Rőszer T. Understanding the mysterious M2 macrophage through activation markers and effector mechanisms. Mediators Inflamm. 2015; 2015: 816460.
30. Robles-Vera I, Toral M, de la Visitación N, Sánchez M, Gómez-Guzmán M, Muñoz R, et al. Changes to the gut microbiota induced by losartan contributes to its antihypertensive effects. Br J Pharmacol. 2020; 177 (9): 2006–23.
31. Zhao J, Lu N, Qu Y, Liu W, Zhong H, Tang N, et al. Calcium-sensing receptor-mediated macrophage polarization improves myocardial remodeling in spontaneously hypertensive rats. Exp Biol Med (Maywood). 2024; 249: 10112.
32. Böttcher C, Schlickeiser S, Sneeboer MAM, Kunkel D, Knop A, Paza E, et al. Human microglia regional heterogeneity and phenotypes determined by multiplexed single-cell mass cytometry. Nat Neurosci. 2019 Jan 17; 22 (1): 78–90.
33. Mendoza-Mari Y, Stojanovic M, Miulli DE, Agrawal DK. Microglial response to inflammatory stimuli under electromagnetic field exposure. Arch Clin Biomed Res. 2025; 9 (4): 304–15.
34. Cohen M, Ben-Yehuda H, Porat Z, Raposo C, Gordon S, Schwartz M. Newly formed endothelial cells regulate myeloid cell activity following spinal cord Injury via expression of CD200 ligand. J Neurosci. 2017; 37 (4): 972–85.
35. Lively S, Wong R, Lam D, Schlichter LC. Sex- and development-dependent responses of rat microglia to pro- and anti-inflammatory stimulation. Front Cell Neurosci. 2018; 12: 433.
36. Li L, Jiang W, Yu B, Liang H, Mao S, Hu X, et al. Quercetin improves cerebral ischemia/reperfusion injury by promoting microglia/macrophages M2 polarization via regulating PI3K/Akt/NF-κB signaling pathway. Biomed Pharmacother. 2023; 168: 115653.
37. Paouri E, Tzara O, Kartalou G-I, Zenelak S, Georgopoulos S. Peripheral tumor necrosis factor-alpha (TNF-α) modulates amyloid pathology by regulating blood-derived immune cells and glial response in the brain of AD/TNF transgenic mice. J Neurosci. 2017; 37 (20): 5155–71.
38. Chistiakov DA, Killingsworth MC, Myasoedova VA, Orekhov AN, Bobryshev Y V. CD68/macrosialin: not just a histochemical marker. Lab Invest. 2017; 97 (1): 4–13.

39. Adler J, Parmryd I. Quantifying colocalization by correlation: The Pearson correlation coefficient is superior to the Mander's overlap coefficient. Cytom Part A. 2010; 77A (8): 733–42.
40. Ling E-A, Kaur C, Lu J. Origin, nature, and some functional considerations of intraventricular macrophages, with special reference to the epiplexus cells. Microsc Res Tech. 1998; 41: 43–56.
41. Bolborea M, Dale N. Hypothalamic tanycytes: potential roles in the control of feeding and energy balance. Trends Neurosci. 2013; 36 (2): 91–100.

Литература

1. Silvin A, Qian J, Ginhoux F. Brain macrophage development, diversity and dysregulation in health and disease. Cell Mol Immunol. 2023; 20: 1277–89.
2. Li Q, Barres BA. Microglia and macrophages in brain homeostasis and disease. Nat Rev Immunol. 2017; 18 (4): 225–42.
3. Brioschi S, Zhou Y, Colonna M. Brain macrophages in development, homeostasis and disease. J Immunol [Internet]. 2020 Jan 15 [cited 2026 Jan 15]; 204 (2): 294. Available from: https://pmc.ncbi.nlm.nih.gov/articles/PMC7034672/.
4. Mrdjen D, Pavlovic A, Hartmann FJ, Schreiner B, Utz SG, Leung BP, et al. High-dimensional single-cell mapping of central nervous system immune cells reveals distinct myeloid subsets in health, aging, and disease. Immunity [Internet]. 2018 Feb 20 [cited 2026 Jan 15]; 48 (2): 380–95.e6. Available from: https://www.sciencedirect.com/science/article/pii/S1074761318300323?via%3Dihub.
5. Haruwaka K, Ikegami A, Tachibana Y, Ohno N, Konishi H, Hashimoto A, et al. Dual microglia effects on blood brain barrier permeability induced by systemic inflammation. Nat Commun. 2019; 10 (1): 5816.
6. Bisht K, Okojie KA, Sharma K, Lentferink DH, Sun Y-Y, Chen H-R, et al. Capillary-associated microglia regulate vascular structure and function through PANX1-P2RY12 coupling in mice. Nat Commun. 2021; 12 (1): 5289.
7. Taketomi T, Tsuruta F. Towards an understanding of microglia and border-associated macrophages. Biology (Basel). 2023 Aug 5; 12 (8): 1091.
8. Engelhardt B, Vajkoczy P, Weller RO. The movers and shapers in immune privilege of the CNS. Nat Immunol. 2017; 18 (2): 123–31.
9. Vara-Pérez M, Movahedi K. Border-associated macrophages as gatekeepers of brain homeostasis and immunity. Immunity. 2025; 58 (5): 1085–100.
10. Greenberg SM, Bacskai BJ, Hernandez-Guillamon M, Pruzin J, Sperling R, van Veluw SJ. Cerebral amyloid angiopathy and Alzheimer disease — one peptide, two pathways. Nat Rev Neurol. 2020; 16 (1): 30–42.
11. Amici SA, Dong J, Guerau-de-Arellano M. Molecular mechanisms modulating the phenotype of macrophages and microglia. Front Immunol. 2017; 8: 1520.
12. Wan Y, Hua Y, Garton HJL, Novakovic N, Keep RF, Xi G. Activation of epiplexus macrophages in hydrocephalus caused by subarachnoid hemorrhage and thrombin. CNS Neurosci Ther. 2019; 25 (10): 1134–41.
13. Котова ММ, Апухтин КВ, Никитин ВС, Калуев АВ. К вопросу о функциональной гетерогенности микроглии и астроглии. Российский физиологический журнал им ИМ Сеченова. 2024; 110 (11): 1824–45.
14. Tamura Y, Yamato M, Kataoka Y. Animal models for neuroinflammation and potential treatment methods. Front Neurol [Internet]. 2022 Jun 27 [cited 2026 Jan 15]; 13: 890217. Available from: www.frontiersin.org.
15. Guzik TJ, Nosalski R, Maffia P, Drummond GR. Immune and inflammatory mechanisms in hypertension. Nat Rev Cardiol. 2024 Jun; 21 (6): 396–416.
16. Fang Z, Shen G, Amin N, Lou C, Wang C, Fang M. Effects of neuroinflammation and autophagy on the structure of the blood–brain barrier in ADHD model. Neuroscience. 2023; 530: 17–25.
17. Cohen EM, Mohammed S, Kavurma M, Nedoboy PE, Cartland S, Farnham MMJ, et al. Microglia in the RVLM of SHR have reduced P2Y12R and CX3CR1 expression, shorter processes, and lower cell density. Auton Neurosci Basic Clin. 2019; 216: 9–16.
18. Гусельникова В. В., Разенкова В. А., Суфиева Д. А., Коржевский Д. Э. Активация микроглии в головном мозге спонтанно гипертензивных крыс. Вестник Российского государственного медицинского университета. 2023; (3): 53–60.
19. Куликова П. В., Гусельникова В. В. Морфологическая характеристика клеток глии черного вещества головного мозга у спонтанно гипертензивных крыс линии SHR. Медицинский академический журнал. 2024; 24 (2): 93–99.
20. Razenkova VA, Kirik OV., Korzhevskii DE. Microglia immunophenotyping in paraffin sections of the brain. Cell Tissue Biol. 2025; 19 (6): 597–604.
21. Gonzalez-Marrero I, Hernández-Abad LG, Castañeyra-Ruiz L, Carmona-Calero EM, Castañeyra-Perdomo A. Changes in the choroid plexuses and brain barriers associated with high blood pressure and ageing. Neurol (English Ed). 2022; 37 (5): 371–82.
22. Mills CD, Kincaid K, Alt JM, Heilman MJ, Hill AM. M-1/M-2 macrophages and the Th1/Th2 paradigm. J Immunol. 2000; 164 (12): 6166–173.
23. Mosser DM, Edwards JP. Exploring the full spectrum of macrophage activation. Nat Rev Immunol. 2008; 8 (12): 958.
24. Xue J, Schmidt S V., Sander J, Draffehn A, Krebs W, Quester I, et al. Transcriptome-based network analysis reveals a spectrum model of human macrophage activation. Immunity. 2014; 40 (2): 274–88.
25. Ji Y, Li X, Yao X, Sun J, Yi J, Shen Y, et al. Macrophage polarization: molecular mechanisms, disease implications, and targeted therapeutic strategies. Front Immunol. 2025 Dec 12; 16: 1732718.
26. Orihuela R, McPherson CA, Harry GJ. Microglial M1/M2 polarization and metabolic states. Br J Pharmacol. 2016; 173 (4): 649–65.
27. Prinz M, Erny D, Hagemeyer N. Ontogeny and homeostasis of CNS myeloid cells. Nat Immunol. 2017; 18 (4): 385–92.
28. Martinez FO, Gordon S. The M1 and M2 paradigm of macrophage activation: time for reassessment. F1000Prime Rep. 2014; 6:13.
29. Rőszer T. Understanding the mysterious M2 macrophage through activation markers and effector mechanisms. Mediators Inflamm. 2015; 2015: 816460.
30. Robles-Vera I, Toral M, de la Visitación N, Sánchez M, Gómez-Guzmán M, Muñoz R, et al. Changes to the gut microbiota induced by losartan contributes to its antihypertensive effects. Br J Pharmacol. 2020; 177 (9): 2006–23.
31. Zhao J, Lu N, Qu Y, Liu W, Zhong H, Tang N, et al. Calcium-sensing receptor-mediated macrophage polarization improves myocardial remodeling in spontaneously hypertensive rats. Exp Biol Med (Maywood). 2024; 249: 10112.
32. Böttcher C, Schlickeiser S, Sneeboer MAM, Kunkel D, Knop A, Paza E, et al. Human microglia regional heterogeneity and phenotypes determined by multiplexed single-cell mass cytometry. Nat Neurosci. 2019 Jan 17; 22 (1): 78–90.
33. Mendoza-Mari Y, Stojanovic M, Miulli DE, Agrawal DK. Microglial response to inflammatory stimuli under electromagnetic field exposure. Arch Clin Biomed Res. 2025; 9 (4): 304–15.
34. Cohen M, Ben-Yehuda H, Porat Z, Raposo C, Gordon S, Schwartz M. Newly formed endothelial cells regulate myeloid cell activity following spinal cord Injury via expression of CD200 ligand. J Neurosci. 2017; 37 (4): 972–85.
35. Lively S, Wong R, Lam D, Schlichter LC. Sex- and development-dependent responses of rat microglia to pro- and anti-inflammatory stimulation. Front Cell Neurosci. 2018; 12: 433.
36. Li L, Jiang W, Yu B, Liang H, Mao S, Hu X, et al. Quercetin improves cerebral ischemia/reperfusion injury by promoting microglia/macrophages M2 polarization via regulating PI3K/Akt/NF-κB signaling pathway. Biomed Pharmacother. 2023; 168: 115653.
37. Paouri E, Tzara O, Kartalou G-I, Zenelak S, Georgopoulos S. Peripheral tumor necrosis factor-alpha (TNF-α) modulates amyloid

pathology by regulating blood-derived immune cells and glial response in the brain of AD/TNF transgenic mice. J Neurosci. 2017; 37 (20): 5155–71.
38. Chistiakov DA, Killingsworth MC, Myasoedova VA, Orekhov AN, Bobryshev Y V. CD68/macrosialin: not just a histochemical marker. Lab Invest. 2017; 97 (1): 4–13.
39. Adler J, Parmryd I. Quantifying colocalization by correlation: The Pearson correlation coefficient is superior to the Mander's overlap coefficient. Cytom Part A. 2010; 77A (8): 733–42.
40. Ling E-A, Kaur C, Lu J. Origin, nature, and some functional considerations of intraventricular macrophages, with special reference to the epiplexus cells. Microsc Res Tech. 1998; 41: 43–56.
41. Bolborea M, Dale N. Hypothalamic tanycytes: potential roles in the control of feeding and energy balance. Trends Neurosci. 2013; 36 (2): 91–100.

ARTIFICIAL INTELLIGENCE ALGORITHMS FOR ASSESSMENT OF THE MAJOR VESSEL TORTUOSITY

Ilina AA[1,2]✉, Lakman IA[2], Bikmeyev AT[3], Enikeeva AR[1], Badykova EA[1], Zagidullin NSh[1], Bryukhanova OA[1]

[1] Bashkir State Medical University, Ufa, Russia

[2] Ufa University of Science and Technology, Ufa, Russia

[3] Mavlyutov Institute of Mechanics, Ufa Federal Research Center of Russian Academy of Science, Ufa, Russia

Tortuosity of the coronary, cerebral arteries, aorta and its branches remains an important vascular problem, which, on the one hand, complicates selection of the X-ray surgical treatment tactics, and on the other hand worsens the disease outcome. The lack of common standards for assessment of tortuosity of the coronary, cerebral arteries, aorta and its branches reduces the diagnosis accuracy in patients at high risk of cardiovascular events. The use of machine learning for automated tortuosity assessment represents one possible solution to this problem. The study aimed to analyze and compare accuracy, feasibility, and limitations of the available methods for automated assessment of tortuosity of the coronary, cerebral arteries, aorta and its branches using the machine learning tools. The systematic review was conducted in accordance with the PRISMA protocol. The search for papers published in 2015–2025 in the PubMed, Scopus, and eLibrary databases was performed using the following keywords: deep learning, machine learning, artificial intelligence, vessel tortuosity, curvature. Six papers out of 240 were included in the analysis. The analysis has shown that 80% of approaches are based on convolutional neural networks, and skeletonization aimed to isolate small blood vessels from the artery represents an essential preprocessing phase. In 50% of papers, tortuosity was determined qualitatively based on the presence of bending angles over 45°. Quantitatively, tortuosity was determined as a distance coefficient and a measure of curvature. In three studies out of six, verification of estimates was carried out by comparing the results with expert opinions (accuracy was 0.92–0.94). The study limitations are as follows: monocentricity, the use of data from one type of equipment.

Keywords: vessel tortuosity, coronary arteries, cerebral arteries, aorta and its branches, machine learning, artificial intelligence, tortuousity index

Author contribution: Ilina AA, Bikmeyev AT — search for papers, manuscript writing; Lakman IA — study design, data processing, manuscript writing and editing; Enikeeva AR, Badykova EA — experts in manual selection of papers, Zagidullin NSh — expert in manual selection of papers, manuscript writing and editing; Bryukhanova OA — manuscript editing.

✉ **Correspondence should be addressed:** Anastasia A. Ilina
Lenina, 3, Ufa, 450008, Russia; anastasiailina35@gmail.com

Received: 22.12.2025 **Accepted:** 26.01.2026 **Published online:** 05.02.2026

DOI: 10.24075/brsmu.2026.005

Copyright: © 2026 by the authors. **Licensee:** Pirogov University. This article is an open access article distributed under the terms and conditions of the Creative Commons Attribution (CC BY) license (https://creativecommons.org/licenses/by/4.0/).

АЛГОРИТМЫ ИСКУССТВЕННОГО ИНТЕЛЛЕКТА ДЛЯ ОЦЕНКИ ИЗВИТОСТИ МАГИСТРАЛЬНЫХ СОСУДОВ

А. А. Ильина[1,2]✉, И. А. Лакман[2], А. Т. Бикмеев[3], А. Р. Еникеева[1], Е. А. Бадыкова[1], Н. Ш. Загидуллин[1], О. А. Брюханова[1]

[1] Башкирский государственный медицинский университет, Уфа, Россия

[2] Уфимский университет науки и технологий, Уфа, Россия

[3] Институт механики имени Р. Р. Мавлютова, Уфимский федеральный исследовательский центр Российской академии наук, Уфа, Россия

Извитость коронарных, цереброваскулярных артерий, аорты и ее ветвей остается одной из значимых сосудистых проблем, которая с одной стороны осложняет выбор тактики рентгенохирургического лечения, а с другой — ухудшает прогноз самого заболевания. Отсутствие единых стандартов оценки извитости коронарных, цереброваскулярных артерий, аорты и ее ветвей снижает точность диагностики пациентов с высоким риском сердечно-сосудистых событий. Одним из возможных решений данной проблемы является применение машинного обучения для автоматической оценки извитости. Целью исследования было провести анализ и сравнение точности, клинической применимости и ограничений существующих методов автоматической оценки извитости коронарных, цереброваскулярных артерий, аорты и ее ветвей с использованием инструментов машинного обучения. Систематический обзор проводили по протоколу PRISMA с поиском статей в базах данных PubMed, Scopus и eLibrary за период с 2015 по 2025 гг. по ключевым словам: deep learning, machine learning, artificial intelligence, vessel tortuosity, curvature. Из 240 выявленных публикаций в анализ было включено шесть. Анализ показал, что 80% подходов основаны на сверточных нейронных сетях, обязательным этапом предобработки изображений является скелетирование для отсечения мелких сосудов от артерии. В 50% статей извитость артерий определяется качественно по наличию углов изгибов более 45°. Количественно извитость определяли как коэффициент расстояния и мера кривизны. Верификацию оценок в трех из шести исследований проводили при сравнении результатов с мнениями экспертов (точность составила 0,92–0,94). Ограничения исследования — моноцентричность, использование данных одного типа оборудования.

Ключевые слова: извитость сосудов, коронарные артерии, цереброваскулярные артерии, аорта и ее ветви, машинное обучение, искусственный интеллект, количественная мера оценки извитости

Вклад авторов: А. А. Ильина, А. Т. Бикмеев — поиск источников, написание статьи; И. А. Лакман — дизайн исследования, обработка данных, написание и редактирование статьи; А. Р. Еникеева, Е. А. Бадыкова — эксперты ручного отбора публикаций, Н. Ш. Загидуллин — эксперт ручного отбора публикаций, написание и редактирование статьи, О. А. Брюханова — редактирование статьи.

✉ **Для корреспонденции:** Анастасия Александровна Ильина
ул. Ленина, д. 3, г. Уфа, 450008, Россия; anastasiailina35@gmail.com

Статья получена: 22.12.2025 **Статья принята к печати:** 26.01.2026 **Опубликована онлайн:** 05.02.2026

DOI: 10.24075/vrgmu.2026.005

Авторские права: © 2026 принадлежат авторам. **Лицензиат:** РНИМУ им. Н. И. Пирогова. Статья размещена в открытом доступе и распространяется на условиях лицензии Creative Commons Attribution (CC BY) (https://creativecommons.org/licenses/by/4.0/).

High arterial tortuosity induces arterial dysfunction due to a number of reasons: first, tortuous arteries can create turbulent and slow blood flow, leading to decreased efficiency of blood supply to tissues and organs [1]; second, increased stress on the vessel wall may occur due to uneven pressure distribution in the vessel, ultimately leading to endothelial damage [2]; third, difficulties arise with diagnostics (for example, when using angiography) and vascular surgery [3]. Furthermore, standard imaging methods and arterial tortuosity assessment based on these methods are a matter of debate [4].

Cardiovascular disorders associated with the coronary artery abnormalities remain one of the leading causes of premature death all over the world [5]. Radiology plays a key role in detection of those; coronary angiography is acknowledged as a gold standard due to high vascular structure imaging accuracy [6]. The available diagnostic methods usually do not focus on assessing the coronary artery tortuosity, despite possible relationship between tortuosity and adverse outcomes, such as ischemia, spontaneous blood vessel dissection, and complications associated with stent placement [7].

The lack of the common standard of arterial tortuosity assessment and severity limits the diagnostic accuracy [8]. Theoretically, machine learning algorithms, in particular machine vision algorithms, which are widely used in X-ray image recognition tasks, could help solve the problem [9]. However, there are many challenges to training intelligent algorithms in practice. Thus, the coronary angiography technical specifics, including the use of the limited number of standard views, do not allow one to obtain an integrated picture of the vascular bed anatomy. Imaging is also hampered by the overlap of vessels, their shadows, the presence of small branches and bone structures that obscure the image. Further complexities arise from the artifacts associated with the patient's heart movement and breathing, as well as from inconsistent rate and uneven filling of blood vessels with the contrast agent [10]. Therefore, there is a need to summarize the available research allowing for further evaluation of the potential of approaches capable of improving the assessment of arterial tortuosity, specifically tortuosity of the coronary arteries of the heart.

The study aimed to analyze and compare accuracy, feasibility, and limitations of the available methods for assessment of tortuosity of the coronary, cerebral arteries, aorta and its branches using machine learning tools.

METHODS

To answer the research question (“How to automatically determine the presence and degree of arterial tortuosity based on medical images?”) the PRISMA protocol was used that is conventionally used for systematic reviews. The search criterion was as follows: studies published not earlier than in 2015 and focused on the intelligent algorithms, methods, and techniques used to assess vascular tortuosity. The earlier studies were not considered due to the fact that the reported technologies were dated. The access to the paper full text was an essential selection criterion. PubMed, Scopus, eLibrary were the databases, in which the search for the review sources was performed. The keywords for the search query in English were as follows: deep learning, machine learning, artificial intelligence, computer vision, coronary, cerebral, carotid, aorta, vessel, artery, tortuosity, curvature. Accordingly, the following keywords in Russian were used: извитость, сосуд, артерия, машинное обучение, компьютерное зрение, искусственный интеллект. The search queries were generated using the OR and AND logical operators for disjunction and conjunction of the terms. The search for papers in the PubMed and Scopus databases was accomplished using appropriate R libraries: pubmedR and rscopus (it was possible, since the authors previously registered in citation databases and got access via API). The “snowball” strategy was used for a broader search for papers in accordance with the research question: we found the necessary paper and conducted further search for the cited and citing sources. Inclusion criteria for the second paper selection phase: presence of characteristics of vascular tortuosity assessment algorithms, methods, and techniques, including information about their accuracy and feasibility. If the article mentioned image preprocessing and processing steps, these were also included in the analysis. Exclusion criteria: discrepancy to the review subject (for example, tortuosity of umbilical vessels). The study limitations and funding were not taken into account when selecting papers. Compliance of each paper with the inclusion criteria was assessed by two independent experts when performing manual selection of papers. In case of disagreement in their opinion regarding any paper, a verification expert was involved. The concurrence of opinions from experts was determined based on the Cronbach's alpha.

Criteria for inclusion of papers in the systematic review: fact of containing the description and/or name of the tortuosity assessment method/technique (TAM-T); fact of containing the description of the TAM-T results; fact of considering arteries only; analysis of blood vessels in adult patients with the mature vascular system (over the age of 18) only; fact of considering images of blood vessels obtained by coronary angiography (CAG), computed tomography (CT) or optical coherence tomography (OCT).

Exclusion criteria: no TAM-T results; description of the study of umbilical vein and/or vessel tortuosity; description of the study of blood vessels in patients under the age of 18; description of the animal study or study involving models, such as computer simulation and microfluid devices.

The sources selected were analyzed with regard to the following: what types of images were used to determine arterial tortuosity; what number of images was used to train machine learning algorithms; what machine learning algorithm was used to recognize images of blood vessels; how blood vessel images were pre-processed; how the arterial tortuosity was quantified; quality metrics for tortuosity assessment.

RESULTS

Primary search in accordance with the specified strategy of combining keywords allowed us to find 240 papers in three databases. In this phase of paper selection, 82 duplicate studies were filtered out, and four papers were not selected due to other reasons (lack of available full-text versions). The remaining publications were re-screened for paper titles and abstracts that matched the answer to the research question, which allowed us to filter out another 69 studies. Full-text versions of the papers selected were analyzed when manually selected by experts, and only one paper was a matter of debate (Cronbach's alpha 0.96). Eventually, among full-test versions selected only six answered the research question, so six papers were selected to analyze and compare the vascular tortuosity assessment algorithms, methods, and techniques. The Figure presents the scheme of paper selection in accordance with the PRISMA protocol.

Convolutional neural networks were used as an arterial tortuosity modeling tool in five papers out of six selected. Thus, two convolutional neural network models (CNN and nnU-Net)

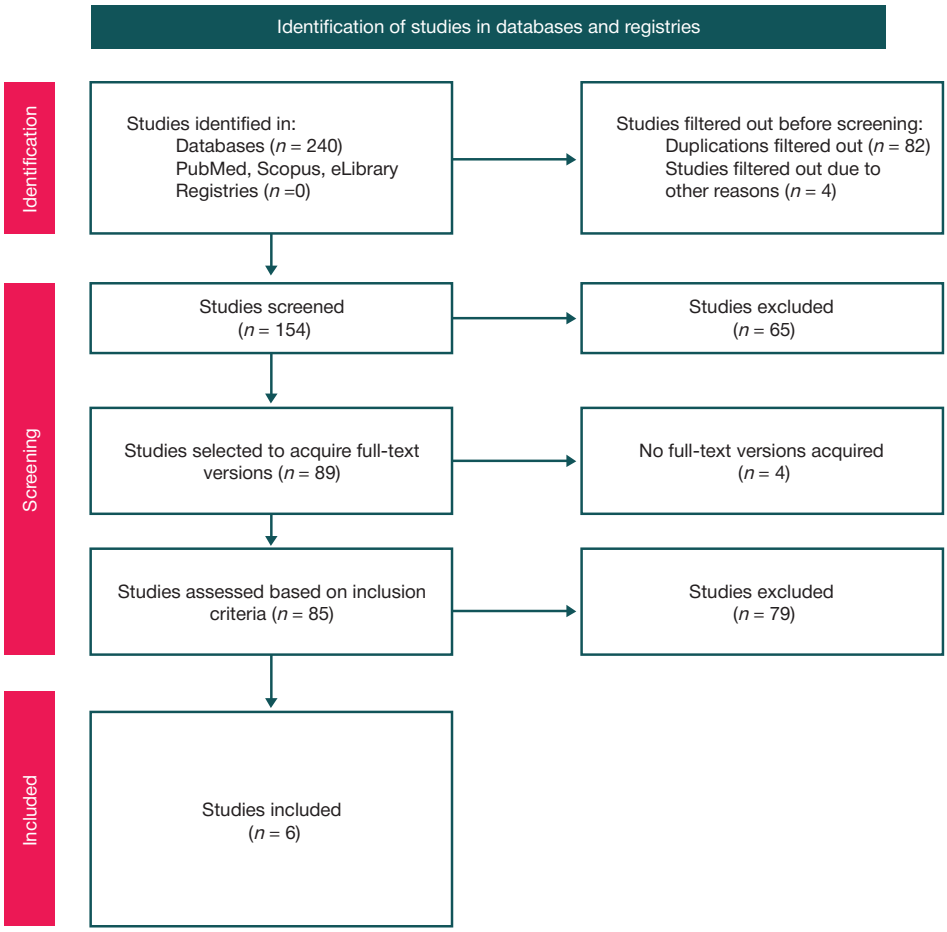

Fig. PRISMA paper selection scheme for the study

for automatic segmentation of coronary arteries and quantitative assessment of their morphological characteristics, including vascular tortuosity, were trained in 2024 [11]. This study involved the analysis of CT angiography images of 281 patients. The input information pre-processing included thresholding with the threshold for selection of blood vessel lumen tailored by an expert (radiologist). Manual adjustment was performed in the over-segmented and under-segmented regions of blood vessel images. Blood vessels were segmented manually using the 3D Slicer free open source software for medical imaging, then the automatic centerline extraction was performed (the so-called vessel skeletonization) using the VMTK (Vascular Modeling Toolkit) library integrated in the 3D Slicer, and the major morphological characteristics of the vessel were calculated. Several approaches were used to assess arterial tortuosity. Global tortuosity was defined as the ratio of the actual blood vessel path length to the direct distance between its ends. Local tortuosity was assessed along the centerline at each point using the 1 cm-long support arcs centered at the point considered. In addition, the tortuosity angle was calculated as arccosine of the scalar product of vectors approximating the blood vessel arc ascending and descending sections by the least squares method. The resulting tortuosity index of blood vessels assessed was determined for each patient as a number of vascular branches having at least three bends with the angle ≥ 45°. In this study, a convolutional neural network (CNN) was trained for automatic blood vessel segmentation, and morphological characteristics were assessed using the nnU-Net neural network-based two-stage cascade approach [11]. At the first stage the multi-view 2.5D U-Net was created. For that three 2D models were trained using the images sliced in orthogonal directions (sagittal, coronal, and axial). Such an approach to vascular tortuosity assessment is particularly useful, since tortuosity can be found in only one view, while in another view it is not always noticeable. At the second stage the data obtained were combined with the original image and used to train the 3D U-Net network. It is noteworthy that the authors assessed the strength of their findings, for that they compared the results of the multi-view 2.5D model and the cascade 3D model. As a result, the value of the Dice coefficient averaged across all patient blood vessel images, as a measure of the quality of image recognition accuracy, increased from 0.791 [0.60; 0.88] to 0.895 [0.75; 0.92]. The fact that all the images used for training were obtained at the same center with the same CT scanner can be noted as a drawback. The use of data from different sources, including open sources, including images of blood vessels of healthy volunteers, might improve stability of the tortuosity assessment model.

In 2023, an automatic segmentation, labeling, and arterial tortuosity assessment method based on artificial neural networks was proposed [12]. To train models, the authors formed a dataset of 566 CT angiography scans from acute ischemic stroke patients, among which 165 images were randomly selected. The pre-processing phase included spatial alignment and intensity normalization. The experts performed segmentation manually, as in the previous solution, in 3D Slicer. The authors tested three segmentation model variants (based on the nnU-Net, UNETR, SwinUNETR neural network models), and nnU-Net turned out to be the most effective (the Dice coefficient was 0.93 ± 0.02). Training involved data augmentation and five-fold cross-validation (additional cross-verification). Next, like in the study [11], the surface model of

Table. Characteristics of the studies included in the systematic review

Authors, year of the study, reference	Type of images analyzed	Image pre-processing methods	Image processing methods	Machine learning method	Sample characteristics	Vessel tortuosity assessment method	Model quality metrics
Nannini G. et al., 2024 [11]	CT angiography	Thresholding with manual selection of the cut-off value	Manual blood vessel segmentation (3D Slicer), centerline extraction	CNN, U-Net	281 patients	≥ 3 bends > 45°, distance coefficient	Dice coefficient: 0.895
Canals P. et al., 2023 [12]	CT angiography	Spatial alignment, color intensity normalization	Manual blood vessel segmentation (3D Slicer), anatomical landmarks, centerlines, calculation of morphological and geometric characteristics	nnU-Net, gU-Net	566 stroke patients	Blood vessel diameter and length, angles of deflection	No
Cobo M. et al., 2023 [13]	Coronary angiography	Cropping	No	Convolutional neural network (Xception)	401 patients , 658 images	≥ 3 bends with the angle ≥ 45°	Accuracy: 0.87, sensitivity 0.87, specificity 0.88
Nageler G. et al., 2023 [14]	CT angiography	No	Segmentation	nnU-Net, 3D CNN	379 post EVT due to acute ischemic stroke	< 90 acute, > 90 obtuse	AUC: 0.92
Gao H. et al., 2022 [15]	3DRA angiography	Segmentation involving the use of thresholding, smoothing, removal of disconnected branches, aneurysm removal	Calculation of geometric characteristics	Logistic regression, ENT, SVM, XGBoost, Random Forest	226 patients post DSA	Curvature, torsion, distance coefficient	Best AUC — 0.762 (SVM)
Witherford M. et al., 2022 [16]	CT angiography	No	Creation of a 3D model of blood vessels	–	234 patients with aortic aneurysm	Distance coefficient	–

blood vessels was extracted from the binary image map using the VMTK library, then filtering and smoothing were applied. A total of 24 characteristics were calculated for each node based on the centerlines obtained, including radii (mean, proximal, distal, minimum and maximum), proximal to distal radius ratio, relative segment length, directions (total and initial), number of points per segment, segment's center of mass coordinates. The authors formed a graph of blood vessel centerlines, the nodes of which denoted vascular segments with the artery names specified. Segments were classified using the graph U-Net neural network after normalization of characteristics and increasing the graph connectivity. The researchers identified and analyzed 33 geometric and morphological characteristics of vascular tortuosity. These included blood vessel diameter, relative segment length, and absolute and relative deflection angles for the major arteries (aorta, brachiocephalic trunk, common carotid and subclavian arteries). Morphological characteristics included the aorta type and the presence of the bovine aortic arch variant. The authors did not calculate a unified tortuosity coefficient, but performed comparative analysis of tortuosity parameters in various groups of patients. They developed an algorithm allowing them to identify the abnormally tortuous blood vessels. All the data used were obtained from the same medical center and one CT equipment manufacturer, which limited generalizability of the results and the method versatility. The automatic analysis sometimes made serious mistakes when determining the key points, which reduced measurement reliability compared to the manual approach. The main sources of error were related to improper blood vessel labeling, segmentation inaccuracy, erroneous centerline extraction and data processing, which affect the overall method accuracy. However, blind validation yielded the recognition accuracy of 0.94.

In 2023, the authors of another paper also used a convolutional neural network, but they proposed an alternative approach to vascular tortuosity assessment that was different from the conventional sequence of actions algorithm [13]. The method to directly classify angiography scans based on the use of convolutional neural networks (CNN) determining the presence or absence of vascular tortuosity was developed. The source material was the dataset of 658 coronary angiography images obtained from 401 patients. To expand the sample, two views were used: Spider (in the form of images taken at a random angle forming a “web”) and 45°. Due to the limited amount of data, the image augmentation technology was used (scaling, shifting and changing the brightness of images). As a result, the authors defined tortuosity as the presence of three or more successive bends with the angle ≥ 45° in any part of the coronary artery. Images were segmented with the Xception convolutional neural network using early stopping in order to avoid retraining of the image recognition algorithm. The so-called transfer learning was used to optimize the algorithm training task, the essence of which was as follows: in the neural network model pre-trained on ImageNet, the last fully connected layer was replaced with the one adapted for the binary classification task. Such an approach made it possible to preserve universal features from ImageNet and adapt these to the medical image specifics. Standard parameters were calculated to estimate the proposed model quality: accuracy (0.87), sensitivity (0.87), specificity (0.88). The main limitations of the method proposed are associated with the image quality and resolution, insufficient variety of images showing different vascular tortuosity types.

In the same year, the automatic method for classifying the internal carotid artery based on the bending angle value was developed [14]. A total of 379 CT angiography scans were used to train algorithms. To expand the sample, both left and right internal carotid arteries of each patient were included in the analysis. As in the above studies, segmentation was performed manually with 3D Slicer using three tags: aorta, left common carotid artery (CCA) + internal carotid artery (ICA), right CCA + ICA. To automate the process of artery segmentation, a neural network with the nnU-Net architecture was trained. Then the hybrid segmentation involving the use of automated prediction with manual verification and adjustment was applied.

The 3D Slicer angle tool was used to measure the ICA bending angles allowing for more accurate consideration of spatial arrangement of individual blood vessels. Angles were classified as acute (≤ 90°) or obtuse (> 90°) depending on their effect on the endovascular intervention duration (angles ≤ 90° turned out to be associated with longer endovascular interventions).

At the image pre-processing stage the following was performed to train the model: cropping of the volume based on segmentation, distinction between the left and right ICA, voxel size unification (0.5 mm), extending the volume size to 400 × × 400 × 605 voxels, and rescaling (a procedure that adds pixels and performs smoothing) to 128 × 128 × 196. The CCA + ICA was the network input, and the binary class (angle > 90° or angle ≤ 90°) was the output. Based on the testing results, the model constructed by the authors showed the AUC classifier evaluation metrics (area under the ROC curve) of 0.92. The major study limitations include the monocentric design, lack of external data validation, planar measurement of angles on 3D segmentations, and loss of information when dichotomizing angles. Furthermore, it was impossible to assess some ICA segments due to insufficient contrast enhancement, which could result in bias of results.

In another study (2022), comparative analysis of the applicability of several machine learning algorithms for the internal carotid artery tortuosity assessment was performed [15]. The analysis included 3DRA angiography scans of 62 patients. At the pre-processing stage, segmentation, smoothing, and removal of the unconnected blood vessel branches were performed using Mimics and Geomagic Studio, then the VMTK library was used for aneurism removal to construct the maternal artery model. Centerlines were calculated in Aneufuse, and the following characteristics were used for tortuosity assessment: curvature, torsion, and the distance coefficient calculated as the ratio of the direct distance between the segment starting and ending points to the centerline length. The average, maximum and range curvature and torsion values were calculated. As a result, the machine learning model for predicting the in-stent stenosis was constructed based on 75 clinical, structural, and morphological variables. The model was trained using logistic regression and four machine learning algorithms: Elastic Net neural network, Support Vector Machines, extreme Gradient Boosting, and Random Forest. When performing test validation, the Support Vector Machines (SVM) algorithm had the best parameters of the AUC-ROC metrics (SVM): 0.891 (test set) and 0.762 (validation set). Among tortuosity parameters, the length coefficient and maximum curvature affected the prognosis most. The key drawbacks of the study, i.e. small sample size (62 patients) and the retrospective single-center design, lowered generalizability of the data obtained. The tortuosity analysis was performed at a global level, without taking into account local blood vessel characteristics, which could affect the accuracy of assessing the relationship with treatment outcomes.

In 2022, the analysis of preoperative anatomy and intraoperative arterial deformities in patients with aortic aneurysms was also conducted [16]. Multiplanar reconstruction with subsequent construction of the 3D blood vessel model was performed in 234 patients. Models were constructed using the CYDAR proprietary software based on preoperative CT scans, where branches of the major arteries were marked (celiac trunk, superior mesenteric, renal and iliac ones). These models were used to create interactive maps during surgery, which allowed for adjustment of anatomical marker positions in three planes in the real-time mode. To assess vascular tortuosity, the tortuosity coefficients were calculated as a ratio of the direct distance to Euclidean distance for the key segments: visceral region (from the celiac trunk to the inferior renal artery), common iliac arteries, and the entire iliac segment. When conducting research, the authors adhered to the standards of the Society for Vascular Surgery in terms of measurement standardization.

The table providing the main characteristics of the arterial tortuosity assessment methods and algorithms was created to summarize the analysis results.

DISCUSSION

The systematic review conducted allowed us to identify six published studies answering the research question ("How to automatically determine the presence and degree of arterial tortuosity based on medical images?"). All the studies were novel, these were published in 2022–2024. The authors of three papers out of six examined tortuosity of the internal carotid artery and supraaortic vessels, in one study — the aorta; in two studies, tortuosity of the coronary arteries was assessed. In five studies out of six, neural networks were used as the main machine learning algorithm; in 50% of papers, 3D Slicer, the freely distributed software for analyzing medical (primarily X-ray) images, was used as a pre-processing tool. In all papers, skeletonization was accomplished at the preliminary stage of the blood vessel image analysis, which was especially important for recognizing and separating the main blood vessels from branches of small vessels, and in three of the six studies, the open source library VMTK was used for this purpose. In three studies out of six, verification was performed when comparing the results with the expert opinions.

As for the answer to the research question, only three papers considered the use of the exact number in the form of the distance coefficient for vascular tortuosity quantification. Furthermore, in one paper, the curvature coefficient (through the second derivative of the approximated function describing the vessel) was also calculated, along with torsion. In three other papers, tortuosity of blood vessels was qualitatively assessed. Any quantification allows one to assess the vessel tortuosity degree, but automatic assessment of the presence of tortuosity itself as a fact of the presence of abnormality is also important. Thus, it has been shown that the presence of coronary artery tortuosity is associated with the early arterial hypertension manifestation [17]. Furthermore, automatic assessment of the presence of vascular tortuosity is important for planning, monitoring and evaluation of the consequences of surgical intervention for stenting. For example, in 2021 the effect of vascular tortuosity on clinical sequelae after stent placement was studied, and conclusions were made that stent implantation in tortuous coronary arteries in pregnancy was associated with the increased rate of coronary artery thrombosis based on the aggregated data of six studied [18]. The paper by other researchers (2021) provides the research results proving that the presence of coronary tortuosity is associated with hypertension, hyperlipidemia, and left ventricular diastolic dysfunction (it is noteworthy that in this study tortuosity was defined as the presence of ≥ 3 bends at an angle greater than 45°) [19]. At the same time, the tortuosity degree quantification allows one to assess the relationship between tortuosity and coronary blood flow alteration, which can cause the decrease in perfusion pressure and, as a consequence, lead to myocardial ischemia [20]. It is noteworthy that the qualitative and quantitative approaches to tortuosity assessment were compared in terms of their effects on the development of coronary artery disease (CAD) [21]. The authors determined tortuosity qualitatively based on angle measurement. They showed that patients with

the coronary artery tortuosity were more common in the group of patients with nonobstructive CAD. The authors quantified tortuosity by determining the tortuosity index, based on which they showed that the highest coronary artery tortuosity index values were reported in patients with ischemia of the lateral wall supplied by the left circumflex artery. It was concluded that both qualitative and quantitative coronary blood vessel tortuosity assessment was important for detection of the coronary artery disease predictors. The study conducted in 2023 showed that cerebrovascular tortuosity also affects plaque formation in the carotid bulb [21]. Furthermore, there are data (2024) that tortuosity is a risk factor of the cervicocerebral artery dissection representing the cause of ischemic stroke in the young [22], which once more emphasizes the need for automatic arterial tortuosity assessment with the use of AI tools.

The use of arterial tortuosity quantitative assessment models in clinical practice is associated primarily with the possibility of its seamless integration into clinical scales for stratifying the risk of vascular surgery complications, as well as implementation in the form of separate modules and a system for supporting medical decision-making. For example, SYNTAX Score and SYNTAX Score II consider arterial tortuosity, and according to the papers by domestic authors, these scores are significantly correlated to clinical outcomes in patients with severe coronary artery lesions post percutaneous coronary interventions. In 2019 it was shown that the higher coronary bed structural complexity reflected by the SYNTAX Score was associated with the worse outcome within four years of follow-up after PCI [23]. According to some data, the revascularization technique selection (PCI or CABG) has a significant impact on clinical outcomes in patients with high SYNTAX Score values [24]. However, the disadvantage of these scores is that the tortuosity assessment remains subjective. Considering the fact that coronary artery tortuosity directly affects the vascular bed geometry, intervention complexity, risk of incomplete revascularization and stent thrombosis, the automatic quantitative tortuosity assessment by artificial intelligence methods can be considered as a potential additional parameter to refine the lesion structural complexity. This opens up the possibility for more objective preoperative stratification of patients, optimization of the choice of revascularization tactics and, as a consequence, reduced incidence of ischemic and thrombotic complications.

CONCLUSIONS

The systematic review allowed us to summarize the options for automatic assessement of tortuosity of the coronary, cerebral arteries, aorta and its branches. Arterial tortuosity affects the decision-making tactics when analyzing coronary angiography scans, for example, to assess the possibility of coronary artery stenting or bypass surgery. In this regard, the automatic qualitative tortuosity assessment is important in terms of the speed of decision-making in the operating and preparation rooms. Automatic quantitative assessment of the arterial tortuosity degree is also important, since it can be used as a predictor of adverse cardiovascular events and cerebrovascular disorders.

References

1. Baharoglu MI, Schirmer CM, Hoit DA, Gao BL, Malek AM. Aneurysm inflow-angle as a discriminant for rupture in sidewall cerebral aneurysms: morphometric and computational fluid dynamic analysis. Stroke. 2010; 41 (7): 1423–30. PMID: 20508183.
2. Tawakul A, Alluqmani MM, Badawi AS, Alawfi AK, Alharbi EK, Aljohani SA, et al. Risk Factors for Cerebral Vasospasm After Subarachnoid Hemorrhage: A Systematic Review of Observational Studies. Neurocrit Care. 2024; 41 (3): 1081–99. PMID: 39048760.
3. Callewaert BL, Willaert A, Kerstjens-Frederikse WS, De Backer J, Devriendt K, Albrecht B, et al. Arterial tortuosity syndrome: clinical and molecular findings in 12 newly identified families. Hum Mutat. 2008; 29 (1): 150–8. PMID: 17935213.
4. Kim JH, Yang H, Son NH, Jang CK, Lee JW, Cho KC. Discrepancy in vessel tortuosity measurements of anterior circulation cerebral artery between digital subtraction angiography and magnetic resonance angiography. J Cerebrovasc Endovasc Neurosurg. 2025; 27 (3): 212–8. PMID: 40147427
5. Nedkoff L, Briffa T, Zemedikun D, Herrington S, Wright FL. Global Trends in Atherosclerotic Cardiovascular Disease. Clin Ther. 2023; 45 (11): 1087–91. DOI: PMID: 37914585.
6. Kheiri B, Simpson TF, Osman M, German DM, Fuss CS, Ferencik M, et al. Computed tomography vs invasive coronary angiography in patients with suspected coronary artery disease: a meta-analysis. J Am Coll Cardiol Img. 2022; 15 (12): 2147–9. PMID: 36481083.
7. Kahe F, Sharfaei S, Pitliya A, Jafarizade M, Seifirad S, Habibi S, et al. Coronary artery tortuosity: a narrative review. Coron Artery Dis. 2020; 31 (2): 187–92. PMID: 31211725.
8. Zebic MP, Arambasic J, Mlinarevic D, Saric S, Labor M, Bosnjak I, et al. Coronary Tortuosity Index vs. Angle Measurement Method for the Quantification of the Tortuosity of Coronary Arteries in Non-Obstructive Coronary Disease. Diagnostics (Basel). 2023; 14 (1): 35. PMID: 38201343.
9. Obuchowicz R, Lasek J, Wodziński M, Piórkowski A, Strzelecki M, Nurzynska K. Artificial Intelligence-Empowered Radiology-Current Status and Critical Review. Diagnostics (Basel). 2025; 15 (3): 282. PMID: 39941212.
10. Sun Z, Choo GH, Ng KH. Coronary CT angiography: current status and continuing challenges. Br J Radiol. 2012; 85 (1013): 495-510. PMID: 22253353.
11. Nannini G, Saitta S, Baggiano A, Maragna R, Mushtaq S, Pontone G, Redaelli A. A fully automated deep learning approach for coronary artery segmentation and comprehensive characterization. APL Bioeng. 2024; 8 (1): 016103. PMID: 38269204.
12. Canals P, Balocco S, Díaz O, Li J, García-Tornel A, Tomasello A, et al. A fully automatic method for vascular tortuosity feature extraction in the supra-aortic region: unraveling possibilities in stroke treatment planning. Comput Med Imaging Graph. 2023; 104: 102170. PMID: 36634467.
13. Cobo M, Pérez-Rojas F, Gutiérrez-Rodríguez C, Heredia I, Maragaño–Lizama P, Yung–Manriquez F, et al. Novel deep learning method for coronary artery tortuosity detection through coronary angiography. Sci Rep. 2023; 13 (1): 11137. PMID: 37429940.
14. Nageler G, Gergel I, Fangerau M, Breckwoldt M, Seker F, Bendszus M, et al. Deep Learning-based Assessment of Internal Carotid Artery Anatomy to Predict Difficult Intracranial Access in Endovascular Recanalization of Acute Ischemic Stroke. Clin Neuroradiol. 2023; 33 (3): 783–92. PMID: 36928398.
15. Gao H, You W, Wei D, Lv J, Sun W, Li Y. Tortuosity of parent artery predicts in-stent stenosis after pipeline flow-diverter stenting for internal carotid artery aneurysms. Front Neurol. 2022; 13: 1034402. PMID: 36313497;
16. Witheford M, Borghese O, Mastracci TM, Maurel B. An observational assessment of aortic deformation during infrarenal and complex endovascular aortic aneurysm repair. J Vasc Surg. 2022; 76 (3): 645–55.e3. PMID: 35367562.
17. Enikeeva AR, Buzaev IV, Badykova EA, Lakman IA, Iskhakova YuO, Bikmeev AT, i dr. Faktory riska izvitosti koronarnyh arterij: original'noe issledovanie. Rossijskij kardiologicheskij zhurnal. 2025; 30 (6): 18–24. DOI: 10.15829/1560-4071-2025-6045. Russian.
18. Konigstein M, Ben-Yehuda O, Redfors B, Zhang Z, Kandzari DE,

Hermiller JB, et al. Impact of Coronary Artery Tortuosity on Outcomes Following Stenting: A Pooled Analysis From 6 Trials. JACC Cardiovasc Interv. 2021; 14 (9): 1009-18. PMID: 33640388.
19. Elamragy A, Yakoub S, AbdelGhany M, Ammar W. Coronary tortuosity relation with carotid intima-media thickness, coronary artery disease risk factors, and diastolic dysfunction: is it a marker of early atherosclerosis? The Egyptian Heart Journal. 2021; 73: 1–9. PMID: 33788058.
20. Kahe F, Sharfaei S, Pitliya A, Jafarizade M, Seifirad S, Habibi S, et al. Coronary artery tortuosity: a narrative review. Coronary artery disease. 2020; 31 (2): 187–92. PMID: 31211725.
21. Ren L, Xu R, Zhao C, Li W, Wang S, Cao C, et. al. Tortuosity and Proximal-Specific Hemodynamics Associated with Plaque Location in the Carotid Bulb Stenosis. J Vasc Res. 2023; 60 (3): 160–71. PMID: 37499638.
22. Salih M, Taussky P, Ogilvy CS. Association between cervicocerebral artery dissection and tortuosity — a review on quantitative and qualitative assessment. Acta Neurochir (Wien). 2024; 166 (1): 285. DOI: 10.1007/s00701-024-06171-2. PMID: 38977512.
23. Grigorev VS, Petrosyan KV, Abrosimov AV, Alekyan BG, Goluhova EZ, Buziashvili YuI, i dr. Rol'shkal SYNTAX Score i SYNTAX Score II v stratifikacii pacientov s tyazhelym porazheniem koronarnogo rusla v techenie chetyrekh let nablyudeniya posle vypolneniya CHKV. Byulleten' NCSSKH im. A. N. Bakuleva RAMN. Serdechno-sosudistye zabolevaniya. 2019; 20 (S11): 144. Russian.
24. Gorbachev IA, Goluhova EZ, Merzlyakov VYu, Petrosyan KV, Lukashkin MA, Salomov MA. Vybor metodiki revaskulyarizacii miokarda u pacientov s mnogososudistym porazheniem koronarnyh arterij s vysokim znacheniem SYNTAX Score. Byulleten' NCSSKH im. A. N. Bakuleva RAMN. Serdechno-sosudistye zabolevaniya. 2022; 23 (S3): 34. Russian.

Литература

1. Baharoglu MI, Schirmer CM, Hoit DA, Gao BL, Malek AM. Aneurysm inflow-angle as a discriminant for rupture in sidewall cerebral aneurysms: morphometric and computational fluid dynamic analysis. Stroke. 2010; 41 (7): 1423–30. PMID: 20508183.
2. Tawakul A, Alluqmani MM, Badawi AS, Alawfi AK, Alharbi EK, Aljohani SA, et al. Risk Factors for Cerebral Vasospasm After Subarachnoid Hemorrhage: A Systematic Review of Observational Studies. Neurocrit Care. 2024; 41 (3): 1081–99. PMID: 39048760.
3. Callewaert BL, Willaert A, Kerstjens-Frederikse WS, De Backer J, Devriendt K, Albrecht B, et al. Arterial tortuosity syndrome: clinical and molecular findings in 12 newly identified families. Hum Mutat. 2008; 29 (1): 150–8. PMID: 17935213.
4. Kim JH, Yang H, Son NH, Jang CK, Lee JW, Cho KC. Discrepancy in vessel tortuosity measurements of anterior circulation cerebral artery between digital subtraction angiography and magnetic resonance angiography. J Cerebrovasc Endovasc Neurosurg. 2025; 27 (3): 212–8. PMID: 40147427
5. Nedkoff L, Briffa T, Zemedikun D, Herrington S, Wright FL. Global Trends in Atherosclerotic Cardiovascular Disease. Clin Ther. 2023; 45 (11): 1087–91. DOI: PMID: 37914585.
6. Kheiri B, Simpson TF, Osman M, German DM, Fuss CS, Ferencik M, et al. Computed tomography vs invasive coronary angiography in patients with suspected coronary artery disease: a meta-analysis. J Am Coll Cardiol Img. 2022; 15 (12): 2147–9. PMID: 36481083.
7. Kahe F, Sharfaei S, Pitliya A, Jafarizade M, Seifirad S, Habibi S, et al. Coronary artery tortuosity: a narrative review. Coron Artery Dis. 2020; 31 (2): 187–92. PMID: 31211725.
8. Zebic MP, Arambasic J, Mlinarevic D, Saric S, Labor M, Bosnjak I, et al. Coronary Tortuosity Index vs. Angle Measurement Method for the Quantification of the Tortuosity of Coronary Arteries in Non-Obstructive Coronary Disease. Diagnostics (Basel). 2023; 14 (1): 35. PMID: 38201343.
9. Obuchowicz R, Lasek J, Wodziński M, Piórkowski A, Strzelecki M, Nurzynska K. Artificial Intelligence-Empowered Radiology-Current Status and Critical Review. Diagnostics (Basel). 2025; 15 (3): 282. PMID: 39941212.
10. Sun Z, Choo GH, Ng KH. Coronary CT angiography: current status and continuing challenges. Br J Radiol. 2012; 85 (1013): 495-510. PMID: 22253353.
11. Nannini G, Saitta S, Baggiano A, Maragna R, Mushtaq S, Pontone G, Redaelli A. A fully automated deep learning approach for coronary artery segmentation and comprehensive characterization. APL Bioeng. 2024; 8 (1): 016103. PMID: 38269204.
12. Canals P, Balocco S, Díaz O, Li J, García-Tornel A, Tomasello A, et al. A fully automatic method for vascular tortuosity feature extraction in the supra-aortic region: unraveling possibilities in stroke treatment planning. Comput Med Imaging Graph. 2023; 104: 102170. PMID: 36634467.
13. Cobo M, Pérez-Rojas F, Gutiérrez-Rodríguez C, Heredia I, Maragaño–Lizama P, Yung–Manriquez F, et al. Novel deep learning method for coronary artery tortuosity detection through coronary angiography. Sci Rep. 2023; 13 (1): 11137. PMID: 37429940.
14. Nageler G, Gergel I, Fangerau M, Breckwoldt M, Seker F, Bendszus M, et al. Deep Learning-based Assessment of Internal Carotid Artery Anatomy to Predict Difficult Intracranial Access in Endovascular Recanalization of Acute Ischemic Stroke. Clin Neuroradiol. 2023; 33 (3): 783–92. PMID: 36928398.
15. Gao H, You W, Wei D, Lv J, Sun W, Li Y. Tortuosity of parent artery predicts in-stent stenosis after pipeline flow-diverter stenting for internal carotid artery aneurysms. Front Neurol. 2022; 13: 1034402. PMID: 36313497;
16. Witheford M, Borghese O, Mastracci TM, Maurel B. An observational assessment of aortic deformation during infrarenal and complex endovascular aortic aneurysm repair. J Vasc Surg. 2022; 76 (3): 645–55.e3. PMID: 35367562.
17. Еникеева А. Р., Бузаев И. В., Бадыкова Е. А., Лакман И. А., Исхакова Ю. О., Бикмеев А. Т. и др. Факторы риска извитости коронарных артерий: оригинальное исследование. Российский кардиологический журнал. 2025; 30 (6): 18–24. DOI: 10.15829/1560-4071-2025-6045.
18. Konigstein M, Ben-Yehuda O, Redfors B, Zhang Z, Kandzari DE, Hermiller JB, et al. Impact of Coronary Artery Tortuosity on Outcomes Following Stenting: A Pooled Analysis From 6 Trials. JACC Cardiovasc Interv. 2021; 14 (9): 1009-18. PMID: 33640388.
19. Elamragy A, Yakoub S, AbdelGhany M, Ammar W. Coronary tortuosity relation with carotid intima-media thickness, coronary artery disease risk factors, and diastolic dysfunction: is it a marker of early atherosclerosis? The Egyptian Heart Journal. 2021; 73: 1–9. PMID: 33788058.
20. Kahe F, Sharfaei S, Pitliya A, Jafarizade M, Seifirad S, Habibi S, et al. Coronary artery tortuosity: a narrative review. Coronary artery disease. 2020; 31 (2): 187–92. PMID: 31211725.
21. Ren L, Xu R, Zhao C, Li W, Wang S, Cao C, et. al. Tortuosity and Proximal-Specific Hemodynamics Associated with Plaque Location in the Carotid Bulb Stenosis. J Vasc Res. 2023; 60 (3): 160–71. PMID: 37499638.
22. Salih M, Taussky P, Ogilvy CS. Association between cervicocerebral artery dissection and tortuosity — a review on quantitative and qualitative assessment. Acta Neurochir (Wien). 2024; 166 (1): 285. DOI: 10.1007/s00701-024-06171-2. PMID: 38977512.
23. Григорьев В. С., Петросян К. В., Абросимов А. В., Алекян Б. Г., Голухова Е. З., Бузиашвили Ю. И., и др. Роль шкал SYNTAX Score и SYNTAX Score II в стратификации пациентов с тяжелым поражением коронарного русла в течение четырех лет наблюдения после выполнения ЧКВ. Бюллетень НЦССХ им. А. Н. Бакулева РАМН. Сердечно-сосудистые заболевания. 2019; 20 (S11): 144.
24. Горбачев И. А., Голухова Е. З., Мерзляков В. Ю., Петросян К. В., Лукашкин М. А., Саломов М. А. Выбор методики реваскуляризации миокарда у пациентов с многососудистым поражением коронарных артерий с высоким значением SYNTAX Score. Бюллетень НЦССХ им. А. Н. Бакулева РАМН. Сердечно-сосудистые заболевания. 2022; 23 (S3): 34.

LINGUO-SEMANTIC DESCRIPTORS OF PAINFUL SENSATIONS AS A MIRROR THERAPY EFFECTIVENESS CRITERION IN TRAUMA-RELATED AMPUTATION

Petrash EA[1]✉, Nikishina VB[1], Uynina-Pakulova NYu[1], Minaev AS[1], Melkonyan GG[2], Lytkina KA[2], Karpenko AS[3]

[1] Pirogov Russian National Research Medical University, Moscow, Russia

[2] Hospital for War Veterans No. 3 of the Moscow City Department of Health, Moscow, Russia

[3] Moscow State Institute of International Relations (University) of the Ministry of Foreign Affairs of the Russian Federation, Moscow, Russia

Assessment of phantom pain linguosemantic descriptors in patients with traumatic amputation during the use of mirror visual feedback is conditioned by the need to find criteria for the psychological phantom pain adjustment effectiveness. The study aimed to assess the dynamic changes in linguosemantic pain descriptors in patients with traumatic amputation showing manifestations of phantom pain syndrome as a criterion for evaluating the effectiveness of mirror visual feedback. The total sample size was 87 males post traumatic amputation of one lower limb (age 23–55 years). The research methods were as follows: Mini Mental State Examination (MMSE), original form for registering linguosemantic descriptors of phantom painful sensations, Visual Analog Scale (VAS) for phantom pain. The detected dynamic changes in linguosemantic descriptors of phantom painful sensations in patients with traumatic amputation of the limb showing manifestations of phantom pain syndrome during treatment involving the use of mirror visual feedback makes it possible to consider the following as effectiveness criteria: an increase in the number of pain descriptors represented mainly by concrete and tangible nouns (makes it possible to reduce phantom pain severity rated using a 10-point scale), as well as the increase in the number of descriptors that characterize non-painful unpleasant sensations at the linguosemantic level.

Keywords: manifestations of phantom pain syndrome, descriptors of phantom pain, linguistic and semantic descriptors, mirror visual feedback

Author contribution: equivalent.

Compliance with ethical standards: the study approved by the Ethics Committee of the Pirogov University (protocol No. 249 dated 17 March 2025) was compliant with the requirements of the Fundamentals of Legislation "On the Protection of Citizens' Health"; all subjects submitted the informed consent for assessment.

✉ **Correspondence should be addressed:** Ekaterina A. Petrash
Ostrovityanova, 1, Moscow, 117997, Russia; petrash@mail.ru

Received: 29.01.2026 **Accepted:** 19.02.2026 **Published online:** 26.02.2026

DOI: 10.24075/brsmu.2026.007

Copyright: © 2026 by the authors. **Licensee:** Pirogov University. This article is an open access article distributed under the terms and conditions of the Creative Commons Attribution (CC BY) license (https://creativecommons.org/licenses/by/4.0/).

ЛИНГВОСЕМАНТИЧЕСКИЕ ДЕСКРИПТОРЫ БОЛЕВЫХ ОЩУЩЕНИЙ КАК КРИТЕРИЙ ОЦЕНКИ ЭФФЕКТИВНОСТИ ЗЕРКАЛЬНОЙ ТЕРАПИИ ПРИ ТРАВМАТИЧЕСКОЙ АМПУТАЦИИ

Е. А. Петраш[1]✉, В. Б. Никишина[1], Н. Ю. Юнина-Пакулова[1], А. С. Минаев[1], Г. Г. Мелконян[2], К. А. Лыткина[2], А. С. Карпенко[3]

[1] Российский национальный исследовательский медицинский университет имени Н. И. Пирогова, Москва, Россия

[2] Госпиталь для ветеранов войн № 3 Департамента здравоохранения города Москвы, Москва, Россия

[3] Московский государственный институт международных отношений (университет) Министерства иностранных дел Российской Федерации, Москва, Россия

Изучение лингвосемантических дескрипторов фантомно-болевых ощущений у пациентов с травматической ампутацией в процессе применения зеркальной визуальной обратной связи обусловлено необходимостью поиска критериев эффективности психологической коррекции фантомно-болевых ощущений. Целью исследования было изучить динамику лингвосемантических дескрипторов болевых ощущений у пациентов с травматической ампутацией с проявлениями фантомно-болевого синдрома как критерия оценки эффективности зеркальной визуальной обратной связи. Общий объем выборки составил 87 мужчин, перенесших травматическую ампутацию одной нижней конечности (возраст — 23–55 лет). Методы исследования: краткая шкала оценки психического статуса MMSE, авторская форма регистрации лингвосемантических дескрипторов фантомно-болевых ощущений, визуальная аналоговая шкала (ВАШ) для оценки интенсивности фантомно-болевых ощущений. Выявленная динамика лингвосемантических дескрипторов фантомно-болевых ощущений у пациентов с травматической ампутацией конечностей с проявлениями фантомно-болевого синдрома в процессе терапии с использованием зеркальной визуальной обратной связи позволяет в качестве критериев эффективности рассматривать следующие: увеличение количества дескрипторов болевых ощущений, представляемых преимущественно в форме конкретных и вещественных существительных (позволяет снизить интенсивность выраженности фантомно-болевых ощущений, оцениваемой по десятибалльной шкале), а также увеличение количества дескрипторов, на лингвосемантическом уровне характеризующих неболевые неприятные ощущения.

Ключевые слова: проявления фантомно-болевого синдрома, дескрипторы фантомно-болевых ощущений, лингвосемантические дескрипторы, зеркальная визуальная обратная связь

Вклад авторов: равнозначный.

Соблюдение этических стандартов: исследование одобрено этическим комитетом Пироговского университета (протокол заседания № 249 от 17 марта 2025 г.), проведено в соответствии с требованиями Основ законодательства «Об охране здоровья граждан»; все участники подписали добровольное информированное согласие на обследование.

✉ **Для корреспонденции:** Екатерина Анатольевна Петраш
ул. Островитянова, д. 1, г. Москва, 117997, Россия; petrash@mail.ru

Статья получена: 29.01.2026 **Статья принята к печати:** 19.02.2026 **Опубликована онлайн:** 26.02.2026

DOI: 10.24075/vrgmu.2026.007

Авторские права: © 2026 принадлежат авторам. **Лицензиат:** РНИМУ им. Н.И. Пирогова. Статья размещена в открытом доступе и распространяется на условиях лицензии Creative Commons Attribution (CC BY) (https://creativecommons.org/licenses/by/4.0/).

The relevance of studying linguistic and semantic descriptors of painful sensations in patients with trauma-related amputation showing manifestations of phantom pain syndrome when using mirror visual feedback results from the fact that manifestation of phantom pain in patients with trauma-related amputation is, on the one hand, combined with manifestations of post-traumatic stress disorders, adjustment disorders, etc., and on the other hand the fact of having phantom pain manifestations affects and sometimes alters motivation for treatment in this group of patients. This impairs social and psychological adaptation, along with socialization in general in the long run [1]. According to the earlier research data, a large proportion of patients with amputations report severe manifestations of phantom pain, which requires special attention during psychological follow-up, rehabilitation training, and rehabilitation of such patients [2].

The mechanism underlying the phantom pain phenomenon is still a matter of debate. When considering the mechanisms underlying the emergence of phantom pain, four major groups can be distinguished formed based on the perceptual organization levels: peripheral, spinal, subcortical, and cortical mechanisms of phantom pain development [3] (Fig. 1).

At the peripheral level of perceptual organization the mechanism underlying the development of phantom painful sensations is determined by neuroma formation in the damaged area. Peripheral mechanisms can affect the processes occurring in the upstream structures, but do not cause phantom painful sensations [4]. At the spinal level of perceptual organization the emergence of phantom painful sensations results from alteration of the neuronal synaptic activity and involvement of nociceptive neurons due to the increased afferent innervation area. This leads to the formation of the abnormal algia system producing painful sensations. Furthermore, the activity of inhibitory neurons is significantly decreased, which interferes with the inhibition of afferent impulses transmitted to the brain [5, 6].

At the subcortical level of perceptual organization the mechanism underlying the development of phantom painful sensations is determined primarily by specific functioning of thalamic structures associated with amputation of any part of the body [7–9]. The thalamus can become sensitized due to the increase in the number of Na^+ channels in thalamic neurons (this has much in common with peripheral sensitization). As a result, pain sensitivity may increase again [9]. The cortical level is represented by three mechanisms underlying the emergence of phantom pain. The first mechanism is associated with functional alterations in the somatosensory and primary motor cortex resulting from the loss of any body part [10–15]. The second one is related directly to the processes associated with the body schema functions within the framework of the proprioceptive memory concept [16–20]. The third central mechanism underlying the development of phantom painful sensations is considered within the framework of the integrative model referred to as neuromatrix [14, 21, 22].

Regardless of the mechanisms underlying the development of phantom painful sensations, a unique role in psychological follow-up of patients with trauma-related amputation of the limb showing manifestations of phantom pain syndrome is played by subjective experiences of pain in the amputated limb. In addition to somatic (physical) sensations, subjective experience of pain is accompanied (characterized) by psychological perception of a physical defect, as well as the experience of traumatic situation of the limb amputation. Psychologically, the phenomenon of subjective experience of pain associated with the loss of the limb (phantom painful sensations) is determined as a combination of pseudo-sensory sensations developed post amputations and is manifested by the illusion of the presence of the body part lost [23–26]. Subjectively, the phantom painful sensations are described using the characteristics of their localization, nature (burning, twisting, sharp, etc.), as well as subjective intensity assessment.

Thus, subjective experiences of phantom painful sensations in patients with amputation of the limb represent a target for psycho-corrective interventions when dealing with this group of patients.

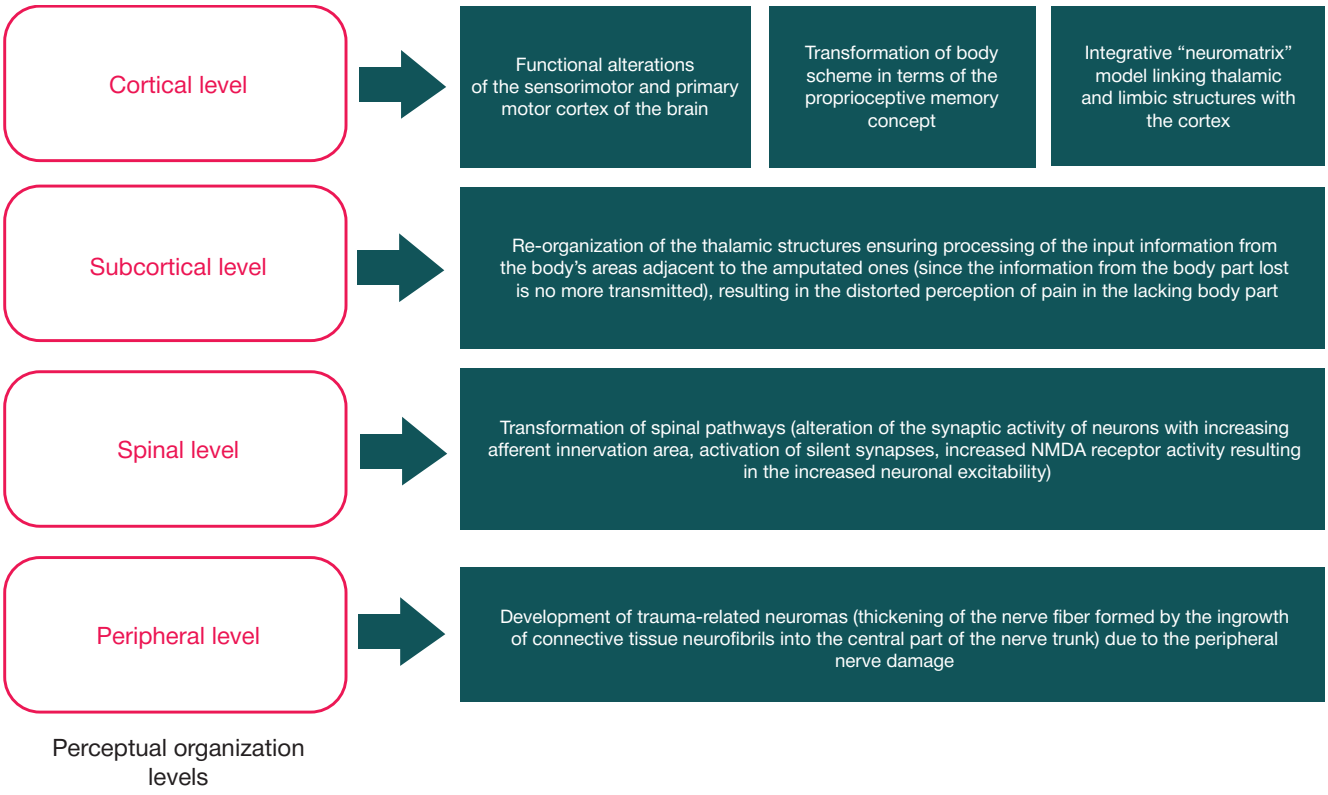

Fig. 1. Scheme hierarchical organization of the mechanisms underlying the emergence of phantom pain

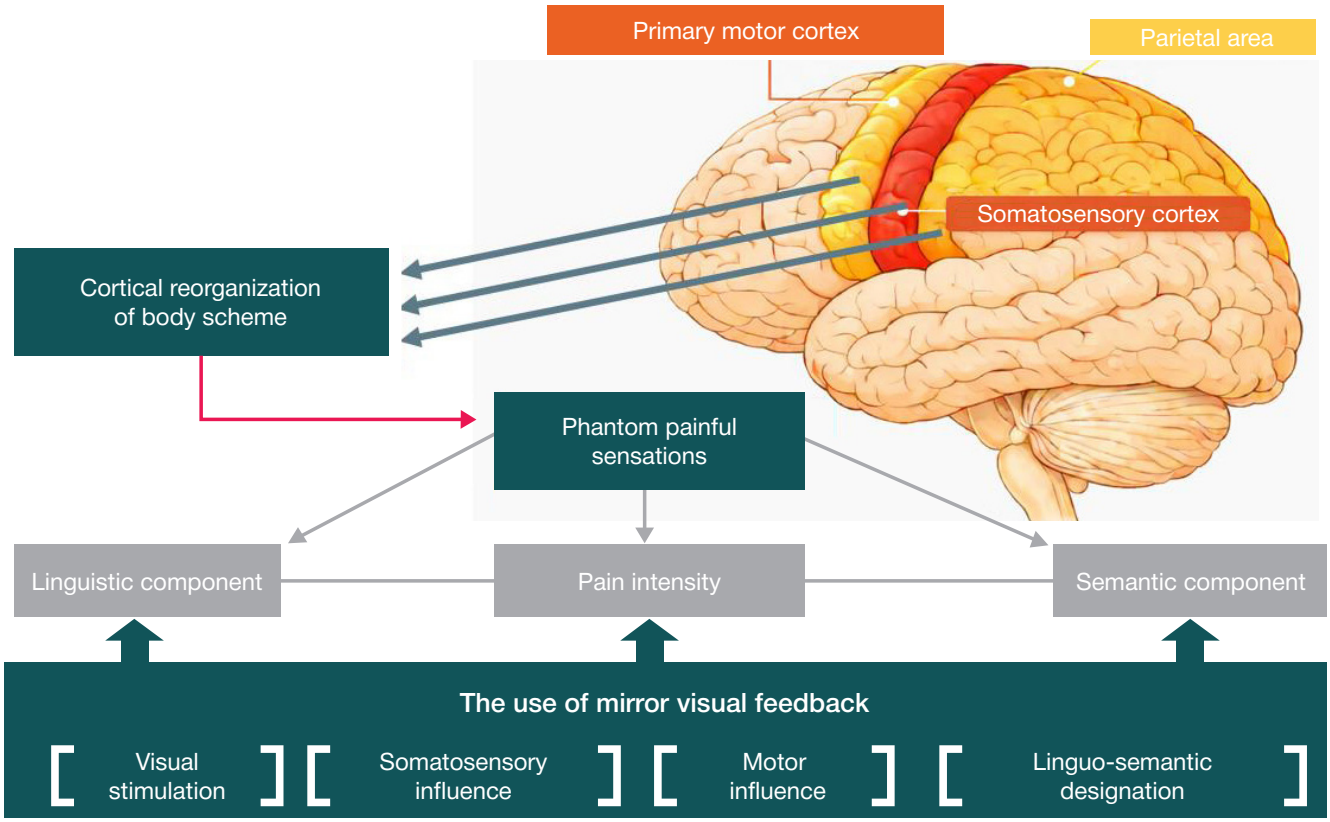

Fig. 2. Scheme of the conceptual model of the dynamic changes in linguistic and semantic descriptors of painful sensations in patients with trauma-related amputation of the limb showing manifestations of phantom pain syndrome during therapy involving the use of mirror visual feedback

In the today's practice of psycho-correction of the phantom pain syndrome manifestations, there is a wide variety of methods aimed at different targets and with different levels of evidence [27–30]. In this paper we will present the procedure of using the mirror visual feedback (mirror illusion) method during psycho-correction of phantom painful sensations, as well as the criteria to assess the procedure effectiveness.

V.S. Ramachandran was the first to propose the use of the mirror visual feedback (or mirror illusion) [13]. In the further studies conducted by both foreign (Deconinck F.J.A., Smorenburg A.R.P., Benham A., Ledebt A., Feltham M.G., Savelsbergh G.J.P., 2015; Zhang JJQ, Fong KNK, Welage N, Liu KPY., 2018) [31, 32] and domestic (Mokienko O.A., Bobrov P.D., Soloveva A.A., Isaev M.R., Kerechanin Ya.V., Ratnikova V.Yu. et al. 2025) [33] researchers, it has been reliably determined that the mirror visual feedback ensures activation of mirror neurons and motor structures of the brain in the hemisphere ipsilateral relative to the active arm, triggering activation of brain plasticity processes [31, 32]. These neurophysiological mechanisms provided the basis for mirror therapy [33]. The efficacy of using mirror visual feedback to adjust the phantom pain syndrome manifestations has been proven at the level of clinical (neurophysiological) manifestations [26, 31, 33]. However, there is no consensus on the criteria of the effectiveness of using this method to adjust manifestations of subjective pain experiences in patients with amputation of the limb.

Considering pathophysiological basis of the emergence of phantom painful sensations, it can be noted that during cortical rearrangement reported in specific cortical areas of the brain, during therapy involving the use of mirror visual feedback, the subjective experience of phantom painful sensations is transformed, which is manifested at the level of linguistic and semantic components (sensory linguistic descriptors and metaphorical constructs — representations of pain), as well as subjective assessment of their intensity. The mechanism underlying the effect of mirror visual feedback during therapy of phantom painful sensations is based on eliminating conflict between the visual and somatosensory afferentation (proprioceptive memory concept) and blocking maladaptive rearrangement processes in specific cortical areas (Fig. 2).

The phantom painful sensations occurring in patients with trauma-related amputation of the limb are designated and marked using the verbal (speech) means studied in linguo-semantic characteristics — descriptors. The linguo-semantic descriptors of phantom painful sensations are represented by various components: sensory descriptors, metaphorical constructs, affective-evaluative markers, and discursive strategies. The specifics of using linguo-semantic constructs to describe phantom painful sensations can include pain severity characteristics. The corrective effect of using mirror visual feedback is based on the fact that these components are influenced by visual stimulation, somatosensory effect, motor effect, and the linguo-semantic designation processes. The mechanism of the use of mirror illusion is based on eliminating conflict between the visual and somatosensory afferentation (proprioceptive memory concept) and blocking maladaptive rearrangement processes in specific cortical areas.

The study aimed to assess the dynamic changes of linguistic and semantic descriptors of painful sensations in patients with trauma-related amputation of the limb showing manifestations of phantom pain syndrome as a criterion to assess the effectiveness of using the mirror visual feedback.

METHODS

The study involved males aged 23–55 years post trauma-related amputation of lower limbs, presenting with phantom painful sensations. The sample size was 87 individuals post amputation

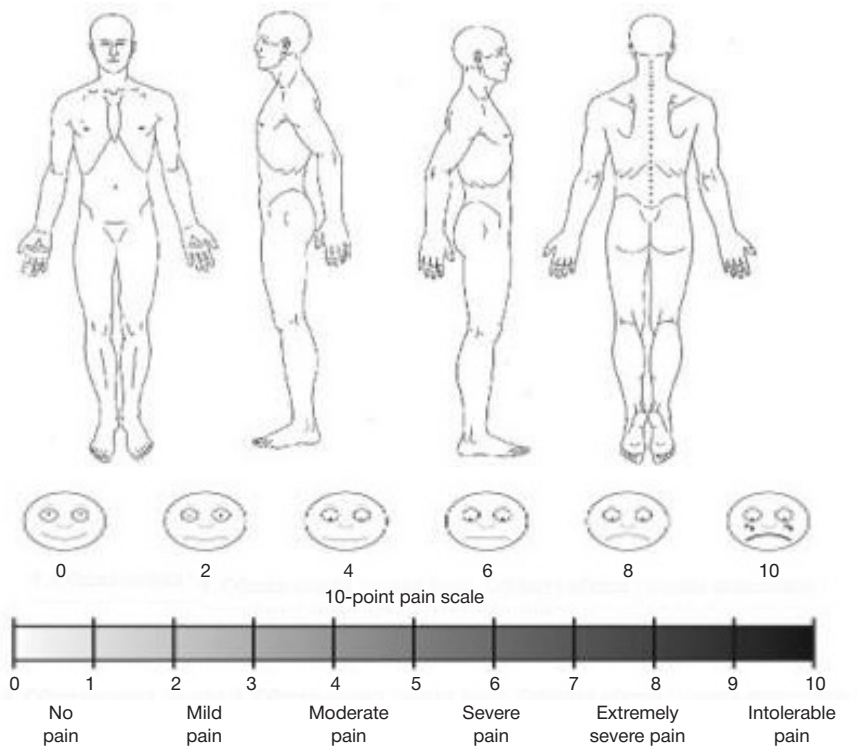

Fig. 3. Example form in the phase of psychological diagnosis of linguo-semantic descriptors of pain in patients with trauma-related amputation showing manifestations of phantom pain syndrome

of one lower limb (being through rehabilitation in a specialized medical institution, 6–18 months had passed since the date of amputation). All the respondents, who were through rehabilitation at the time of assessment, received pain management medications and physiotherapy prescribed by primary care physicians. Inclusion criteria: preserved cognitive function estimated using MMSE (Mini-Mental State Examination) — score 26–30 in quantitative terms. Exclusion criteria: postoperative period (post amputation of the limb); early recovery period (up to 6 months since the date of amputation); severe pain syndrome; other medical contraindications determined by a rehabilitation physician.

Research phases

A common form for recording of phantom pain manifestation was developed in order to implement the first (diagnostic) research phase. The form consists of four sections to be filled sequentially one after another, starting from the first one. At first, during the clinical interview, the patient named and recorded certain characteristics of phantom painful sensations (phantom pain descriptors), without limiting the number of those, and recorded the severity score (1–10 points) for each specified descriptor. Then he formulated and recorded a holistic image of pain (as a verbal description) in the form, and also noted pain severity on a scale ranging from 1 to 10. After that, he had to indicate the level of amputation of the lower limb on the body projections using a black pen, and then shade the regions of the amputated limb where phantom pain was localized with a blue pen. Furthermore, the regions of localization for the phantom pain descriptors recorded in the initial section of the questionnaire were marked with arrows in the body projections, adjacent to the shaded areas. At the final stage of filing the form, the patient had to assess the overall phantom pain severity using the Visual Analog Scale (VAS) and circle the number from 1 to 10 (Fig. 3).

The second research phase (phase of psychological correction) involved 40 patients, who were assessed by the rehabilitation physician and admitted to remedial classes before the psychological correction course involving the use of the FaBo mirror [34]. Among 47 patients, who were not involved in the phase of psychological correction using FaBo mirror, 21 individuals had pulled out; 26 individuals were not admitted to mirror therapy by a rehabilitation physician for medical reasons.

The algorithm for conducting training sessions is illustrated in Fig. 4.

Each patient with lower limb amputation attended five training sessions within the mirror visual feedback program for adjustment of phantom painful sensations.

The results obtained were quantified using the following methods: descriptive statistics (the mean, standard deviation, frequency analysis, mode, median, range) and comparative statistics (Wilcoxon signed-rank test, Fisher angular transformation, $p < 0.05$).

RESULTS

The relationship between the subjective phantom painful sensation severity estimates and the rates of selecting the descriptors to describe phantom painful sensations allowed us to reveal high variability in both the number of descriptors and the descriptor severity levels. However, the most common ones (central descriptors) are represented by three variants: “burning”, “shots”, and “tingling” (Fig. 5).

The rates of sensory descriptors in the group of war veterans with amputation of the lower limb are distributed as follows: “burning” (60%), “shots” (60%), “tingling” (46%), “nagging pain” (20%), “spasm” (16%), “throbbing pain” (6%), “freezing” (4%), “pulling pain” (12%), “itching” (12%), “twisting” (18%), “chills” (4%), “numbness” (8%), “compression” (12%), “dull ache” (6%), “shock” (10%), “lancinating pain” (6%). When comparing the rates of linguo-semantic descriptors with their intensity on a 10-point scale, discrepancy is reported: with the maximum rates of phantom painful sensations in the form of burning, shots, and tingling, the most intense are dull ache and the sensation referred to as “itching”.

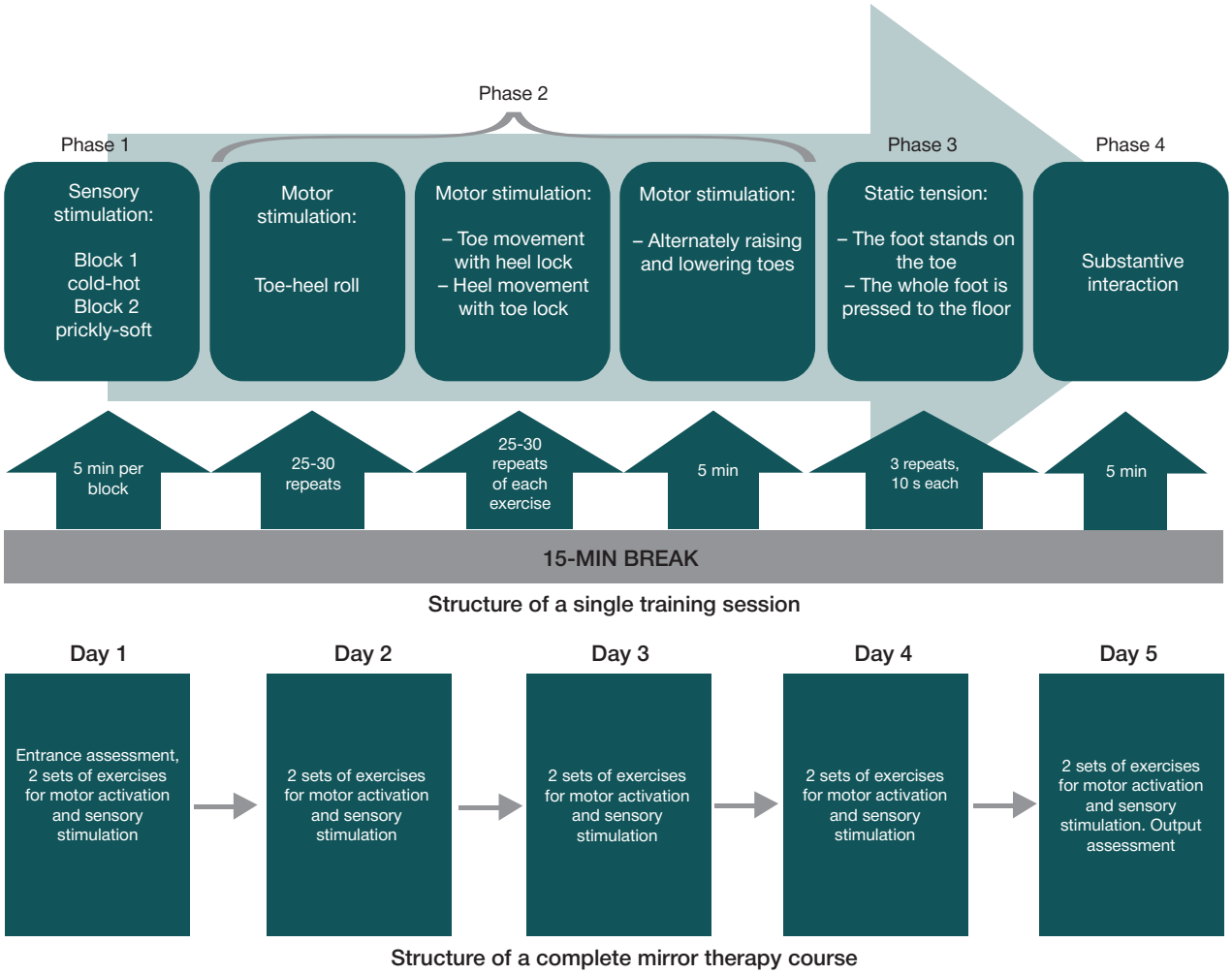

Fig. 4. Algorithm to conduct the psychological correction procedure involving the use of the FaBo mirror in patients with trauma-related amputation of lower limbs

We differentiate linguo-semantic descriptors of phantom painful sensations into two groups: the descriptors, the names of which are based on nouns, and the descriptors, the names of which are based on adjectives. The noun-based linguo-semantic descriptors are, in turn, divided into two groups: the descriptors designated by concrete and material nouns; the descriptors designated by verbal nouns. The share of the linguo-semantic descriptors represented by the adjectives describing qualitative characteristics of phantom painful sensations is 25%. The share of concrete and material nouns

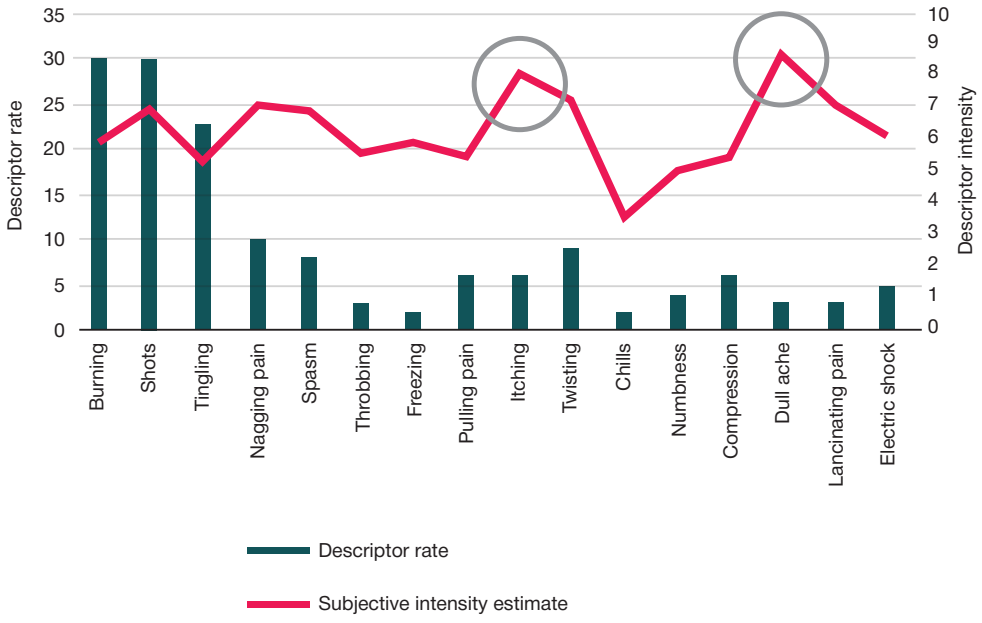

Fig. 5. Relationship between the rates of selecting the descriptors to describe phantom painful sensations and the subjective estimates of their intensity in patients

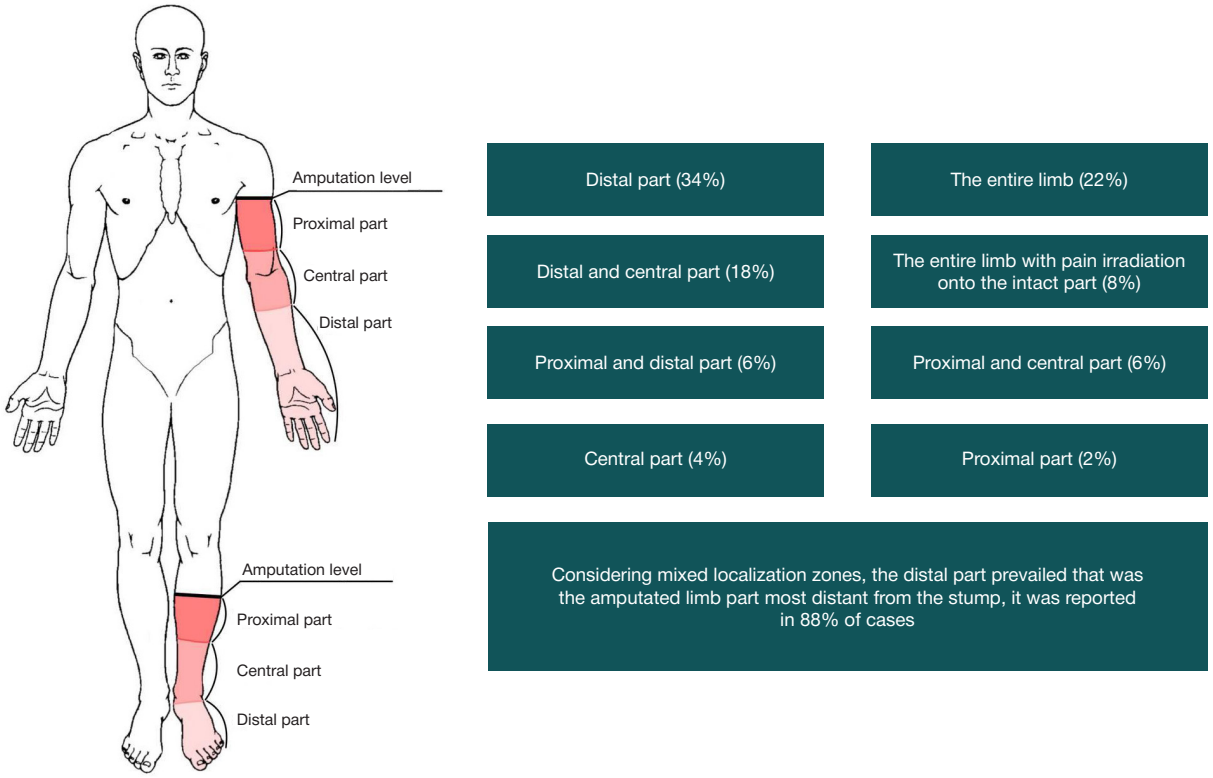

Fig. 6. Scheme of phantom painful sensation localization in patients with trauma-related amputation of lower limbs

characterizing individual meanings, personal meanings, and categorical structures of consciousness in designation of linguo-semantic descriptors is 31% of the total number of descriptors. The vast majority of descriptors are designated by patients with trauma-related amputation of lower limbs with verbal nouns, denoting the objectification of action. This linguo-semantic descriptor form, transforming the dynamic process into a static term, consolidates phantom painful sensations at the level of linguistic semantic meaning.

As for their qualitative characteristics, the descriptors were divided into two groups based on the criterion of painful nature: naturally, painful sensations predominate and account for 75% of the total number of descriptors (“burning”, “shots”, “tingling”, “nagging pain”, “spasm”, “throbbing pain”, “pulling pain”, “twisting”, “compression”, “dull ache”, “shock”, “lancinating pain”). The non-painful descriptors characterizing unpleasant sensations in the phantom limb that are not pain account for 25% and include such labels, as “freezing”, “itching”, “chills”, “numbness”.

The following trends are distinguished based on the subjective assessment of phantom painful sensation localization: in the distal part of the amputated limb — 34%, in the distal to central part of the amputated limb — 18%, the entire amputated part of the limb — 22%, the proximal to distal part of the amputated limb — 6%, the entire amputated part of the limb with the spread onto the intact part of the stump — 8%, central part of the amputated limb — 4%, proximal to central part of the amputated limb — 6%, proximal part of the amputated limb — 2% (Fig. 6).

According to the results of the painful sensation localization subjective assessment, the vast majority of patients with amputation of lower limbs specify the distal part of the amputated limb, which is most distant from the stump, — 88% of cases.

In addition to quantitative analysis, qualitative analysis was also carried out. The patients had to provide the description of a phantom painful sensation holistic image and estimate its subjective severity on a 10-point scale. A total of 88% of patients with phantom painful sensations were able to provide holistic images of pain. Three groups were formed based on the phantom pain image characteristics. The first group of images is characterized by involuntary movement of various parts of the amputated limb (in 61% of patients). The following speech constructs are used to describe the image of phantom pain sensations: “toes curl”, “toes are twisted”, “toes bend”, “the foot bends”, “the toes are stretching”. Clinical example: “the toes are intertwined and one of those digs its nail into the other and pierces it through”. The second group of images is characterized by changes in the size and integrity of the amputated part of the limb; it is represented in 20% of patients with amputation of lower limbs. When talking, the patients use such speech construct, as “the leg is swelling”, “a piece of meat was torn off”, “the nail digs into another toe”, “the leg has grown and is resting against the back of the bed”, “the nails are moving away from the toes”. Such representation of the holistic image of phantom painful sensations, as “the leg has grown and is resting against the back of the bed”, can be considered the clinical example. Patients of the third group represent the images through description of the exposure to the external stimulus (43% of patients). Such speech constructs, as “someone is pressing a bone on the skin”, “the toes are burnt with a lighter”, “the leg is in the water”, “the leg is clamped in a vice”, “the leg is pierced with an awl”, “an object falls on the foot”, were used to verbally describe the holistic image.

The correlation analysis procedure allowed us to distinguish two strategies of linguo-semantic designation of phantom painful sensations in patients with trauma-related amputation of lower limbs. The first strategy is determined by high differentiation of descriptors with their low intensity in terms of differentiation, but high aggregate intensity. This strategy is confirmed by the identified inverse significant correlations between the intensity of distinct linguo-semantic descriptors and the total number of descriptors describing phantom pain manifestations; as well as by the direct significant correlations ($r = 0.424$) between subjective estimates of the holistic image of

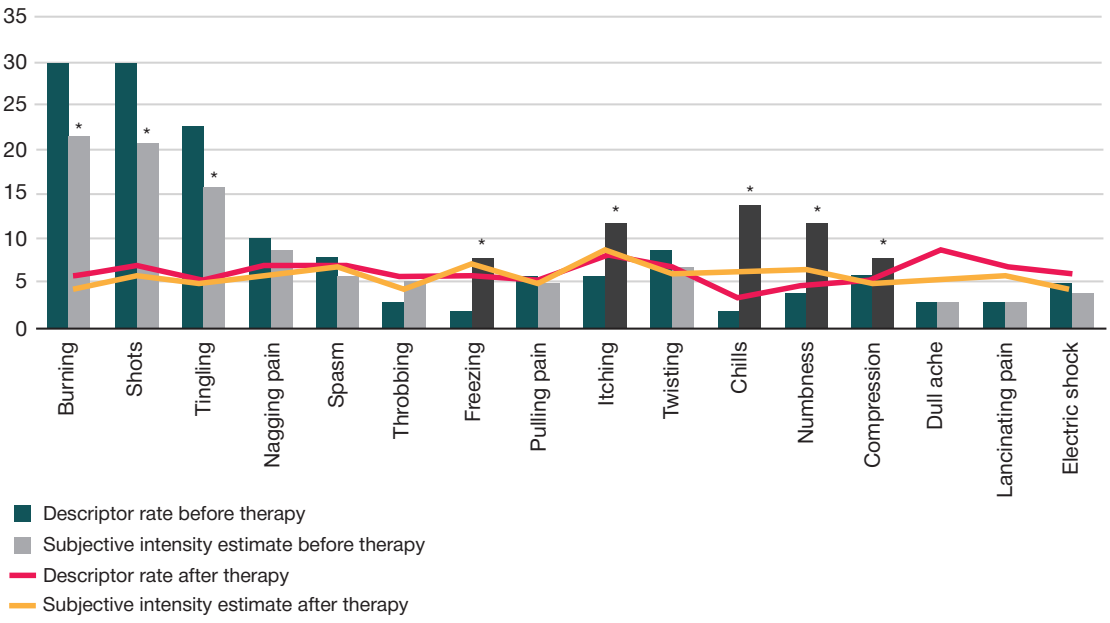

Fig. 7. Relationship between the phantom pain descriptor rates and manifestation intensity in patients before and after the training course involving the use of the FaBo mirror

phantom painful sensations and the VAS pain severity scores. This system of correlations includes the descriptors characterized by maximum rates or maximum intensity. Thus, the total number of descriptors is related to the intensity of burning (r = –0.536) and tingling (r = –0.429) being the most common descriptors; when the intensity is high, the number of descriptors is correlated to the intensity of nagging pain (r = –0.418) and twisting (r = –0.504). The data obtained suggest that the more differentiated is the linguo-semantic designation of the phantom pain manifestation, the lower is the intensity of single manifestations characterizing the phantom pain painful nature.

The second strategy of the linguo-semantic designation of phantom painful sensations in patients with trauma-related amputation of lower limbs is manifested by low differentiation of the descriptors with their high intensity (both aggregate intensity and intensity of distinct descriptors). This strategy is confirmed by the identified direct significant correlations between the total number of descriptors and the intensity of low-rate linguo-semantic descriptors: chills (r = 0.522), numbness (r = 0.427), freezing (r = 0.416), pulling (r = 0.402) and clenching (r = 0.411) pain; as well as between subjective estimates of the intensity of distinct descriptors and the VAS pain severity scores. Thus, it is clear that the more differentiated descriptors are used by the patient to designate the phantom pain manifestations, the higher the intensity of non-painful sensations represented by war veterans with amputation of lower limbs in the linguo-semantic constructs describing the phantom pain manifestations.

The second phase of the study involved 36 individuals admitted to remedial classes involving the use of mirror visual feedback out of 40 patients with trauma-related amputation of lower limbs; they completed the full course, consisting of five training sessions. Re-evaluation was conducted after completing the training course.

Assessment of the significance of differences in the number of descriptors and intensity of their manifestations revealed significant differences in both rates of descriptors and subjective estimates of their intensity. This shows that the rate of such descriptors, as “burning” (p = 0.021), “shots” (p = 0.018), and “tingling” (p = 0.018), which prevailed before the remedial training course, significantly decreased after completing the course of five training sessions. However, these descriptors remained predominant. We should also note a significant increase in the rates of the linguo-semantic meaning the non-painful sensations: “freezing” (p = 0.024), “itching” (p = 0.031), “chills” (p = 0.019), “numbness” (p = 0.021), and “compression” (p = 0.022) (Fig. 7).

Assessment of the dynamic changes in the relationship of the linguistic forms used to designate the descriptors of painful sensations and their semantic contents after the end of the remedial training course involving the use of mirror visual feedback also revealed significant differences. The percentage of verbal nouns decreased significantly (from 44 to 35%), which suggests a shift towards predominance of concrete and material nouns. The percentage of the descriptors characterizing painful sensations also decreased with increasing percentage of the descriptors describing unpleasant (non-painful) sensations (from 75 to 68%). According to reliable indicators, the system of correlations between the number of descriptors of painful sensations in patients with trauma-related amputation of lower limbs having phantom pain and the intensity of painful sensations remained unchanged after the remedial training course (the changes affected the values of significant correlation coefficients only).

Thus, the research results obtained showed that mostly verbal nouns characterizing the painful sensations’ duration (meaning an action, process, or result of an action) are used as linguo-semantic descriptors of phantom painful sensations in patients with trauma-related amputation of lower limbs showing manifestations of phantom pain syndrome with the pronounced intensity that describe various painful sensations.

It should be noted that four patients with trauma-related amputation of the lower limb showing manifestations of phantom pain out of 40 refused further procedures, reporting increased phantom painful sensations, after one or two training sessions. Patients complained that during and after the procedures, the intensity of phantom painful sensations increased, arising against the background of involuntary phantom movements of the amputated part of the limb, which imitated the exercises and movements performed during the procedure: “I feel the amputated part more clearly, how it bends and flexes, aches and hurts”.

DISCUSSION

The image of pain is a holistic linguo-semantic structure, the result of integration of various sensory modalities of

painful sensations. The image of phantom painful sensations presented in the authors' interpretation is most close to the linguo-semantic metaphorical constructs — figurative expressions that contain causal and affective interpretations. Such constructs often reflect not only the intensity of phantom painful sensations, but also the patient's attitude towards this [35]. The differentiated nature of the verbal description of phantom painful sensations in patients with trauma-related amputation of the limbs involving the use of linguo-semantic descriptors is in line with the results of the studies focused on neurophysiological correlates involving the use of mirror visual feedback, i.e. bilateral activation of primary sensorymotor areas of the cerebral cortex [33], which, in turn, corresponds to the cortical level of perceptual organization of the mechanisms underlying the emergence of phantom painful sensations. Subjective assessment of the phantom painful sensation localization mainly in distal parts of the amputated limb can be considered as the indirect evidence of the peripheral level of perceptual organization of the mechanisms underlying the emergence of phantom painful sensations [4].

The image of phantom painful sensations is represented by variability of linguo-semantic descriptors and the image description reflects the contents of the unique experience of reliving and interpretation of various phantom painful sensations. Integration of various sensation types in the verbal description of the image of pain (tactile, muscular, stereognostic) suggests the involvement of the associative cortex of posterior brain regions ensuring synthesis and processing of multimodal information, along with the primary motor and somatosensory cortex.

CONCLUSIONS

The linguo-semantic representation of the image of phantom painful sensations with involuntary movement of various parts of the amputated limb and disruption of the integrity of these parts is characterized by qualitative differences from the phantom pain representation described in terms of exposure to the external stimulus. The other two groups of the linguo-semantic representation of the holistic image of pain (in terms of the external influence or changes in the size and integrity of the amputated limbs) reflect the verbalized process of experiencing the maladaptive cortical rearrangement in the primary motor and somatosensory cortex, rearrangement of sensory maps, while the latter group at the level of the linguo-semantic characteristics represents the holistic image of phantom painful sensations in terms of the subjective sensory-perceptive experience allowing one to explain the origin of such sensations "as if I were holding my hands over a fire," "as if I were standing with my foot in water"). The identified dynamic changes of the linguo-semantic descriptors of phantom painful sensations in patients with trauma-related amputation of the limbs showing manifestations of phantom pain syndrome during therapy involving the use of mirror visual feedback allows one to consider the following as the effectiveness criteria: the increase in the number of descriptors of painful sensations represented mainly in the form of concrete and material nouns (allowing one to reduce the intensity of phantom painful sensation assessed on the 10-point scale), as well as the increase in the number of descriptors characterizing non-painful unpleasant sensations at the linguo-semantic level.

References

1. Morgan L., Aldington D. Comorbid chronic pain and post-traumatic stress disorder in UK veterans: a lot of theory but not enough evidence. Br J Pain, 2020.
2. Resnik L, Ekerholm S, Borgia M, Clark MA. A national study of Veterans with major upper limb amputation: Survey methods, participants, and summary findings. 2019.
3. Wu H, Saini C, Medina R, Hsieh SL, Meshkati A, Sung K. Pain without presence: a narrative review of the pathophysiological landscape of phantom limb pain. Front Pain Res. 2025; 6: 1419762.
4. Collins KL. A review of current theories and treatments for phantom limb pain. The Journal of Clinical Investigation. 2018; 128 (6): 2168–76.
5. Kondratev IA, Dzhodzhua AV, Anankin AA, i dr. Sovremennye predstavleniya o fantomnoj boli i metodah eyo lecheniya. Vestnik nacional'nogo mediko-hirurgicheskogo centra im. N. I. Pirogova. 2025; 20 (3). Russian.
6. Kuffler DP. Evolving techniques for reducing phantom limb pain. Exp Biol Med. 2023; 248 (7): 561–72.
7. Andoh J, Milde C, Diers M, et al. Assessment of cortical reorganization and preserved function in phantom limb pain: a methodological perspective. Sci Rep. 2020.
8. Florence SL, Hackett TA, Strata F. Thalamic and cortical contributions to neural plasticity after limb amputation. J Neurophysiol. 2000; 83 (5): 3154–9.
9. Zhao P, Waxman SG, Hains BC. Sodium channel expression in the ventral posterolateral nucleus of the thalamus after peripheral nerve injury. Mol Pain. 2006.
10. Kaas JH. The reorganization of somatosensory and motor cortex after peripheral nerve or spinal cord injury in primates. Prog Brain Res. 2000.
11. Rasmusson DD. Reorganization of raccoon somatosensory cortex following removal of the fifth digit. J Comp Neurol. 1982.
12. Makin TR, Flor H. Brain (re)organisation following amputation: Implications for phantom limb pain. NeuroImage. 2020.
13. Ramachandran VS, Hirstein W. The perception of phantom limbs. The D. O. Hebb lecture. Brain: A Journal of Neurology. 1998.
14. Katz J, Melzack R. Pain "memories" in phantom limbs: review and clinical observations. Pain. 1990.
15. Maravita A, Iriki A. Tools for the body (schema). Trends in Cognitive Sciences. 2004.
16. Anderson-Barnes VC, McAuliffe C, Swanberg KM, Tsao JW. Phantom limb pain — a phenomenon of proprioceptive memory? Med Hypotheses. 2009.
17. Di Pino G, Piombino V, Carassiti M, Ortiz-Catalan M. Neurophysiological models of phantom limb pain: what can be learnt. Minerva Anestesiol. 2021.
18. Giaxoglou K. The Language of Pain: Expression or Description? Journal of Greek Linguistics. 2009; 9.
19. Chiyohara S, Furukawa JI, Noda T, Morimoto J, Imamizu H. Proprioceptive short-term memory in passive motor learning Sci Rep. 2023.
20. Moseley LG. I can't find it! Distorted body image and tactile dysfunction in patients with chronic back pain. Pain. 2008.
21. Bittar RG, Otero S, Carter H, Aziz TZ. Deep brain stimulation for phantom limb pain. Journal of Clinical Neuroscience. 2005.
22. Giummarra MJ, Gibson SJ, Georgiou-Karistianis N, Bradshaw JL. Central mechanisms in phantom limb perception: The past, present and future. Brain Research Reviews. 2007.
23. Nikishina VB, Bobyncev II, Petrash EA, Minyahina KA. Deskriptory intraceptivnyh oshchushchenij pri fantomno-bolevom sindrome u lyudej s amputaciej nizhnih konechnostej. Kurskij nauchno-prakticheskij vestnik «CHelovek i ego zdorov'e». 2015; 3: 133–39. Russian.
24. Zhang K, Ding L, Wang X, et al. Mirror therapy reduces excessive variability of motor network in stroke patients: a randomized controlled trial. Eur J Phys Rehabil Med. 2025; 61: 184–94.
25. Zhuang J, Lei X, Guo X, Ding L, Jia J. Motor and parietal cortex activity responses to mirror visual feedback in patients with subacute stroke: An EEG study. Clin Neurophysiol Pract. 2025; 10: 12–21.
26. Xie H-M, Zhang K-X, Wang S, et al. Effectiveness of Mirror Therapy for Phantom Limb Pain: A Systematic Review and Metaanalysis. Arch Phys Med Rehabil. 2022; 103: 988–97.
27. Sanabria-Mazo JP, Colomer-Carbonell A, Fernández-Vázquez Ó,

et al. A systematic review of cognitive behavioral therapy-based interventions for comorbid chronic pain and clinically relevant psychological distress. Front Psychol. 2023.
28. Bicego A, Delmal P, Ledoux D, et al. Self-Hypnosis for Phantom Limb Pain: A Multiple-Case Study. OBM Integrative and Complementary Medicine. 2022.
29. Lendaro E, Van der Sluis CK, Hermansson L, et al. Extended reality used in the treatment of phantom limb pain: a multicenter, double-blind, randomized controlled trial. PAIN. 2025; 166 (3): 571–86.
30. Marshall Wilensky. Eye Movement Desensitization and Reprocessing (EMDR) as a Treatment for Phantom Limb Pain. British Columbia School of Professional Psychology. Vancouver, British Columbia, Canada. 2006.
31. Deconinck FJA, Smorenburg ARP, Benham A, Ledebt A, Feltham MG, Savelsbergh GJP. Reflections on Mirror Therapy: A Systematic Review of the Effect of Mirror Visual Feedback on the Brain. Neurorehabilitation and Neural Repair. 2015; 29: 349–61.
32. Zhang JJQ, Fong KNK, Welage N, Liu KPY. The Activation of the Mirror Neuron System during Action Observation and Action Execution with Mirror Visual Feedback in Stroke: A Systematic Review. Neural Plast. 2018; 2018: 2321045.
33. Mokienko OA, Bobrov PD, Soloveva AA, Isaev MR, Kerechanin YaV, Ratnikova VYu, i dr. Nejrofiziologicheskie markery illyuzii, vyzvannoj zerkal'noj vizual'noj obratnoj svyaz'yu. Vestnik RGMU. 2025; 5: 91–99. DOI: 10.24075/vrgmu.2025.052. Russian.
34. Nikishina VB, SHagina ED, YUnina-Pakulova NYu, Petrash EA. Metodicheskie rekomendacii po sposobu korrekcii fantomnyh bolej metodom zerkal'noj terapii «Zerkalo FaBo». Moskva, 2024; 45 s. Russian.
35. Meltzoff AN, Moore MK. Explaining facial imitation: A theoretical model. Early Development and Parenting. 1997.

Литература

1. Morgan L., Aldington D. Comorbid chronic pain and post-traumatic stress disorder in UK veterans: a lot of theory but not enough evidence. Br J Pain, 2020.
2. Resnik L, Ekerholm S, Borgia M, Clark MA. A national study of Veterans with major upper limb amputation: Survey methods, participants, and summary findings. 2019.
3. Wu H, Saini C, Medina R, Hsieh SL, Meshkati A, Sung K. Pain without presence: a narrative review of the pathophysiological landscape of phantom limb pain. Front Pain Res. 2025; 6: 1419762.
4. Collins KL. A review of current theories and treatments for phantom limb pain. The Journal of Clinical Investigation. 2018; 128 (6): 2168–76.
5. Кондратьев И. А., Джоджуа А. В., Ананкин А. А. и др. Современные представления о фантомной боли и методах её лечения. Вестник национального медико-хирургического центра им. Н. И. Пирогова. 2025; 20 (3).
6. Kuffler DP. Evolving techniques for reducing phantom limb pain. Exp Biol Med. 2023; 248 (7): 561–72.
7. Andoh J, Milde C, Diers M, et al. Assessment of cortical reorganization and preserved function in phantom limb pain: a methodological perspective. Sci Rep. 2020.
8. Florence SL, Hackett TA, Strata F. Thalamic and cortical contributions to neural plasticity after limb amputation. J Neurophysiol. 2000; 83 (5): 3154–9.
9. Zhao P, Waxman SG, Hains BC. Sodium channel expression in the ventral posterolateral nucleus of the thalamus after peripheral nerve injury. Mol Pain. 2006.
10. Kaas JH. The reorganization of somatosensory and motor cortex after peripheral nerve or spinal cord injury in primates. Prog Brain Res. 2000.
11. Rasmusson DD. Reorganization of raccoon somatosensory cortex following removal of the fifth digit. J Comp Neurol. 1982.
12. Makin TR, Flor H. Brain (re)organisation following amputation: Implications for phantom limb pain. NeuroImage. 2020.
13. Ramachandran VS, Hirstein W. The perception of phantom limbs. The D. O. Hebb lecture. Brain: A Journal of Neurology. 1998.
14. Katz J, Melzack R. Pain "memories" in phantom limbs: review and clinical observations. Pain. 1990.
15. Maravita A, Iriki A. Tools for the body (schema). Trends in Cognitive Sciences. 2004.
16. Anderson-Barnes VC, McAuliffe C, Swanberg KM, Tsao JW. Phantom limb pain — a phenomenon of proprioceptive memory? Med Hypotheses. 2009.
17. Di Pino G, Piombino V, Carassiti M, Ortiz-Catalan M. Neurophysiological models of phantom limb pain: what can be learnt. Minerva Anestesiol. 2021.
18. Giaxoglou K. The Language of Pain: Expression or Description? Journal of Greek Linguistics. 2009; 9.
19. Chiyohara S, Furukawa JI, Noda T, Morimoto J, Imamizu H. Proprioceptive short-term memory in passive motor learning Sci Rep. 2023.
20. Moseley LG. I can't find it! Distorted body image and tactile dysfunction in patients with chronic back pain. Pain. 2008.
21. Bittar RG, Otero S, Carter H, Aziz TZ. Deep brain stimulation for phantom limb pain. Journal of Clinical Neuroscience. 2005.
22. Giummarra MJ, Gibson SJ, Georgiou-Karistianis N, Bradshaw JL. Central mechanisms in phantom limb perception: The past, present and future. Brain Research Reviews. 2007.
23. Никишина В. Б., Бобынцев И. И., Петраш Е. А., Миняхина К. А. Дескрипторы интрацептивных ощущений при фантомно-болевом синдроме у людей с ампутацией нижних конечностей. Курский научно-практический вестник «Человек и его здоровье». 2015; 3: 133–39.
24. Zhang K, Ding L, Wang X, et al. Mirror therapy reduces excessive variability of motor network in stroke patients: a randomized controlled trial. Eur J Phys Rehabil Med. 2025; 61: 184–94.
25. Zhuang J, Lei X, Guo X, Ding L, Jia J. Motor and parietal cortex activity responses to mirror visual feedback in patients with subacute stroke: An EEG study. Clin Neurophysiol Pract. 2025; 10: 12–21.
26. Xie H-M, Zhang K-X, Wang S, et al. Effectiveness of Mirror Therapy for Phantom Limb Pain: A Systematic Review and Metaanalysis. Arch Phys Med Rehabil. 2022; 103: 988–97.
27. Sanabria-Mazo JP, Colomer-Carbonell A, Fernández-Vázquez ó, et al. A systematic review of cognitive behavioral therapy-based interventions for comorbid chronic pain and clinically relevant psychological distress. Front Psychol. 2023.
28. Bicego A, Delmal P, Ledoux D, et al. Self-Hypnosis for Phantom Limb Pain: A Multiple-Case Study. OBM Integrative and Complementary Medicine. 2022.
29. Lendaro E, Van der Sluis CK, Hermansson L, et al. Extended reality used in the treatment of phantom limb pain: a multicenter, double-blind, randomized controlled trial. PAIN. 2025; 166 (3): 571–86.
30. Marshall Wilensky. Eye Movement Desensitization and Reprocessing (EMDR) as a Treatment for Phantom Limb Pain. British Columbia School of Professional Psychology. Vancouver, British Columbia, Canada. 2006.
31. Deconinck FJA, Smorenburg ARP, Benham A, Ledebt A, Feltham MG, Savelsbergh GJP. Reflections on Mirror Therapy: A Systematic Review of the Effect of Mirror Visual Feedback on the Brain. Neurorehabilitation and Neural Repair. 2015; 29: 349–61.
32. Zhang JJQ, Fong KNK, Welage N, Liu KPY. The Activation of the Mirror Neuron System during Action Observation and Action Execution with Mirror Visual Feedback in Stroke: A Systematic Review. Neural Plast. 2018; 2018: 2321045.
33. Мокиенко О. А., Бобров П. Д., Соловьева А. А., Исаев М. Р., Керечанин Я. В., Ратникова В. Ю. и др. Нейрофизиологические маркеры иллюзии, вызванной зеркальной визуальной обратной связью. Вестник РГМУ. 2025; 5: 91–99. DOI: 10.24075/vrgmu.2025.052.
34. Никишина В. Б., Шагина Е. Д., Юнина-Пакулова Н. Ю., Петраш Е. А. Методические рекомендации по способу коррекции фантомных болей методом зеркальной терапии «Зеркало ФаБо». Москва, 2024; 45 с.
35. Meltzoff AN, Moore MK. Explaining facial imitation: A theoretical model. Early Development and Parenting. 1997.

RESULTS OF SIMULTANEOUS COMBINED LASER TREATMENT OF NEWLY DIAGNOSED PRIMARY OPEN-ANGLE GLAUCOMA

Tahchidi KhP[1], Doga AV[2], Obodova KV[3]✉

[1] Pirogov Russian National Research Medical University, Moscow, Russia
[2] Fyodorov Eye Microsurgery Federal State Institution, Moscow, Russia
[3] Yekaterinburg Eye Microsurgery Center, Yekaterinburg, Russia

Today, selection of the optimal treatment method in patients with the early-stage primary open-angle glaucoma (POAG) remains an urgent problem of ophthalmology. There are various approaches to treating such patients, including the use of topical therapy and laser treatments. The study aimed to assess the hypotensive effect and clinical and functional outcomes of the simultaneous combined laser treatment, including YAG-LAT and the subsequent one-time SLT in the same localization zones, in patients with the newly diagnosed early-stage POAG and moderately elevated intraocular pressure (IOP). The study included 100 eyes with stage I POAG, which were divided into two groups: group I — 50 eyes before and after YAG-LAT and SLT; group II – 50 eyes that underwent SLT only. The follow-up period was 12 months. In patients of groups I and II, a decrease in IOP by 28 and 30.5% relative to the baseline IOP was reported at 1 month, and by 32.2 and 32% at 3 months, respectively. The intergroup difference in the extent of IOP decrease at 1 and 3 months was non-significant ($p > 0.05$). There was still good hypotensive effect, up to 29.3% of the preoperative value, 12 months after YAG-LAT and SLT. Twelve months after SLT, the hypotensive effect was 17%. The intergroup difference in the extent of IOP decrease at 12 months was significant ($p < 0.05$). Glaucoma stabilization was reported in groups I and II, but in group II, antihypertensive therapy was required in 63% of cases. The simultaneous combined laser treatment technology (YAG-LAT and SLT) showed a pronounced, persistent hypotensive effect and glaucoma stabilization when used for treatment of the newly diagnosed early-stage POAG.

Keywords: newly identified primary open-angle glaucoma, first-line therapy, selective laser trabeculoplasty, YAG laser activation of the trabecula, alternative drug therapy strategy, hypotensive therapy

Author contribution: Tahchidi KhP, Doga AV — study concept and design, manuscript editing; Obodova KV — study concept and design, material collection, analysis, and processing, statistical data processing, manuscript writing.

Compliance with ethical standards: the study was approved by the Ethics Committee of the Yekaterinburg Eye Microsurgery Center (protocol No. 6 dated 22 January 2026)

✉ **Correspondence should be addressed:** Kseniya V. Obodova
Bardina, 4A, Yekaterinburg, 620149, Russia; zxx1991@yandex.ru

Received: 17.12.2025 **Accepted:** 25.01.2026 **Published online:** 01.02.2026

DOI: 10.24075/brsmu.2026.004

Copyright: © 2026 by the authors. **Licensee:** Pirogov University. This article is an open access article distributed under the terms and conditions of the Creative Commons Attribution (CC BY) license (https://creativecommons.org/licenses/by/4.0/).

РЕЗУЛЬТАТЫ ОДНОВРЕМЕННОГО КОМБИНИРОВАННОГО ЛАЗЕРНОГО ЛЕЧЕНИЯ ВПЕРВЫЕ ВЫЯВЛЕННОЙ ПЕРВИЧНОЙ ОТКРЫТОУГОЛЬНОЙ ГЛАУКОМЫ

Х. П. Тахчиди[1], А. В. Дога[2], К. В. Ободова[3]✉

[1] Российский национальный исследовательский медицинский университет имени Н. И. Пирогова, Москва, Россия
[2] Национальный медицинский исследовательский центр, Межотраслевой научно-технический комплекс «Микрохирургия глаза» имени С. Н. Федорова, Москва, Россия
[3] Екатеринбургский центр, Межотраслевой научно-технический комплекс «Микрохирургия глаза», Екатеринбург, Россия

На сегодняшний день выбор оптимального метода лечения пациентов с начальной стадией первичной открытоугольной глаукомы (ПОУГ) остается актуальной проблемой в офтальмологии. Существуют различные подходы к лечению таких пациентов, среди которых использование местной топической терапии и лазерные методы лечения. Целью работы было провести исследование состояния гипотензивного эффекта и клинико-функциональных результатов одновременного комбинированного лазерного лечения, включающего YAG-ЛАТ и последующую за ней, по тем же зонам локализации, одномоментную СЛТ у пациентов с начальной стадией впервые выявленной ПОУГ с умеренно повышенным уровнем ВГД. В исследование вошли 100 глаз с ПОУГ I стадии, они были разделены на две группы: I группа — 50 глаз до и после проведения YAG-ЛАТ и СЛТ; II группа — 50 глаз, которым была выполнена только СЛТ. Срок наблюдения — 12 месяцев. У пациентов I и II групп через месяц отмечено снижение ВГД на 28 и 30,5%, через 3 месяца на 32,2 и 32% от исходного уровня ВГД соответственно. Различие между группами по степени снижения ВГД через 1 и 3 месяца было статистически незначимым ($p > 0,05$). Через 12 месяцев после YAG-ЛАТ и СЛТ сохранялся хороший гипотензивный эффект, составивший до 29,3% от его дооперационного значения. После СЛТ гипотензивный эффект через 12 месяцев достигал 17%. Различие между группами по степени снижения ВГД через 12 месяцев статистически значимо ($p < 0,05$). В I и II группах наблюдалась стабилизация глаукомного процесса, но во II группе в 63% случаев потребовалась гипотензивная терапия. Технология одновременного комбинированного лазерного лечения (YAG-ЛАТ и СЛТ) показала выраженный, стойкий гипотензивный эффект и стабилизацию глаукомного процесса при лечении начальной стадии впервые выявленной ПОУГ.

Ключевые слова: впервые выявленная первичная открытоугольная глаукома, терапия первой линии, селективная лазерная трабекулопластика, YAG-лазерная активация трабекулы, альтернативная стратегия медикаментозной терапии, гипотензивная терапия

Вклад авторов: Х. П. Тахчиди, А. В. Дога — концепция и дизайн исследования, редактирование рукописи; К. В. Ободова — концепция и дизайн исследования, сбор, анализ и обработка материала, статистическая обработка данных, написание рукописи.

Соблюдение этических стандартов: исследование одобрено этическим комитетом АО «Екатеринбургский центр МНТК «Микрохирургия глаза» (протокол № 6 от 22 января 2026 г.).

✉ **Для корреспонденции:** Ксения Викторовна Ободова
ул. Бардина, д. 4А, г. Екатеринбург, Россия; zxx1991@yandex.ru

Статья получена: 17.12.2025 **Статья принята к печати:** 25.01.2026 **Опубликована онлайн:** 01.02.2026

DOI: 10.24075/vrgmu.2026.004

Авторские права: © 2026 принадлежат авторам. **Лицензиат:** РНИМУ им. Н. И. Пирогова. Статья размещена в открытом доступе и распространяется на условиях лицензии Creative Commons Attribution (CC BY) (https://creativecommons.org/licenses/by/4.0/).

Glaucoma is a chronic progressive disease of the optic nerve that finally results in irreversible blindness, if left without proper and timely treatment. According to the federal statistical observation data, a total of 1,249,617 glaucoma patients aged over 18 accounting for 1077.8 per 100,000 adult population of the Russian Federation (RF) were registered in 2022 in the RF [1]. The number of glaucoma patients increases annually: 57.5 million people were affected in 2015, their number increased to 65.5 million by the year 2020 [2]. All these data confirm that primary open-angle glaucoma (POAG) is one of the most important socially significant problems all over the world [3]. The early-stage glaucoma has no specific symptoms. Visual acuity usually does not decrease. However, despite this fact, the programmed death of nervous cells and optic nerve fibers is triggered. In this regard, it is necessary to start glaucoma treatment as early as possible, at early stages, to reduce much of the cases of blindness due to glaucomatous optic atrophy [4]. The potential of modern diagnosis methods allows one to detect the slightest glaucomatous alterations in patients. A multicenter scientific-analytical cohort study of 6,407 individuals (12,814 eyes) was conducted in the RF between December 2019 and October 2020, based on the results of which stage I glaucoma was diagnosed in a half of cases in the group with POAG (1995 eyes). This confirms good prospects in the diagnosis and treatment of glaucomatous optic neuropathy (GON) [5]. Therefore, the proper and timely treatment of early-stage glaucoma with the stable hypotensive effect determines the good prognosis in terms of vision for this disorder. According to the Russian (POAG Clinical Guidelines, RF 2024) and foreign regulatory documents, topical drug therapy and selective laser trabeculoplasty can be prescribed as a starter treatment method for early-stage POAG [6]. In the world today, considering the laser technology active development, laser treatment methods are extensively used to treat early-stage POAG. One of the main reasons to switch from hypotensive eyedrops to laser surgery when treating early-stage POAG is low patient compliance with the topical hypotensive therapy due to possible local and systemic side effects [7–9].

The majority of topical hypotensive drugs used to treat glaucoma contain preservatives, which, in turn, negatively affect the condition of the ocular surface and conjunctiva. Considering the fact that glaucoma is a chronic disorder and that treatment with hypotensive eyedrops is lifelong, the long-term use of such drugs lower the efficacy of glaucoma surgery [10]. According to foreign studies, the common cause of intraocular pressure (IOP) decompensation in patients with POAG post filtering surgery is scarring of the artificially created pathways for the intraocular fluid drainage due to the long-term use of the preservative-containing topical hypotensive drugs [11]. The approaches to treatment of early-stage POAG change due to the personalized medicine development. Therefore, in addition to achieving the target IOP it is necessary to consider the influence of treatment on the patient's quality of life. Treatment must be safe, cost-effective, and efficient.

Selective laser trabeculoplasty (SLT) is successfully used as a first choice intervention. This is a more cost-effective treatment option for POAG, than drug therapy [12]. SLT is recommended by the European Glaucoma Society and the World Glaucoma Association as first-line therapy for glaucoma. This is due to the fact that it helps stabilize IOP in a few years without using topical hypotensive therapy, thereby increasing patient compliance with treatment. The patient stops experiencing side effects of topical hypotensive drugs, and no monthly financial costs are required, so SLT is a cost-effective method to treat glaucoma [13, 14]. According to the Russian literature, the studies focused on the SLT efficacy when used as first-line therapy showed that the hypotensive effect of this laser surgical procedure was not durable enough, it accounted for 11–20% of the baseline IOP by month 12 of follow-up [15, 16]. Due to this fact the new combination laser technologies having a more pronounced hypotensive effect have started appearing in Russia.

A combination laser technology using different mechanisms of affecting the trabecular mesh (YAG laser activation of the trabecula and SLT), which complement each other based on the mechanism of action and ensure the more pronounced persistent hypotensive effect at various glaucoma stages, was developed and patented in 2024 at the glaucoma diagnosis and treatment department of the Yekaterinburg Eye Microsurgery Center [17]. According to the authors, the YAG-LAT + SLT technique developed ensured the glaucomatous process stabilization through achieving the necessary target intracranial pressure (ICP) depending on the glaucoma stage [18].

We found no data on the simultaneous use of combination laser techniques for treatment of the newly diagnosed POAG before hypotensive therapy prescription in the literature.

The study aimed to assess the hypotensive effect and clinical and functional outcomes of the simultaneous combination laser treatment, including YAG laser activation of the trabecula (YAG-LAT) and the subsequent one-time selective laser trabeculoplasty (SLT) in the same localization zones, in patients with the newly diagnosed early-stage POAG and moderately elevated IOP.

METHODS

Clinical assessment was based on evaluation of the clinical and functional state of 100 patients (100 eyes) with the newly diagnosed early-stage POAG aged 37–83 years. The nonrandomized prospective clinical and functional analysis of treatment outcomes in these patients was conducted. The gender distribution was as follows: 38 males (38%) and 62 females (62%). The follow-up period was 12 months.

Patients were divided into two groups. Group I included 50 patients (50 eyes), who underwent simultaneous YAG-LAT and SLT. The gender distribution was as follows: 30 females (60%) and 20 males (40%). The patients' age was 37–80 years.

Group II included 50 patients (50 eyes), who underwent SLT only. The gender distribution was as follows: 32 females (64%) and 18 males (36%). The patients' age was 38–83 years. The gender and age differences between groups of patients were non-significant.

Inclusion criteria: newly diagnosed stage I POAG (before prescription of hypotensive eyedrops) with the moderately increased IOP (Po, 22–28 mmHg), II–III degree of pigmentation on the anterior chamber angle.

Exclusion criteria: bullous keratopathy, high IOP (Po, ≥ 29 mmHg), corrected visual acuity less than 0.4; reduced transparency of optical media that interfere with the computed perimetry, poor computed perimetry quality (fixation loss > 25%, false positives and false negatives > 25%); high refractive errors; central retinal dystrophy.

Monitoring of the clinical and functional analysis in patients with the newly diagnosed POAG was performed before using the combination laser technique, as well as 1, 3, 6, and 12 months after laser treatment.

The clinical and functional analysis of patients with the newly diagnosed POAG conducted at all the follow-up terms specified included the following: visometry, gonioscopy, slit lamp examination, induction-based tonometry with the

Table 1. Mean values of clinical and functional parameters in groups I and II before laser surgery, M ± σ

Parameter	Group I	Group II	*p*
BCVA	0.8 ± 0.1	0.8 ± 0.2	> 0.05
IOP, mmHg	26.0 ± 1.7	26.3 ± 1.5	> 0.05
MD, dB	2.6 ± 1.5	2.4 ± 1.7	> 0.05
sLV, dB	3.7 ± 1.9	3.0 ± 1.5	> 0.05
Average RNFL, μm	98.0 ± 5.2	100.5 ± 4.9	> 0.05
Average GCC, μm	90.0 ± 4.2	92.0 ± 4.8	> 0.05

Note: BCVA — best-corrected visual acuity; RNFL — retinal nerve fiber layer.

use of the iCare TA01i tonometer (Icare Finland Oy, Finland), indirect ophthalmoscopy. The IOP values measured using the iCare tonometer were considered as "true" IOP (Po), since this tonometry type has a slight effect on the eye's fibrous membrane.

To accurately diagnose early-stage POAG, the optical coherence tomography (RTVue 100 system, Optovue, USA) data were used, i.e. the retinal nerve fiber layer and ganglion cell complex thickness, optic nerve head profile, along with the unconventional computed perimetry methods (Octopus 600 system, Haag-Streit Diagnostics, Switzerland). The PULSAR perimetry was used to diagnose the visual field, since this method was developed specifically for early detection of glaucoma; it showed sensitivity and specificity, when used to detect early-stage glaucoma [19]. When using computed perimetry, the G pattern and dynamic strategy were used. The G pattern is characterized by high density of test points in the paracentral zone for increasing the likelihood of detecting the glaucomatous optic neuropathy (GON) early signs.

Patients of group I underwent combination treatment (YAG-LAT and SLT) as follows.

At first, in phase I, the Visulas YAG-3 Nd:YAG laser (wavelength 1064 nm) (Carl Zeiss Meditec Inc., Germany) was used to perform YAG-LAT in the lower part of the anterior chamber angle (180 degrees) via application of 50–60 single pulses with the energy of 0.9–1.0 mJ at equal distances from one another; the spot diameter was 8–10 μm, and the laser exposure time was 3 ns [20].

Then, in phase II, we switched to the Ellex Solo Nd:YAG laser (Ellex Medical Pty Ltd., Australia) with frequency doubling (532 nm) to perform SLT in the same zone of the lower part of the anterior chamber angle (180 degrees) with 70–75 non-overlapping laser applications with the energy of 0.5–0.6 mJ; the spot diameter was 400 μm, and the laser exposure time was 3 ns.

Patients of group II received only SLT performed using the doubled-frequency (532 nm) Ellex Solo Nd:YAG laser (Ellex Medical Pty Ltd., Australia); the spot diameter was 400 μm, and the laser exposure time was 3 ns; 70–80 non-overlapping laser applications with the energy of 0.7–0.9 mJ were used in the lower part of the anterior chamber angle (180 degrees).

In the postoperative period, patients of group I, who received simultaneous combination laser treatment, were prescribed instillation of nonsteroidal anti-inflammatory drugs for 7 days (bromfenac 0.09%, 1 drop once a day); topical hypotensive therapy was not prescribed.

After receiving SLT only (group II), no anti-inflammatory agent instillation or topical hypotensive therapy was prescribed.

According to the preoperative assessment data, the average baseline IOP was 26.1 ± 1.7 mmHg in patients of group I without local hypotensive therapy, while in patients of group II without topical hypotensive therapy it was 26.3 ± 1.5 mmHg; the intergroup difference is also non-significant ($p > 0.05$).

Mean clinical and functional parameter values in patients of groups I and II before laser surgery are provided in Table 1.

Statistical analysis of the results was conducted using STATISTICA 10.0 and Excel 2020. The data obtained were processed using variation statistics with normal distribution determined using the Shapiro–Wilk test. The data are presented as the mean (M) and standard deviation (σ), (M ± σ). Student's *t*-test was used to compare mean values and assess significance of differences. The differences were considered significant at $p < 0.05$. Significance of differences between identical indicators was calculated using the Mann–Whitney *U*-test; significance of differences between the indicators reported before and after treatment within the same group was calculated using the Wilcoxon test.

RESULTS

The IOP decreased by 28% of the baseline a month after using the combination laser treatment involving YAG-LAT and SLT (group I); at 3 months it decreased by 32.2% of the baseline IOP. In patients, who received SLT only (group II), the IOP decrease relative to baseline was 30.5% within a month and 32% within 3 months. The difference in the extent of IOP decrease reported within a month and 3 months between groups I and II was non-significant ($p > 0.05$).

There was still persistent hypotensive effect that accounted for 29.3% of the preoperative value 12 months after the simultaneous combination laser treatment involving YAG-LAT and SLT. There was no persistent hypotensive effect in the long term after SLT (within 12 months), and the IOP decrease relative to baseline was 17%. The differences in the extent of IOP decrease relative to baseline between groups I and II were significant ($p < 0.05$) in the long term (within 12 months).

The IOP values (Po, mmHg) reported at various follow-up terms are provided in Table 2.

In the long term (within 12 months) after the simultaneous combination laser treatment (YAG-LAT + SLT), the target IOP was achieved in 82% of cases (41 eyes out of 50); in 18% of cases (9 eyes out of 50), normal IOP was achieved by prescribing topical hypotensive therapy (latanoprost 0.005% once daily). In a year, in patients post SLT only, the target IOP was achieved in 37% of cases (18 eyes out of 50), while in 63% of cases (32 eyes out of 50) there was a need for prescription of topical hypotensive therapy (latanoprost 0.005% once daily). The target IOP values were determined by the Russian regulatory documents (POAG Clinical Guidelines, RF 2024): Po 16–18 mmHg. The slit lamp examination of individuals in groups I and II revealed dystrophic changes in the anterior segment of the eye, exogenous pigmentation and pseudo-exfoliation of the iris and lens. Gonioscopy showed that the anterior chamber angle was of medium width or wide, open, with the II–III degree of pigmentation. Ophtalmoscopy showed that individuals in groups I and II had the pale pink optic disc with clear margins;

Table 2. Mean IOP, Po (mmHg), at various follow-up terms, M ± σ

Group	Before surgery	After surgery			
		1 month	3 months	6 months	12 months
I (n = 50)	26.1 ± 1.7	18.8 ± 2.1	17.7 ± 1.9	18.8 ± 2.5	18.7 ± 2.6
II (n = 50)	26.3 ± 1.5	18.3 ± 2.9	17.9 ± 1.5	20.5 ± 2.8	21.9 ± 2.5
p	> 0.05	> 0.05	> 0.05	< 0.05	< 0.05

in the central retinal area, foveal and macular reflexes were preserved, no abnormalities were revealed.

During the 12-month follow-up all patients of group I (50 eyes) showed stabilization of visual functions and glaucomatous process; the glaucomatous process stabilization was also reported in all patients of group II (50 eyes), but in this group it was achieved by prescribing topical hypotensive eyedrops, which were necessary in 63% of cases (31 eyes). The glaucomatous process stabilization in patients with early-stage glaucoma was confirmed by computed perimetry and optical coherence tomography (OCT) of the optic disc and retinal ganglion cells. The difference in this parameter reported for patients of groups I and II by the end of follow-up (after 12 months) was non-significant (p > 0.05).

The dynamic changes of the average clinical and functional parameter values in patients of groups I and II before laser surgery and after 12 months are provided in Table 3.

In the early postoperative period, 10% of patients with early-stage POAG and moderately increased IOP post simultaneous combination laser treatment (group I, 5 eyes) reported eye redness and light sensitivity; the slit lamp examination revealed conjunctival injection without any signs of inflammation in the anterior chamber. All the above symptoms disappeared during topical anti-inflammatory treatment in the form of bromfenac 0.09% eyedrops once daily for 7 days.

As for patients with early-stage POAG post SLT (group II), in the early postoperative period 14% (7 eyes) showed the reactive IOP increase, which recovered spontaneously without hypotensive therapy prescription; in 16% of cases (8 eyes), inflammatory eye injection occurred, which was jugulated by topical steroid anti-inflammatory therapy in the form of dexamethasone 0,1% eyedrops 3 times daily for 7 days.

DISCUSSION

In contrast to the use of SLT only, the simultaneous combination laser surgery technique (YAG-LAT and SLT) used for treatment of patients with the newly diagnosed early-stage POAG makes it possible to achieve the more pronounced persistent hypotensive effect of surgery within 12 months (up to 29.3% of baseline IOP within a year after laser surgery). The fact of achieving the target IOP (Po 16–18 mmHg) was reported in 82% of patients in group I, who received no topical hypotensive therapy. In a comparative aspect with group II of patients, who received SLT only, the IOP decrease within a year accounted for 17% of baseline IOP values, and the target IOP (Po 16–18 mmHg) was achieved only in 37% of patients with the newly diagnosed early-stage POAG. In group II, the extent of IOP decrease within 6–12 months is comparable with the Russian literature data on the efficacy of SLT as first-line therapy for glaucoma. Thus, it was shown in 2014 that the extent of IOP decrease within 12 months after using SLT as first-line therapy was about 20% [15]; similar data were obtained by other researchers [20].

There is a causal relationship between the laser exposure mechanism and the pronounced persistent hypotensive effect when using the simultaneous combination laser treatment. The simultaneous combination laser treatment (YAG-LAT and SLT) involves various mechanisms. In the first phase, when performing YAG laser activation of the trabecula, the main mechanism underlying the effect is related to the micro-hydraulic shock wave generated by laser energy and directed at the trabecula. On the one hand, the wave fragments biomaterial in the trabecular zone (primarily pigment) that impairs drainage and moves biomaterial deeper into the trabecular mesh lumens.

Table 3. Dynamic changes of the average clinical and functional parameter values in patients of groups I and II before laser surgery and after 12 months, M ± σ

Parameter	Before laser surgery	After 12 months	p
	Group I		
BCVA	0.8 ± 0.1	0.8 ± 0.1	> 0.05**
MD, dB	2.6 ± 1.5	2.72 ± 1.4	> 0.05**
sLV, dB	3.7 ± 1.9	3.6 ± 1.7	> 0.05**
Average RNFL, μm	98.0 ± 5.2	101.0 ± 4.6	> 0.05**
Average GCC, μm	90.0 ± 4.2	92.0 ± 3.8	> 0.05**
	Group II		
BCVA	0.8 ± 0.2	0.8 ± 0.1	> 0.05**
MD, dB	2.4 ± 1.7	2.5 ± 1.5	> 0.05**
sLV, dB	3.0 ± 1.5	3.2 ± 1.3	> 0.05**
Average RNFL, μm	100.5 ± 4.9	100.9 ± 5.1	> 0.05**
Average GCC, μm	92.0 ± 4.8	92.9 ± 4.2	> 0.05**
p	> 0.05*	> 0.05*	

Note: * — p > 0.05, the difference between indicators in two groups; ** — p > 0.05, difference between pre-treatment and post-treatment values within a group.

On the one hand, it stretches the trabecula, which results in expansion of the intertrabecular spaces. This, in turn, further increases their permeability for biomaterial particles, improving the overall trabecular permeability.

In the second phase of the simultaneous combination laser treatment, the same localization zones simultaneously undergo SLT, the main mechanism of which is aimed at photothermolysis [21]. At the same time, the conditions for photothermolysis are significantly improved due to the fact that the microhydraulic shock wave breaks down the biomaterial after YAG-LAT, freeing access to the trabecular surface, and also promotes its more compact and uniform movement into the trabecular mesh. This contributes to more accurate focusing, concentration, and distribution of the necessary laser energy across the depth of the mesh intratrabecular spaces on the photothermolysis objects, increasing the SLT procedure efficacy.

CONCLUSIONS

The simultaneous combination laser treatment technique (YAG-LAT combined with SLT) proposed as first-line therapy showed the pronounced stable hypotensive effect throughout the follow-up period when used for treatment of the newly diagnosed early-stage POAG. Furthermore, the patients showed stabilization of visual functions and glaucoma manifestations.

References

1. Neroev VV, Mikhaylova LA, Malishevskaya TN, Petrov SYu, Filippova OM. Glaucoma epidemiology in the Russian Federation. Russian Ophthalmological Journal. 2024; 17 (3): 7–12. Russian.
2. Terminology and Guidelines for Glaucoma. 4th edition. Savona: Euro-pean Glaucoma Society; 2014. DOI: 10.1136/bjophthalmol-2016-egsguideline.001.
3. Libman ES. Medical and social problems in ophthalmology. IX Congress of Ophthalmologists of Russia. Abstracts of reports. Moscow; 2010: 70–71. Russian.
4. Chechenina NG, Shaposhnikova IV, Frolova EA, Lemberg OV. The main sources of glaucoma detection at outpatient appointments. Permanent residence. RMJ. Clinical Ophthalmology. 2008; 4: 19. Russian.
5. Kuroyedov AV, Movsisyan AB, Egorov EA, Erichev VP, Gorodnichiy VV, Brezhnev AYu, Gazizova IR. The profile of patients with primary open-angle glaucoma in the Russian Federation. National Journal glaucoma. 2021; 20 (1): 3–15. Russian.
6. Kuroedov AV, Brezhnev AYu, Lovpache JN, Petrov SYu, Tibieva ZU, Nagornova ZM, Krinitsyna EA, Sergeeva VM. The feasibility of adopting «stepwise» initial approaches in treatment of patients with different stages of glaucoma. National Journal glaucoma. 2018; 17 (4): 27–54. Russian.
7. Töteberg-Harms M, Meier-Gibbons F. Is laser trabeculoplasty the new star in glaucoma treatment? Current Opinion in Ophthalmology. 2021; 32: 141–47. PMID: 33470670.
8. Newman-Casey PA, Robin AL, Blachley T, et al. The most common barriers to glaucoma medication adherence: a cross-sectional survey. Ophthalmology. 2015; 122 (7): 1308–16.
9. Baudouin C, Labbe A, Liang H, et al. Preservatives in eyedrops: the good, the bad and the ugly. Prog Retinal Eye Res. 2010; 29 (4): 312–24.
10. Malyugin BE, Sidorova AV, Starostina AV, et al. Pharmacological modulation of wound healing in glaucoma surgery. Russian Annals of Ophthalmology. 2022; 138 (4): 136–43. Russian.
11. European Glaucoma Society: Terminology and guidelines for glaucoma. 3rd edition. Savona: Italy Editrice Dogma, 2008.
12. Erichev VP, Ragozina EA. Selective laser trabeculoplasty as the initial treatment of primary open-angle glaucoma. National Journal glaucoma. 2020; 19 (1): 47–54. Russian.
13. Garg A, Vickerstaff V, Nathwani N, Garway-Heath D, Konstantakopoulou E, Ambler G, et al. Primary selective laser trabeculoplasty for open-angle glaucoma and ocular hypertension: Clinical outcomes, predictors of success, and safety from the laser in glaucoma and ocular hypertension trial. Ophthalmology. 2019; 126: 1238–48.
14. Ansari E. 10-year outcomes of first-line selective laser trabeculoplasty (SLT) for primary open-angle glaucoma (POAG). Graefes Arch Clin Exp Ophthalmol. 2021; 259 (6): 1597–604.
15. Seleznev AV. Characteristics of the hypotensive effectiveness of selective laser trabeculoplasty in primary open-angle glaucoma. Bulletin of the Ivanovo Medical Academy. 2014; 9 (4): 83. Russian.
16. Doga AV, Obodova KV. Modern approaches to the treatment of patients with the initial stage of primary open-angle glaucoma. Fyodorov Journal of Ophthalmic Surgery. 2025; 1 (143): 103–14. Russian.
17. Obodova KV, Strenev NV. A method of combined laser treatment of primary open-angle glaucoma in the presence of pigmentation of the anterior chamber angle structures. Patent RUS № 2024113910/22.05.2024. Russian.
18. Doga AV, Obodova KV, Strenev NV. Combined use of YAG laser trabecular activation and selective laser trabeculoplasty in the treatment of primary open-angle glaucoma. Fyodorov Journal of Ophthalmic Surgery. 2024; 4: 70–77. Russian.
19. Gonzalez de la Rosa M, Gonzalez-Hernandez M. Pulsar perimetry. A review and new results. Ophthalmologe. 2013; 110: 107–15.
20. Anisimova SYu, Anisimov SI, Kochmala OB, et al. Comparative results of local and laser treatment of newly diagnosed patients with primary glaucoma. National Journal of Glaucoma. 2024; 23 (3): 37–43. Russian.
21. Suetov AA, Doktorova TA, Molodkina NA. The effect of initial conservative hypotensive therapy on the outcomes of selective laser trabeculoplasty in primary open-angle glaucoma. Russian Annals of Ophthalmology. 2025; 141 (5): 16–22. Russian.

Литература

1. Нероев В. В., Михайлова Л. А., Малишевская Т. Н., Петров С. Ю., Филиппова О. М. Эпидемиология глаукомы в Российской Федерации. Российский офтальмологический журнал. 2024; 17 (3): 7–12.
2. Terminology and Guidelines for Glaucoma. 4th edition. Savona: Euro-pean Glaucoma Society; 2014. DOI: 10.1136/bjophthalmol-2016-egsguideline.001.
3. Либман Е. С. Медико-социальные проблемы в офтальмологии. IX Съезд офтальмологов России. Тезисы докладов. М., 2010; с. 70–71.
4. Чеченина Н. Г., Шапошникова И. В., Фролова Е. А., Лемберг О. В. Основные источники выявления глаукомы на амбулаторном приеме. РМЖ. Клиническая офтальмология. 2008; 4: 19.
5. Куроедов А. В., Мовсисян А. Б., Егоров Е. А., Еричев В. П., Городничий В. В., Брежнев А. Ю., Газизова И. Р. Профиль пациентов с первичной открытоугольной глаукомой в Российской Федерации. Национальный журнал Глаукома. 2021; 20 (1): 3–15.
6. Куроедов А. В., Брежнев А. Ю., Ловпаче Д. Н., Петров С. Ю., Тибиева З. У., Нагорнова З. М., Криницына Е. А., Сергеева В. М. Целесообразность применения дифференцированных («ступенчатых») стартовых подходов к лечению больных с разными стадиями глаукомы. Национальный журнал

Глаукома. 2018; 17 (4): 27–54.
7. Töteberg-Harms M, Meier-Gibbons F. Is laser trabeculoplasty the new star in glaucoma treatment? Current Opinion in Ophthalmology. 2021; 32: 141–7. PMID: 33470670.
8. Newman-Casey PA, Robin AL, Blachley T, et al. The most common barriers to glaucoma medication adherence: a cross-sectional survey. Ophthalmology. 2015; 122 (7): 1308–16.
9. Baudouin C, Labbe A, Liang H, et al. Preservatives in eyedrops: the good, the bad and the ugly. Prog Retinal Eye Res. 2010; 29 (4): 312–24.
10. Малюгин Б. Э., Сидорова А. В., Старостина А. В., и др. Фармакотерапевтические подходы к управлению репаративными процессами в хирургии глаукомы. Вестник офтальмологии. 2022; 138 (4): 136–43.
11. European Glaucoma Society: Terminology and guidelines for glaucoma. 3rd edition. Savona: Italy Editrice Dogma, 2008.
12. Еричев В. П., Рагозина Е. А. Селективная лазерная трабекулопластика как стартовый метод лечения первичной открытоугольной глаукомы. Национальный журнал Глаукома. 2020; 19 (1): 47–54.
13. Garg A, Vickerstaff V, Nathwani N, Garway-Heath D, Konstantakopoulou E, Ambler G, et al. Primary selective laser trabeculoplasty for open-angle glaucoma and ocular hypertension: Clinical outcomes, predictors of success, and safety from the laser in glaucoma and ocular hypertension trial. Ophthalmology. 2019; 126: 1238–48.
14. Ansari E. 10-year outcomes of first-line selective laser trabeculoplasty (SLT) for primary open-angle glaucoma (POAG). Graefes Arch Clin Exp Ophthalmol. 2021; 259 (6): 1597–604.
15. Селезнев А. В. Характеристика гипотензивной эффективности селективной лазерной трабекулопластики при первичной открытоугольной глаукоме. Вестник Ивановской медицинской академии. 2014; 9 (4): 83.
16. Дога А. В., Ободова К. В. Современные подходы к лечению больных с начальной стадией первичной открытоугольной глаукомы. Офтальмохирургия. 2025; 1 (143): 103–14.
17. Ободова К. В., Стренев Н. В., авторы. Способ комбинированного лазерного лечения первичной открытоугольной глаукомы при наличии пигментации структур угла передней камеры. Патент РФ на изобретение № 2024113910/ 22.05.2024.
18. Дога А. В., Ободова К. В., Стренев Н. В. Комбинированное применение YAG-лазерной активации трабекулы и селективной лазерной трабекулопластики в лечении первичной открытоугольной глаукомы. Офтальмохирургия. 2024; 4: 70–77.
19. Gonzalez de la Rosa M, Gonzalez-Hernandez M. Pulsar perimetry. A review and new results. Ophthalmologe. 2013; 110: 107–15.
20. Анисимова С. Ю., Анисимов С. И., Кочмала О. Б. и др. Сравнительные результаты местного и лазерного лечения вновь выявленных больных первичной глаукомой. Национальный журнал Глаукома. 2024; 23 (3): 37–43.
21. Суетов А. А., Докторова Т. А., Молодкина Н. А. Влияние исходной консервативной гипотензивной терапии на результаты селективной лазерной трабекулопластики при первичной открытоугольной глаукоме. Вестник офтальмологии. 2025; 141 (5): 16–22.

GAIT PARAMETER ADJUSTMENT AFTER KNEE ARTHROPLASTY BY KINESIOTHERAPY IN SUSPENSION

Minasov BSh[1], Yakupov RR[1], Akbashev VN[1]✉, Evgrafov IO[1], Malsagov YuM[3], Karimov KK[2], Minasov IB[1], Akhmeldinova AA[1], Shveykin AA[1]

[1] Bashkir State Medical University, Ufa, Russia
[2] Avicenna Tajik State Medical University, Dushanbe, Tajikistan
[3] Republican Oncology Dispensary, Plievo, Republic of Ingushetia, Russia

The study is relevant due to persistent postural control impairment and gait disorder in patients post total knee arthroplasty (TKA), despite pain relief and restoration of the range of motion. The study aimed to assess the effects of kinesiotherapy in suspension on the patients' stabilometry and gait phase parameters in the long term after TKA. A prospective comparative study was conducted that involved 93 patients (39 males and 54 females; average age 62.3 ± 5.1 years) enrolled 36 months after surgery. The patients were randomized into the index group (standard rehabilitation involving kinesiotherapy in suspension) and comparison group (standard program). The efficacy was assessed using stabilometry and gait phase analysis before and after the 3-week rehabilitation course. In the index group, a significant decrease in the normalized vectorogram area from 320 ± 60 to 190 ± 40 mm^2 (p = 0.001) and mean center of pressure movement linear speed from 15.5 ± 2.8 to 8.7 ± 2.1 mm/s (p = 0.002) was revealed. The stance phase duration increased by 18%, and the walking phase symmetry increased from 74 ± 5 to 90 ± 4% (p < 0.01). In the comparison group, the changes were non-significant (p > 0.05). The decrease in WOMAC scores was reported for both groups, there were no intergroup differences. The data obtained confirm the efficacy of using kinesiotherapy in suspension to adjust postural and locomotor disorders after TKA.

Keywords: total knee arthroplasty, medical rehabilitation; kinesiotherapy, stabilometry, gait, axial skeleton, stance phase

Author contribution: Minasov BSh — study concept and design, academic advising, manuscript approval; Yakupov RR — study design, clinical phase management, interpretation of the results; Akbashev VN — surgical treatment of patients, clinical assessment of the results; Evgrafov IO — clinical data acquisition, part in the rehabilitation program implementation; Malsagov YuM — clinical and functional assessment of patients, research database creation; Karimov KK — statistical data processing, analysis of the study results; Minasov IB — instrumental tests (stabilometry, gait phase analysis), data processing and interpretation; Akhmeldinova AA — course of kinesiotherapy in suspension, compliance with the rehabilitation protocol; Shveykin AA — scientific literature review, interpretation of the results, manuscript writing.

Compliance with ethical standards: the study was approved by the Ethics Committee of the Bashkir State Medical University (protocol No. 4 dated 25 April 2025) and conducted in accordance with the principles of the World Health Association Declaration of Helsinki (2013). All patients submitted the informed consent to take part in the study.

✉ **Correspondence should be addressed:** Vladislav N. Akbashev
Lenina, 3, Ufa, 450008, Russia; vlad-akb@mail.ru

Received: 05.01.2026 **Accepted:** 20.01.2026 **Published online:** 03.02.2026

DOI: 10.24075/brsmu.2026.003

Copyright: © 2026 by the authors. **Licensee:** Pirogov University. This article is an open access article distributed under the terms and conditions of the Creative Commons Attribution (CC BY) license (https://creativecommons.org/licenses/by/4.0/).

КОРРЕКЦИЯ ПАРАМЕТРОВ ПОХОДКИ ПОСЛЕ ЭНДОПРОТЕЗИРОВАНИЯ КОЛЕННОГО СУСТАВА МЕТОДОМ АППАРАТНО-ПОДВЕСНОЙ КИНЕЗИОТЕРАПИИ

Б. Ш. Минасов[1], Р. Р. Якупов[1], В. Н. Акбашев[1]✉, И. О. Евграфов[1], Ю. М. Мальсагов[3], К. К. Каримов[2], И. Б. Минасов[1], А. А. Ахмельдинова[1], А. А. Швейкин[1]

[1] Башкирский государственный медицинский университет, Уфа, Республика Башкортостан, Россия
[2] Таджикский государственный медицинский университет имени Абуали ибни Сино, Душанбе, Таджикистан
[3] Республиканский онкологический диспансер, Плиево, Республика Ингушетия, Россия

Актуальность исследования обусловлена сохраняющимися нарушениями постурального контроля и походки у пациентов после тотального эндопротезирования коленного сустава (ТЭКС), несмотря на устранение болевого синдрома и восстановление объема движений. Целью исследования было оценить влияние аппаратно-подвесной кинезиотерапии на стабилометрические и фазовые параметры походки у пациентов в отдаленные сроки после ТЭКС. Проведено проспективное сравнительное исследование с участием 93 пациентов (39 мужчин и 54 женщины; средний возраст 62,3 ± 5,1 года), включенных через 36 месяцев после операции. Пациенты были рандомизированы в основную группу (стандартная реабилитация с включением аппаратно-подвесной кинезиотерапии) и группу сравнения (стандартная программа). Эффективность оценивали с использованием стабилометрии и фазового анализа походки до и после трехнедельного курса реабилитации. В основной группе выявлено достоверное снижение нормированной площади векторограммы с 320 ± 60 до 190 ± 40 мм^2 (p = 0,001) и средней линейной скорости перемещения центра давления с 15,5 ± 2,8 до 8,7 ± 2,1 мм/с (p = 0,002). Длительность фазы опоры увеличилась на 18%, симметрия фаз ходьбы — с 74 ± 5 до 90 ± 4% (p < 0,01). В группе сравнения изменения были недостоверны (p > 0,05). Снижение показателей WOMAC отмечено в обеих группах без межгрупповых различий. Полученные данные подтверждают эффективность аппаратно-подвесной кинезиотерапии в коррекции постуральных и локомоторных нарушений после ТЭКС.

Ключевые слова: тотальное эндопротезирование коленного сустава, медицинская реабилитация, кинезиотерапия, стабилометрия, походка, осевой скелет, фаза опоры

Вклад авторов: Б. Ш. Минасов — концепция и дизайн исследования, научное руководство исследованием, утверждение рукописи; Р. Р. Якупов — дизайн исследования, организация клинического этапа, интерпретация результатов; В. Н. Акбашев — хирургическое лечение пациентов, клиническая оценка результатов; И. О. Евграфов — сбор клинического материала, участие в реализации реабилитационной программы; Ю. М. Мальсагов — клинико-функциональное обследование пациентов, формирование базы данных исследования; К. К. Каримов — статистическая обработка данных, анализ результатов исследования; И. Б. Минасов — проведение инструментальных исследований (стабилометрия, фазовый анализ походки), обработка и интерпретация полученных данных; А. А. Ахмельдинова — проведение курса аппаратно-подвесной кинезиотерапии, соблюдение протокола реабилитации; А. А. Швейкин — анализ научной литературы, интерпретация результатов, подготовка текста рукописи.

Соблюдение этических стандартов: исследование одобрено этическим комитетом ФГБОУ ВО «Башкирский государственный медицинский университет» Минздрава России (протокол № 4 от 25 апреля 2025 г.), проведено в соответствии с принципами Хельсинкской декларации Всемирной медицинской ассоциации (в редакции 2013 г.). Все пациенты подписали добровольное информированное согласие на участие в исследовании.

✉ **Для корреспонденции:** Владислав Николаевич Акбашев
ул. Ленина, д. 3, г . Уфа, 450008, Россия; vlad-akb@mail.ru

Статья получена: 05.01.2026 **Статья принята к печати:** 20.01.2026 **Опубликована онлайн:** 03.02.2026

DOI: 10.24075/vrgmu.2026.003

Авторские права: © 2026 принадлежат авторам. **Лицензиат:** РНИМУ им. Н. И. Пирогова. Статья размещена в открытом доступе и распространяется на условиях лицензии Creative Commons Attribution (CC BY) (https://creativecommons.org/licenses/by/4.0/).

Under conditions of the increasing prevalence of degenerative-dystrophic lesions of large joints, the modern clinical practice is shaped as an integrated medical rehabilitation system based on combining medicinal, surgical, and functional technologies [1, 2]. Motor activity that ensures regulation of the connective tissue structural and functional state and the physiological motor stereotype development represents the key mechanism underlying restoration. The key role in these processes is played by the central and peripheral postural regulation links, and the strength imbalance results in the coordination disorder and decreased neuromuscular regulation efficiency [3].

Reduced motor activity is associated with the increase in the prevalence of musculoskeletal degenerative-dystrophic disorders, including those affecting large joints and segments of the pelvic girdle, which are accompanied by chronic systemic disorders with mostly local clinical manifestations [4]. Decompensated knee osteoarthritis reflecting the progressive structural and functional balance loss is accompanied by pain, hypodynamia, and involvement of various organs and systems [5, 6].

Despite the total knee arthroplasty high efficacy for pain relief and restoration of the range of motion, the long-term functional outcome is largely determined by the quality of medical rehabilitation considered as a continuous adaptation process aimed at restoring movement and ensuring the patient's social re-integration [7]. One of the factors limiting the physiological gait restoration is insufficient stabilization of the axial skeleton, primarily the lumbopelvic complex. The impaired neuromuscular control of the stabilizer muscles and asymmetric load result in alteration of the stance and walking phases [8, 9].

In this regard, modern rehabilitation programs are aimed at adjusting postural disorders, proprioceptive control restoration, and motor pattern optimization with the use of kinesiotherapy. The use of stabilization exercises with the load control contributes to better postural stability and return of the gait phase characteristics back to normal. The use of automated and robotic systems makes it possible to objectify assessment of the patients' functional state [10, 11]. At the same time, the data on the clinical efficacy of such methods in the late postoperative period are limited, which determines the relevance of further research.

The scientific novelty of this study lies in conducting a comprehensive instrumental assessment of the impact of kinesiotherapy in suspension on the postural control and locomotion parameters in patients post total knee arthroplasty (TKA). The study aimed to assess the effect of kinesiotherapy in suspension involving the use of the automated complex on the gait stabilometry and phase parameters in patients post TKA in the late postoperative period.

METHODS

A prospective comparative study aimed to assess the effects of kinesiotherapy in suspension on the postural stability indicators and gait parameters in patients post TKA.

Study design

The patients were enrolled 36 months after TKA, which corresponded to the period of the completed functional bone tissue remodeling and made it possible to assess the delayed biomechanical impairment and efficacy of the delayed rehabilitation intervention. A total of 93 patients (39 males, 54 females; average age 62.3 ± 5.1 years) meeting the selection criteria were enrolled.

Surgical intervention

All the patients had earlier undergone primary TKA involving the use of the posterior stabilized (PS) construct. The cemented prostheses (Meril Life Sciences, India) were used. The surgical procedure was performed using a standard method; the medial parapatellar approach was used. Stable fixation of the endoprosthesis components was reported in all patients based on the follow-up clinical and radiography assessment data by the time of enrollment.

Randomization and allocation of groups

Randomization was performed by simple random sampling using a random number generator. The patients were distributed by independent experts, who did not take part in rehabilitation activities. Two groups were formed: comparison group (control; $n = 46$), study group (index; $n = 47$)

Inclusion criteria

1. Age 55–75 years.
2. Primary unilateral TKA due to grade 3–4 osteoarthritis deformans (according to Kellgren–Lawrence).
3. Clinically stable condition, no contraindications to physical exercise.
4. No cognitive impairment (MMSE score ≥ 24).
5. Submitted informed consent to take part in the study
6. Endoprosthesis component stability confirmed by clinical, laboratory, and radiography data.

Exclusion criteria

1. Infectious complications, including periprosthetic joint infection.
2. Instability or displacement of the endoprosthesis components based on the clinical and instrumental assessment data.
3. Bilateral knee arthroplasty.
4. Severe limb deformities (valgus/varus > 15°) or shortening of the operated leg > 2 cm
5. Severe pain at rest (VAS > 5 points).
6. Severe concomitant disorders limiting physical activity: chronic heart failure (CHF), functional class III–IV according to the New York Heart Association (NYHA) classification; chronic obstructive pulmonary disease (COPD), grade III–IV according to the GOLD (Global Initiative for Chronic Obstructive Lung Disease) classification; unstable coronary artery disease (CAD), including progressive effort angina, angina at rest, early post-infarction angina, and the condition post recent acute coronary syndrome (within 3 months) associated with high risk of coronary complications and limited tolerance to physical exertion.
7. Active or progressive disorders of the central nervous system (Parkinson's disease, multiple sclerosis, stroke sequelae < 12 months).
8. Dementia or severe cognitive impairment (MMSE < 24).
9. Severe hearing loss or visual impairment interfering with exercise.
10. Refusal of participation or failure to adhere to the training and visit regimen.

Rehabilitation program

Comparative characteristics of rehabilitation programs are provided in Table 1. The comparison group was through the

Table 1. Comparative characteristics of rehabilitation programs

Direction of therapy	Comparison group (standard program)	Index group (standard + kinesiotherapy)
Physiotherapy	Ultra-high frequency electric field, electrical muscle stimulation	
Breathing exercises	Diaphragmatic breathing exercises	
Passive and active motion	Passive mobilization of the joint, active motion within the permissible range	
Isometric exercises	Tensing muscles of the thigh and gluteal muscles	
Stretching exercises	For the muscles of the thigh, lower leg, and lumbar region	
Coordination and balance exercises	Balancing using the stability ball and balance platform	Suspension exercises with the pressure center control and biological feedback
Kinesiotherapy (in suspension)	Was not used	The suspension system, ORMED Kinezo automated complex (ORMED, Russia) was used
Stabilization of the trunk and axial skeleton	Was not performed	Exercises for activation of the core and pelvic stabilizer muscles
Proprioceptive stimulation	Limited implementation through unstable surfaces	Targeted training involving modulation of the support and moving the center of gravity
Unloaded functional movements	Were not performed	Were performed using suspended unloading
Frequency of sessions	5 times a week, 40–50 min	5 times a week, 50–60 min
Course duration	3 weeks (15 sessions)	3 weeks (15 sessions)

standard rehabilitation program in accordance with the clinical guidelines on restoration after TKA (Table 2). The program included the following physiotherapeutic procedures: exposure to the ultra-high frequency electric field and electrical muscle stimulation (EMS) of the gluteal muscles, as well as the muscles of the thigh and lower leg of the operated and contralateral limbs, breathing exercises, passive and active knee joint mobilization, isometric exercises for the thigh and gluteal muscles, stretching exercises for the lower limb, and coordination exercises using a stability ball and unstable supports. The 40–50 min training sessions were conducted 5 times a week throughout 3 weeks.

In addition to standard therapy, the index group was through the course of kinesiotherapy in suspension (Table 3) involving the use of the automated complex and suspension trainers. The program included exercises aimed at activating deep muscles of the trunk and pelvis (core), proprioceptive training, restoration of the gait phase symmetry, and execution of functional movements with partial bodyweight unloading. The stabilization training elements and biological feedback technologies were used. The 3-week course consisted of 15 daily 50–60 min sessions controlled by the specialist.

Method to assess rehabilitation efficacy

The rehabilitation activity efficacy was assessed twice: before the beginning of the course and after the end of the 3-week cycle (on day 21). Objective instrumental and subjective methods were used.

Stabilometry analysis

The postural stability parameters were assessed using the HUBER 360 stabilometry platform (LPG Systems, France) when standing with the eyes open. The main assessed indicators were as follows:

- normalized vectorogram area (NVA, mm^2) reflecting the value of the center of pressure spatial distribution;
- mean center of pressure movement linear speed (mm/s) being a compensatory activity indicator;

Table 2. Composition and structure of a standard rehabilitation program

Program component	Duration	Aim	Description and execution specifics
Physiotherapy	15 procedures (daily)	Pain relief and reduction of swelling, regeneration stimulation	Electrophoresis with Diclofenac-AKOS, 1% solution for external use; (Sintez, Russia) low-frequency alternating magnetic therapy applied to the knee joint
Breathing exercises	10–15 min / session	Diaphragmatic breathing activation, hypostatic disorder prevention	Performed in a lying and sitting position under the instructor's count; three sets of 10 repetitions
Passive and active motion	10–15 min / session	Restoration of the knee joint motion range	Passive flexion/extension with the instructor's help; active moving in a lying or sitting position, within the painless amplitude
Isometric exercises	7 min / session	Strengthening the gluteal, quadriceps, hamstrings, and lower limb muscles	Static tension of muscles, retention for 3–5 s, 3–4 series of 10 repetitions
Stretching	5–10 min / session	Muscle elasticity improvement, contracture prevention	Metered stretching the anterior and posterior thigh, lower leg, and lumbar region, retention for 15–20 s
Coordination exercises	10 min / session	Stability and balance improvement	Exercises using a stability ball, body weight shifting, execution on unstable platforms with and without support
Overall duration of a single session	40–50 min	Complex motor function restoration	Algorithmic execution of all components under the instructor's supervision, 5 times a week for 3 weeks

Table 3. Composition and structure of the rehabilitation program comprising the kinesiotherapy component used in the study group

Kinesiotherapy component	Duration	Aim	Description and execution specifics
Trunk and pelvis stabilization exercises	10–15 min / session	Activation of the deep stabilizer muscles, shaping axial stability	Executed in the suspension system with the trunk position control; retention and movement in the stato-dynamic modes
Proprioceptive training	10–15 min / session	Neuromuscular control and intermuscular coordination improvement	Tasks to maintain balance with the changing support and load direction; using a platform with the variable force vector
Gait symmetry training	10 min / session	Restoration of the phase balance and even load distribution	Step modeling with the feedback based on the stance and swing phase parameters; visual representation of abnormalities
Unloaded functional movements	10–15 min / session	Motor activity improvement with minimal stress on the joint	Walking, half squats and lifts with partial bodyweight unloading in the suspension system; metered load increase
Biological feedback	Embedded in each module	Increasing movement consciousness and adjustment of motor patterns	Using sensory modules for visual control of body position and symmetry of efforts
Total kinesiotherapy exercise duration	20–30 min / session	Comprehensive improvement of the stabilometry and phase parameters	Was part of the common 50–60 min session daily throughout 3 weeks

• center of pressure oscillation amplitude in the sagittal and frontal planes characterizing stability and balance.

Phase analysis of gait and walking

The gait kinematic characteristics were assessed using the Walker View system (TecnoBody, Italy) equipped with the treadmill and optical sensors. The following parameters were recorded:

• stance phase and swing phase duration;

• double support index (percentage of the entire walking cycle);

• symmetry of the stance phase and walking for the operated and contralateral lower limbs (%);

• step length and cadence, if technically possible.

Assessment of the state using scales

The WOMAC (Western Ontario and McMaster Universities Osteoarthritis Index) scale recommended for assessment of the efficacy of conservative and surgical knee osteoarthritis treatment was used for subjective functional state assessment. The scale consists of 24 questions distributed across three subscales: pain (five items), stiffness (two items), and physical function (17 items). The answers were rated on a 5-point scale: 0 — no symptom, 4 — severe manifestation. The total score was calculated by summing up all scores (maximum score 96 points). Lower scores corresponded to better clinical condition. The results were interpreted in accordance with the generally accepted scale: 0–14 points — excellent, 15–28 points — good, 29–38 points — satisfactory, over 38 points — unsatisfactory.

Statistical data processing

Statistical processing of the data obtained was performed using the SPSS Statistics software package (version 26.0, IBM, USA). The distribution of quantitative variables was tested for normality using the Shapiro–Wilk test before the analysis. The intragroup comparison of the indicators reported before and after the rehabilitation course involved the use of the paired Student's *t*-test (when normally distributed) or Wilcoxon test for related samples (when non-normally distributed). The intergroup comparison was performed using the two-sample Student's

Table 4. Major clinical and functional indicators before and after rehabilitation

Indicator	Group	Before treatment (M ± SD)	After treatment (M ± SD)	*p* (intragroup)	*p* (intergroup)
Stabilometry					
Normalized vectorogram area (mm^2)	Index (*n* = 47)	320 ± 60	190 ± 40	0.001	0.003
	Comparison (*n* = 46)	330 ± 70	290 ± 65	0.12	
Mean center of pressure movement linear speed (mm/s)	Index (*n* = 47)	15.5 ± 2.8	8.7 ± 2.1	0.002	0.005
	Comparison (*n* = 46)	16.1 ± 3.0	14.0 ± 2.9	0.09	
Oscillation amplitude (sagittal area) (mm)	Index (*n* = 47)	10.5 ± 2.1	8.7 ± 1.9	0.06	0.11
	Comparison (*n* = 46)	10.8 ± 2.0	9.5 ± 1.8	0.08	
Gait phases					
Stance phase duration (s)	Index (*n* = 47)	0.68 ± 0.07	0.80 ± 0.05	0.003	0.004
	Comparison (*n* = 46)	0.67 ± 0.06	0.71 ± 0.06	0.15	
Phase symmetry (%)	Index (*n* = 47)	74 ± 5	90 ± 4	0.001	0.002
	Comparison (*n* = 46)	75 ± 6	80 ± 5	0.08	
WOMAC (points)					
Total score	Index (*n* = 47)	36 ± 4	22 ± 3	0.001	0.12
	Comparison (*n* = 46)	37 ± 5	25 ± 4	0.004	

Note: *p* (intragroup) — sifgnificance of differences between the indicators reported before and after treatment within the same group; *p* (intergroup) — sifgnificance of differences between the index group and comparison group after treatment.

t-test (normal distribution) or Mann-Whitney *U*-test. Pearson's chi-squared test (χ^2) was used for categorical variables. The differences were considered significant at $p < 0.05$. All data are presented as the mean and standard deviation (M ± SD).

RESULTS

The 3-week rehabilitation course was associated with the changes in stabilometry and kinematic parameters in both groups showing differences in their extent (Table 4). The stabilometry analysis revealed a significant normalized vectorogram area decrease in the index group ($p < 0.01$). No significant differences were revealed in the comparison group ($p > 0.05$). The mean center of pressure movement linear speed decreased significantly in the index group ($p < 0.01$), while in the comparison group the changes were non-significant ($p > 0.05$). The intergroup analysis revealed significant differences in the normalized vectorogram area and mean center of pressure movement linear speed after the rehabilitation course ($p < 0.01$). The gait analysis revealed a significant increase in the stance phase duration and gait phase symmetry improvement in the index group ($p < 0.01$). In the comparison group, the changes in phase parameters were non-significant ($p > 0.05$). The intergroup differences reported after treatment were significant ($p < 0.01$). As for the WOMAC scores, a significant decrease in the total score compared to baseline was reported in both groups ($p < 0.01$). The intergroup differences reported after the rehabilitation course were non-significant ($p > 0.05$).

DISCUSSION

Kinesiotherapy in suspension has a significant impact on the postural control and gait characteristics in patients post knee arthroplasty. Targeting the deep stabilizer muscles and synergist muscles contributes to shaping the more balanced motor patterns and improvement of motor coordination in the stance and swing phases. The decrease in the center of pressure distribution and the neuromuscular control optimization in the index group are likely to be associated with activation of the deep stabilizer muscles and the increased proprioceptive sensitivity. The combination of these changes contributes to higher stability in the static position and decreased risk of falls, which is in line with the research data showing improvement of postural parameters after TKA. The standard rehabilitation program used in the comparison group had a less pronounced effect on the stabilometry indicators, which emphasizes the importance of targeted exercises involving the use of automated complexes and suspension systems for postural control restoration.

The development of the more balanced locomotion in the index group manifested by the increase in the stance phase duration and movement symmetry improvement reflects the physiological motor stereotype restoration. This results in the reduced asymmetric load on the joints, reduces the risk of the compensatory contralateral limb overload and excess stress on the endoprosthesis components. The findings are consistent with the literature data suggesting that the intense, structured rehabilitation programs are effective for restoration of the gait temporal and spatial parameters after TKA. In the comparison group, the changes were less pronounced, which is in line with the data on the limited efficacy of standard programs when used to adjust biomechanical gait disturbances.

The lack of significant intergroup differences in WOMAC scores, despite the decrease in indicators in both groups, can be due to the limited sensitivity of subjective scales to biomechanical parameter alterations. According to the literature data, WOMAC reflects pain severity and functional limitations to the greater extent, that the postural control and gait characteristics [12]. This highlights the feasibility of using objective assessment methods, such as stabilometry and gait phase analysis, when analyzing the rehabilitation program efficacy.

The findings suggest that kinesiotherapy in suspension as a version of the structured balance training and proprioceptive exercises has a pronounced effect on the postural control and gait characteristics in patients post total knee arthroplasty. The current systematic reviews and meta-analyses show that inclusion of balance training in rehabilitation programs ensures the more pronounced static and dynamic balance improvement compared to the standard programs that are based mainly on the essential functional exercises [13–16]. The literature data suggest that such programs contribute to the walking speed increase, reduction of the time of executing the TUG and 6MWT tests, reduction of the center of pressure distribution, and increase in movement symmetry, which is in line with the results reported for the index group in this study. The mechanisms underlying the changes identified can be explained in terms of neuromuscular regulation. The balance training and training in suspension systems activate the deep stabilizer muscles and synergist muscles, enhance the proprioceptive afferent output, and contribute to developing more adequate postural responses. The neuromuscular control improvement manifested by reduction of the center of pressure oscillation amplitude and optimization of its trajectory was described in a number of studies as the key factor of stability restoration following TKA [13, 17, 18]. The use of suspension systems makes it possible to safely increase the training intensity, reducing pain and fear of falling, which, according to the authors, accelerates the functional mobility restoration and increases the patient's engagement in rehabilitation [19].

Shaping the more balanced locomotion in the index group manifested by the increased stance phase duration and movement symmetry reflects the physiological motor stereotype restoration. In the literature, such changes are considered as a sign of reduction of the asymmetric load on the contralateral limb and prevention of the limb overload in the postoperative period. Furthermore, optimization of the gait temporal and spatial parameters reduces the excess stress on the endoprosthesis components, which is potentially important for the long-term implant preservation. Similar data are reported in the studies showing the efficacy of the intense, structured rehabilitation programs for adjustment of biomechanical gait disturbances following TKA [20, 21]. In the comparison group, the standard rehabilitation program ensured improvement, but the dynamic changes in stabilometry and biomechanical indicators were less pronounced. Such results are consistent with the data reported in the papers emphasizing that conventional programs are aimed mainly at restoring the motion range and muscle strength; these are less likely to affect postural control and coordination mechanisms [22]. This suggests the importance of the targeted inclusion of the exercises focusing on balance and proprioception in the postoperative rehabilitation structure. The lack of significant intergroup differences in WOMAC scores, despite objective differences in the postural control and gait parameters, is also explained in the literature. It is reported that WOMAC to the greater extent reflect pain severity and subjective functional limitations, than subtle biomechanical and stabilometry characteristics of movement [23, 24]. This emphasizes the subjective scales' limited sensitivity when used to assess the efficacy of the programs aimed at adjusting neuromuscular regulation and confirms the feasibility of using

objective instrumental methods (stabilometry and gait phase analysis) to analyze the rehabilitation outcomes.

It should be noted that the American Physical Therapy Association guidelines suggest the need to include the dynamic balance training and robot-assisted or suspension technologies in the programs of rehabilitation after TKA in order to optimize gait and reduce the risk of falls [13]. The data obtained in our study confirm these provisions and demonstrate clinical relevance of using kinesiotherapy in suspension as a component of the structured rehabilitation program.

Thus, the combination of the changes revealed allows us to consider kinesiotherapy in suspension not only as a method to restore muscle strength and the range of motion, but also as a tool for targeting the mechanisms underlying postural control, neuromuscular coordination and the development of the physiological motor stereotype following knee arthroplasty.

CONCLUSIONS

Kinesiotherapy in suspension leads to significant changes in the stabilometry and phase parameters in patients post knee arthroplasty. Reduction of the center of pressure distribution, increased stance phase duration and movement symmetry reflect postural control improvement and physiological gait restoration. These changes are associated with shaping balanced locomotion and restoration of physiological locomotor responses ensuring even distribution of the load on the joints and optimal endoprosthesis functioning conditions, which confirms the efficacy of using kinesiotherapy in suspension in the programs for rehabilitation following TKA, especially in the coordination and stability restoration phases. The lack of intergroup differences in WOMAC scores emphasizes the need to use objective assessment methods in rehabilitation.

References

1. Cieza A, Causey K, Kamenov K, Hanson SW, Chatterji S, Vos T. Global estimates of the need for rehabilitation based on the Global Burden of Disease study 2019: a systematic analysis for the Global Burden of Disease Study 2019. The Lancet. 2020; 396: 2006–17. Available from: https://doi.org/10.1016/S0140-6736(20)32340-0.
2. Negrini S, Selb M, Kiekens C, Todhunter-Brown A, Arienti C, et al. Rehabilitation definition for research purposes. 3rd Cochrane Rehabilitation Methodology Meeting participants. A global stakeholders' initiative by Cochrane Rehabilitation. Eur J Phys Rehabil Med. 2022; 58. Available from: https://doi.org/10.23736/S1973-9087.22.07509-8.
3. Proske U, Gandevia SC. The proprioceptive senses: their roles in signaling body shape, body position and movement, and muscle force. Physiol Rev. 2012; 92: 1651–97. Available from: https://doi.org/10.1152/physrev.00048.2011.
4. Booth FW, Roberts CK, Laye MJ. Lack of Exercise Is a Major Cause of Chronic Diseases. In: Prakash YS, editor. Comprehensive Physiology. Wiley, 2012; p. 1143–211. Available from: https://doi.org/10.1002/cphy.c110025.
5. Hunter DJ, Bierma-Zeinstra S. Osteoarthritis. The Lancet. 2019; 393: 1745–59. Available from: https://doi.org/10.1016/S0140-6736(19)30417-9.
6. Katz JN, Arant KR, Loeser RF. Diagnosis and Treatment of Hip and Knee Osteoarthritis: A Review. JAMA. 2021; 325: 568–78. Available from: https://doi.org/10.1001/jama.2020.22171.
7. Wade DT. What is rehabilitation? An empirical investigation leading to an evidence-based description. Clin Rehabil. 2020; 34: 571–83. Available from: https://doi.org/10.1177/0269215520905112.
8. Van Criekinge T, Winnock De Grave P, Luyckx T, Claeys K. Trunk control, motion and alignment after total knee arthroplasty: a systematic review and meta-analysis. Gait & Posture. 2022; 94: 173–88. Available from: https://doi.org/10.1016/j.gaitpost.2022.03.006.
9. Booij MJ, Van Royen BJ, Nolte PA, Twisk JWR, Harlaar J, Van Den Noort JC. Total knee arthroplasty improves gait adaptability in osteoarthritis patients; a pilot study. Journal of Orthopaedics. 2022; 34: 304–9. Available from: https://doi.org/10.1016/j.jor.2022.08.003.
10. Sloan M, Premkumar A, Sheth NP. Projected Volume of Primary Total Joint Arthroplasty in the U.S., 2014 to 2030. The Journal of Bone and Joint Surgery. 2018; 100: 1455–60. Available from: https://doi.org/10.2106/JBJS.17.01617.
11. Learmonth ID, Young C, Rorabeck C. The operation of the century: total hip replacement. The Lancet. 2007; 370: 1508–19. Available from: https://doi.org/10.1016/S0140-6736(07)60457-7.
12. Hadamus A, Błażkiewicz M, Wydra KT, Kowalska AJ, Łukowicz M, Białoszewski D, et al. Effectiveness of Early Rehabilitation with Exergaming in Virtual Reality on Gait in Patients after Total Knee Replacement. J Clin Med. 2022; 11: 4950. Available from: https://doi.org/10.3390/jcm11174950.
13. Jette DU, Hunter SJ, Burkett L, Langham B, Logerstedt DS, Piuzzi NS, et al. Physical Therapist Management of Total Knee Arthroplasty. Phys Ther. 2020; 100: 1603–31. Available from: https://doi.org/10.1093/ptj/pzaa099.
14. Liao C-D, Lin L-F, Huang Y-C, Huang S-W, Chou L-C, Liou T-H. Functional outcomes of outpatient balance training following total knee replacement in patients with knee osteoarthritis: a randomized controlled trial. Clin Rehabil. 2015; 29: 855–67. Available from: https://doi.org/10.1177/0269215514564086.
15. Domínguez-Navarro F, Igual-Camacho C, Silvestre-Muñoz A, Roig-Casasús S, Blasco JM. Effects of balance and proprioceptive training on total hip and knee replacement rehabilitation: A systematic review and meta-analysis. Gait Posture. 2018; 62: 68–74. Available from: https://doi.org/10.1016/j.gaitpost.2018.03.003.
16. Jaczewska-Bogacka J, Stolarczyk A. Improvement in Gait Pattern After Knee Arthroplasty Followed by Proprioceptive Neuromuscular Facilitation Physiotherapy. Adv Exp Med Biol. 2018; 1096: 1–9. Available from: https://doi.org/10.1007/5584_2018_187.
17. Yu X, Zhuang R, Jin P. Evaluation of the efficacy after Total Knee Arthroplasty by Gait analysis in patients with Knee Osteoarthritis: a meta-analysis. J Orthop Surg Res. 2024; 19: 612. Available from: https://doi.org/10.1186/s13018-024-05091-2.
18. Konnyu KJ, Thoma LM, Cao W, Aaron RK, Panagiotou OA, Bhuma MR, et al. Rehabilitation for Total Knee Arthroplasty: A Systematic Review. Am J Phys Med Rehabil. 2023; 102: 19–33. Available from: https://doi.org/10.1097/PHM.0000000000002008.
19. Buhagiar MA, Naylor JM, Harris IA, Xuan W, Kohler F, Wright R, et al. Effect of Inpatient Rehabilitation vs a Monitored Home-Based Program on Mobility in Patients With Total Knee Arthroplasty: The HIHO Randomized Clinical Trial. JAMA. 2017; 317: 1037. Available from: https://doi.org/10.1001/jama.2017.1224.
20. Pozzi F, Snyder-Mackler L, Zeni J. Physical exercise after knee arthroplasty: a systematic review of controlled trials. Eur J Phys Rehabil Med. 2013; 49: 877–92.
21. Mistry JB, Elmallah RDK, Bhave A, Chughtai M, Cherian JJ, McGinn T, et al. Rehabilitative Guidelines after Total Knee Arthroplasty: A Review. J Knee Surg. 2016; 29: 201–17. Available from: https://doi.org/10.1055/s-0036-1579670.
22. Hamilton DF, Beard DJ, Barker KL, Macfarlane GJ, Tuck CE, Stoddart A, et al. Targeting rehabilitation to improve outcomes after total knee arthroplasty in patients at risk of poor outcomes: randomised controlled trial. BMJ. 2020; 371: m3576. Available from: https://doi.org/10.1136/bmj.m3576.
23. Qu H, Zhen Q, Li H, Jiang Q, Cao X, Zhang L, et al. Effects of Balance and Proprioceptive Training on Rehabilitation After Total Knee and Total Hip Replacement: A Systematic Review and Meta-Analysis. J Aging Phys Act. 2026; 34: 82–90. Available from: https://doi.org/10.1123/japa.2024-0390.
24. Artz N, Elvers KT, Lowe CM, Sackley C, Jepson P, Beswick AD. Effectiveness of physiotherapy exercise following total knee replacement: systematic review and meta-analysis. BMC Musculoskelet Disord. 2015; 16: 15. Available from: https://doi.org/10.1186/s12891-015-0469-6.

Литература

1. Cieza A, Causey K, Kamenov K, Hanson SW, Chatterji S, Vos T. Global estimates of the need for rehabilitation based on the Global Burden of Disease study 2019: a systematic analysis for the Global Burden of Disease Study 2019. The Lancet. 2020; 396: 2006–17. Available from: https://doi.org/10.1016/S0140-6736(20)32340-0.
2. Negrini S, Selb M, Kiekens C, Todhunter-Brown A, Arienti C, et al. Rehabilitation definition for research purposes. 3rd Cochrane Rehabilitation Methodology Meeting participants. A global stakeholders' initiative by Cochrane Rehabilitation. Eur J Phys Rehabil Med. 2022; 58. Available from: https://doi.org/10.23736/S1973-9087.22.07509-8.
3. Proske U, Gandevia SC. The proprioceptive senses: their roles in signaling body shape, body position and movement, and muscle force. Physiol Rev. 2012; 92: 1651–97. Available from: https://doi.org/10.1152/physrev.00048.2011.
4. Booth FW, Roberts CK, Laye MJ. Lack of Exercise Is a Major Cause of Chronic Diseases. In: Prakash YS, editor. Comprehensive Physiology. Wiley, 2012; p. 1143–211. Available from: https://doi.org/10.1002/cphy.c110025.
5. Hunter DJ, Bierma-Zeinstra S. Osteoarthritis. The Lancet. 2019; 393: 1745–59. Available from: https://doi.org/10.1016/S0140-6736(19)30417-9.
6. Katz JN, Arant KR, Loeser RF. Diagnosis and Treatment of Hip and Knee Osteoarthritis: A Review. JAMA. 2021; 325: 568–78. Available from: https://doi.org/10.1001/jama.2020.22171.
7. Wade DT. What is rehabilitation? An empirical investigation leading to an evidence-based description. Clin Rehabil. 2020; 34: 571–83. Available from: https://doi.org/10.1177/0269215520905112.
8. Van Criekinge T, Winnock De Grave P, Luyckx T, Claeys K. Trunk control, motion and alignment after total knee arthroplasty: a systematic review and meta-analysis. Gait & Posture. 2022; 94: 173–88. Available from: https://doi.org/10.1016/j.gaitpost.2022.03.006.
9. Booij MJ, Van Royen BJ, Nolte PA, Twisk JWR, Harlaar J, Van Den Noort JC. Total knee arthroplasty improves gait adaptability in osteoarthritis patients; a pilot study. Journal of Orthopaedics. 2022; 34: 304–9. Available from: https://doi.org/10.1016/j.jor.2022.08.003.
10. Sloan M, Premkumar A, Sheth NP. Projected Volume of Primary Total Joint Arthroplasty in the U.S., 2014 to 2030. The Journal of Bone and Joint Surgery. 2018; 100: 1455–60. Available from: https://doi.org/10.2106/JBJS.17.01617.
11. Learmonth ID, Young C, Rorabeck C. The operation of the century: total hip replacement. The Lancet. 2007; 370: 1508–19. Available from: https://doi.org/10.1016/S0140-6736(07)60457-7.
12. Hadamus A, Błażkiewicz M, Wydra KT, Kowalska AJ, Łukowicz M, Białoszewski D, et al. Effectiveness of Early Rehabilitation with Exergaming in Virtual Reality on Gait in Patients after Total Knee Replacement. J Clin Med. 2022; 11: 4950. Available from: https://doi.org/10.3390/jcm11174950.
13. Jette DU, Hunter SJ, Burkett L, Langham B, Logerstedt DS, Piuzzi NS, et al. Physical Therapist Management of Total Knee Arthroplasty. Phys Ther. 2020; 100: 1603–31. Available from: https://doi.org/10.1093/ptj/pzaa099.
14. Liao C-D, Lin L-F, Huang Y-C, Huang S-W, Chou L-C, Liou T-H. Functional outcomes of outpatient balance training following total knee replacement in patients with knee osteoarthritis: a randomized controlled trial. Clin Rehabil. 2015; 29: 855–67. Available from: https://doi.org/10.1177/0269215514564086.
15. Domínguez-Navarro F, Igual-Camacho C, Silvestre-Muñoz A, Roig-Casasús S, Blasco JM. Effects of balance and proprioceptive training on total hip and knee replacement rehabilitation: A systematic review and meta-analysis. Gait Posture. 2018; 62: 68–74. Available from: https://doi.org/10.1016/j.gaitpost.2018.03.003.
16. Jaczewska-Bogacka J, Stolarczyk A. Improvement in Gait Pattern After Knee Arthroplasty Followed by Proprioceptive Neuromuscular Facilitation Physiotherapy. Adv Exp Med Biol. 2018; 1096: 1–9. Available from: https://doi.org/10.1007/5584_2018_187.
17. Yu X, Zhuang R, Jin P. Evaluation of the efficacy after Total Knee Arthroplasty by Gait analysis in patients with Knee Osteoarthritis: a meta-analysis. J Orthop Surg Res. 2024; 19: 612. Available from: https://doi.org/10.1186/s13018-024-05091-2.
18. Konnyu KJ, Thoma LM, Cao W, Aaron RK, Panagiotou OA, Bhuma MR, et al. Rehabilitation for Total Knee Arthroplasty: A Systematic Review. Am J Phys Med Rehabil. 2023; 102: 19–33. Available from: https://doi.org/10.1097/PHM.0000000000002008.
19. Buhagiar MA, Naylor JM, Harris IA, Xuan W, Kohler F, Wright R, et al. Effect of Inpatient Rehabilitation vs a Monitored Home-Based Program on Mobility in Patients With Total Knee Arthroplasty: The HIHO Randomized Clinical Trial. JAMA. 2017; 317: 1037. Available from: https://doi.org/10.1001/jama.2017.1224.
20. Pozzi F, Snyder-Mackler L, Zeni J. Physical exercise after knee arthroplasty: a systematic review of controlled trials. Eur J Phys Rehabil Med. 2013; 49: 877–92.
21. Mistry JB, Elmallah RDK, Bhave A, Chughtai M, Cherian JJ, McGinn T, et al. Rehabilitative Guidelines after Total Knee Arthroplasty: A Review. J Knee Surg. 2016; 29: 201–17. Available from: https://doi.org/10.1055/s-0036-1579670.
22. Hamilton DF, Beard DJ, Barker KL, Macfarlane GJ, Tuck CE, Stoddart A, et al. Targeting rehabilitation to improve outcomes after total knee arthroplasty in patients at risk of poor outcomes: randomised controlled trial. BMJ. 2020; 371: m3576. Available from: https://doi.org/10.1136/bmj.m3576.
23. Qu H, Zhen Q, Li H, Jiang Q, Cao X, Zhang L, et al. Effects of Balance and Proprioceptive Training on Rehabilitation After Total Knee and Total Hip Replacement: A Systematic Review and Meta-Analysis. J Aging Phys Act. 2026; 34: 82–90. Available from: https://doi.org/10.1123/japa.2024-0390.
24. Artz N, Elvers KT, Lowe CM, Sackley C, Jepson P, Beswick AD. Effectiveness of physiotherapy exercise following total knee replacement: systematic review and meta-analysis. BMC Musculoskelet Disord. 2015; 16: 15. Available from: https://doi.org/10.1186/s12891-015-0469-6.